UNIVERSITAT POLITÈCNICA DE CATALUNYA BARCELONATECH

Micromechanics of quaternary AlCrSiN coatings on hard substrates

Jing Liang

Departament de Ciència dels Materials i Enginyeria Metal·lúrgica
UNIVERSITAT POLITÈCNICA DE CATALUNYA

CIEFMA

Micromechanics of quaternary AlCrSiN coatings on hard substrates

A dissertation submitted to partial fulfilment of the requirements for the degree of

Doctor of Philosophy by

Jing Liang

Advisors: Emilio Jiménez Piqué

Center of Structural Integrity, Micromechanics and Reliability of Materials

Department of Materials Science and Engineering

Universitat Politècnica de Catalunya – Barcelona Tech

Barcelona, Spain

2023

Acknowledgements

Looking back on the past five years, whole period of my Ph.D experience, the excitement and gratitude are filled in my heart. I still remember many memorable moments: the first time setting foot on a foreign land, the nervousness of being interviewed with my poor and stuttering English by the professors of our CIEFMA group, the excitement of receiving the admission notice from the UPC, the anxiety of new research area for me at the beginning, the joy of talking and playing together with great colleagues, these images generally appear in my mind as if it happened yesterday. I don't know how to express the gratitude at this moment and I'm very grateful to everyone I have met and gave me help in my research work during the past five years. You create the memorable moments for me and will be in my heart forever.

First and foremost, I would like to express my heartfelt gratitude to my supervisor, **Prof. Emilio Jiménez Piqué,** his continuous support wise and acute academic perception gave me considerable encourage to strive in the scientific work. In these years, I have been deeply influenced by his sense of responsibility, carefulness, and passion in the work, and these qualities will bring me a very positive effect in my future work. He patiently guide me how to be a qualitied scientific researcher, from the data collection to normatively scientific thinking and writing habits, which greatly improve my work efficiency.

Prof. Luis Llanes, my guide for joining into the CIEFMA group, gave me the opportunity to study and research work in the past five years. He also gave me some very professional and rigorous comments for my work and urge me to become more sensitive to the problems I met.

Joan Josep Roa, supervised in the first two years, took my hand and taught me how to operate the relevant instrument to evaluate the mechanical properties of materials. He also led me to familiarize the whole campus and daily rules of labs.

Fernando García, for his efficient help on use of confocal microscopy, servo-hydraulic testing machine and cutting machine.

Laia Ortiz-Membrado, Sandra Gordon, and Marc Serra, for their great help during experimental work, the advice for choice of different parameters and machines.

Trifon Trifnov, for his unlimited and immeasurable help to make me professional learn how to use the FESEM and FIB.

My colleagues and friends, for all memorable and great moments, we shared during the last five years. Special thankfulness gives to Yafeng, Junhui, Hossein, Joaquim, Daniela(s), Ke, Congcong, Suhong, Mona, and Ana. Thank you for being with me through this wonderful time.

Dr. Ruifeng Du, my dear husband, best friend and soulmate, for his continuous love and support, for his careful care and companionship, for his understanding to my reasonable and unreasonable requirements, filling my life with happiness and hope. The same for **my parents**, my biggest financial and spiritual supporter, let me face all difficulties bravely and confidently, love you forever!

Preface

This thesis is a gathering results of my doctoral studies in the Department of Materials Science and Engineering at Universitat Politècnica de Catalunya – Barcelona Tech (UPC) during the period from February 2018 to July 2023. All work were carried out under the supervision of **Prof. Emilio Jiménez Piqué** at the Centre d'Integritat Estructural, Micromecànica i Fiabilitat dels Materials (CIEFMA), a research group of UPC. Research was supported by the Spanish ministry of Science, Innovation and Universities, through grant number of PGC2018-096855-B-C41. The contents in this doctoral thesis are original work, except described in the acknowledges and comprehensive and detailed references.

Abstract

AlCrSiN quaternary coating is a kind of protective and hard ceramic coating which is widely in tool industry because of its excellent mechanical performance. The formation of AlCrSiN quaternary coating is based on the CrN binary structural ceramic coating through the introduced elements of Alumina (Al) and Silicon (Si) which enhance the mechanical properties, thermal stability and wear resistance. The stable B1 crystalline structure and solid solution strengthen effect promote the coating keep these capabilities. Physical vapor deposition (PVD) is one of the most used and commercial method in cutting tool to improve the performance of hard materials because of their striking properties. As a result, AlCrSiN quaternary coating was prepared by PVD and deposited on substrates with different extent of hardness in this doctoral thesis.

Soft substrates of steel H13 (DIN 1.2344) and Inconel, hard substrate of cemented carbide (WC-Co) and superhard substrate of cubic boron nitride (cBN) are deposited by AlCrSiN quaternary coating in order to profoundly improve the mechanical response of coating-substrate systems. Steel H13 is a type of ferroalloy especially used as hot work steel for processing light metal. And Inconel is a type of Nickle-based alloy widely employed for metal additive manufacturing in various industrial areas due to its outstanding strength and thermal stability. For cutting tools and structural materials, WC-Co have got extensively application and studies because of its better hard hardness and wear resistance. And cBN apply in tool materials due to its better combination of excellent hardness (which is just less than diamond) and abrasive wear resistance.

Within the above presentation, the first section of this thesis was dedicated to explore the mechanical performance of AlCrSiN quaternary coating deposited soft substrate of steel H13 and Inconel 718 after thermal treatment to bring out and simulate the similar service conditions. The comparative study with AlTiSiN quaternary coating was conducted to investigate the evolution of same substrate and temperature environment. The hardness and elastic modulus of AlCrSiN coating increased with all substrates deposited under lower temperature condition

of 500°C, however, they decreased under higher temperature of 800°C, which means a degradation of materials. ACrSiN coating samples presented lower adhesion than AlTiSiN coating for all thermal treatment with larger spalled areas. Regarding the substrates, coatings deposited on Inconel 718 exhibited better mechanical performance remarkably after thermal treatment at both lower and higher temperature, associated with its better performance at high temperature.

For the sequent part, the comparative study of mechanical performance was carried out AlCrSiN quaternary coating deposited on hard substrate of WC-Co and superhard substrate of cBN. The intrinsic hardness and elastic modulus show the same value of AlCrSiN coating deposited on both substrates. The crystalline structure of AlCrSiN coating also was not influenced by the substrates. AlCrSiN coating deposited on WC-Co substrate presented better adhesion than deposited on cBN substrate regardless of suffering progressive and static normal loads. The results of mechanical response under contact Hertzian loads were showed that AlCrSiN coating deposited on WC-Co substrate perform better resistance of monotonic loads and cyclic loads than deposited on cBN substrates. Cohesive failure of AlCrSiN coating was detected when deposited WC-Co substrate, however, adhesive failure was observed when deposited on cBN substrate. The difference in mechanical performance of AlCrSiN coating deposited on different hardness of substrate depend on both adhesion strength and distinck mechanical performance of substrate.

And the final part was focued on the effect of Zr/Ta ions implantation on mechanical properties of AlCrSiN quaternary coating deposited on hard substrate of WC-Co. In these coating-substrate systems, both Zr and Ta ion implantations introduce a degradation of hardness and elastic modulus. The metal bodning of both Al-Al and Cr-Cr were transformed into Al-N and Cr-N metal nitride chemical bonding respectively according to the analysis of X-ray photoelectron spectroscopy (XPS). The crystalline structure of AlCrSiN coating keep similar (Cr,Al)N solid solution regardless of ion implantation. In the case of Zr ion implantation a small amount of zb-AlN was detected. The adhesion strength between coating and substrate was improved after ion implantation, where Ta ion implantation performed the best.

Resumen

Los recubrimientos cuaternarios tipo AlCrSiN es un recubrimiento extremadamente duro utilizado ampliamente en la industria de materiales para herramienta. Este tipo de recubrimiento se forma a través de la adición de alúmina (Al) y silicio (Si) al recubrimiento estructural binario CrN, lo que mejora sus propiedades mecánicas, estabilidad térmica y resistencia al desgaste. La estructura cristalina B1 y el efecto de fortalecimiento de la solución sólida contribuyen a mantener estas capacidades. La deposición física de vapor (PVD) es uno de los métodos más utilizados en herramientas de corte para mejorar el rendimiento de materiales duros, por lo que en esta tesis doctoral se estudiaron recubrimiento cuaternarios de AlCrSiN por PVD depositados sobre sustratos de diferente dureza.

Para ello se utilizaron sustratos blandos de acero H13 e Inconel, un sustrato duro de carburo cementado (WC-Co) y un sustrato superduro de nitruro de boro cúbico (cBN) para mejorar la respuesta mecánica de los sistemas de recubrimiento-sustrato. El acero H13 se utiliza para trabajar en caliente en el procesamiento de metales ligeros, mientras que el Inconel es ampliamente utilizado en la fabricación aditiva de metal debido a su excelente resistencia y estabilidad térmica. Por otro lado, el WC-Co se aplica en herramientas de corte y materiales estructurales debido a su mejor dureza y resistencia al desgaste, y el cBN se utiliza en materiales para herramientas debido a su excelente dureza y resistencia al desgaste abrasivo.

Así pues, la primera sección de esta tesis se dedicó a explorar el rendimiento mecánico del recubrimiento cuaternario de AlCrSiN depositado en un sustrato blando de acero H13 e Inconel 718 después del tratamiento térmico para simular condiciones de servicio similares. Se realizó un estudio comparativo con el recubrimiento cuaternario AlTiSiN para investigar la evolución del mismo sustrato a diferentes temperaturas. Se encontró que la dureza y el módulo elástico del recubrimiento de AlCrSiN aumentaron en todos los sustratos a temperaturas más bajas de 500°C, pero disminuyeron a temperaturas más altas de 800°C, lo que indica una degradación de los materiales. Además, se observó que los recubrimientos depositados sobre Inconel 718 presentaron un mejor desempeño

mecánico notablemente después del tratamiento térmico, tanto a menor como a mayor temperatura, en comparación con los depositados sobre acero H13. También se observó que los recubrimientos de AlTiSiN presentaron una mejor adherencia que los de AlCrSiN en todas las condiciones de tratamiento térmico, con áreas desconchadas más pequeñas.

A continuación, e realizó us estudio comparativo del comportamiento mecánico del recubrimiento cuaternario de AlCrSiN depositado sobre sustrato duro de WC-Co y sustrato superduro de cBN. La dureza intrínseca y el módulo elástico muestran el mismo valor del recubrimiento de AlCrSiN depositado en ambos sustratos. La estructura cristalina del recubrimiento de AlCrSiN no se alteró por los sustratos. El recubrimiento de AlCrSiN depositado sobre sustrato WC-Co presentó mejor adherencia que el depositado sobre sustrato cBN independientemente de sufrir cargas normales progresivas y estáticas. Los resultados de la respuesta mecánica bajo cargas Hertzianas de contacto mostraron que el recubrimiento de AlCrSiN depositado sobre sustrato de WC-Co resiste mejor las cargas monotónicas y las cargas cíclicas que el depositado sobre sustratos de cBN. Se detectó falla cohesiva del revestimiento AlCrSiN cuando se depositó sustrato WC-Co, sin embargo, se observó falla adhesiva cuando se depositó sobre sustrato cBN. La diferencia en el rendimiento mecánico del recubrimiento de AlCrSiN depositado en diferentes durezas del sustrato depende tanto de la fuerza de adhesión como del rendimiento mecánico del sustrato.

Finalmente, se investigó el efecto de la implantación de iones Zr/Ta en las propiedades mecánicas del recubrimiento de AlCrSiN depositado sobre sustrato WC-Co. Los resultados mostraron una degradación de la dureza y el módulo elástico después de la implantación de iones, pero la fuerza de adhesión entre el recubrimiento y el sustrato mejoró. Además, el enlace metálico de Al-Al y Cr-Cr se transformó en enlace químico de nitruro metálico Al-N y Cr-N respectivamente después de la implantación de iones, y se mantuvo una solución sólida de (Cr,Al)N en la estructura cristalina del recubrimiento de AlCrSiN. La implantación de iones de Ta tuvo un mejor desempeño en la mejora de la fuerza de adhesión que la implantación de iones de Zr.

En resumen, el estudio comparativo y el análisis de la implantación de iones muestran que la dureza, el módulo elástico y la fuerza de adhesión son factores importantes a considerar en la selección del sustrato y en la mejora del rendimiento mecánico del recubrimiento de AlCrSiN. Además, la implantación de iones puede ser una técnica efectiva para mejorar la adhesión del recubrimiento al sustrato.

Resum

Los recubrimientos cuaternarios tipo AlCrSiN son un recubrimiento extremadamente duro usado ampliamente en la industria de materiales para herramienta. Aquest tipus de recubriment es forma a través de l'adición d'alúmina (Al) i silici (Si) al recubriment estructural binari CrN, el que millora les seves propietats mecàniques, l'estabilitat tèrmica i la resistència al desgast. L'estructura cristalina B1 i l'efecte de reforç de la solució sòlida contribueixen a mantenir les seves capacitats. La deposició física de vapor (PVD) és un dels mètodes més utilitzats en eines de corte per millorar el rendiment de materials durs, per tal que en aquesta tesi doctoral s'estudiï el recubriment de quadres d'AlCrSiN per PVD dipositats sobre substrats de diferent durada.

Per ello se utilitzaron substrats blandos d'acer H13 i Inconel, un substrat dur de carbur cementado (WC-Co) i un substrat superduro de nitruro de boro cúbico (cBN) per millorar la resposta mecànica dels sistemes de recubriment-sust. L'acer H13 s'utilitza per treballar en calent en el processament de metalls lleugers, mentre que l'Inconel s'utilitza àmpliament en la fabricació aditiva de metall a causa de la seva excel·lent resistència i estabilitat tèrmica. Per un altre lado, el WC-Co s'aplica en eines de corte i materials estructurals a causa de la seva millor duresa i resistència al desgaste, i el cBN s'utilitza en materials per a eines degut a la seva excel·lent duresa i resistència al desgast abrasiu.

Així pues, la primera secció d'aquesta tesi es va dedicar a explorar el rendiment mecànic del recubrimiento cuaternari d'AlCrSiN dipositat en un substrat blanc d'acer H13 i Inconel 718 després del tractament tèrmic per a simular condicions de servei semblants. S'ha realitzat un estudi comparatiu amb el recubrimiento cuaternari AlTiSiN per investigar l'evolució del mateix substrat a diferents temperatures. Es va trobar que la duresa i el mòdul elàstic del recobriment d'AlCrSiN augmentar en tots els substrats a temperatures més baixes de 500°C, però disminuyeron a temperatures més altes de 800°C, el que indica una degradació dels materials. A més, s'ha observat que els recubrimientos depositados sobre Inconel 718 presentaron un millor rendiment mecànic notablement després del tractament tèrmic, tant a menor com a major temperatura, en comparació amb els dipositats sobre acero H13. També s'ha observat que els recubrimientos

d'AlTiSiN presentaron una millor adherència que els d'AlCrSiN en totes les condicions de tractament tèrmic, amb àrees desconchades més petites.

A continuació, e realizó us estudio comparativo del comportamiento mecánico del recubrimiento cuaternario de AlCrSiN depositado sobre substrat duro de WC-Co i substrat superduro de cBN. La duresa intrínseca i el mòdul elàstic mostra el mateix valor del recobriment d'AlCrSiN dipositat en ambdós substrats. La estructura cristalina del recubrimiento de AlCrSiN no es va alterar por los substratos. El recubrimiento de AlCrSiN depositado sobre substrat WC-Co va presentar la millor adherència que el dipositat sobre substrat cBN independentment de patir càrregues normals progressives i estàtiques. Los resultados de la respuesta mecánica bajo cargas Hertzianas de contacto mostraron que el recubrimiento de AlCrSiN depositado sobre substrato de WC-Co resiste mejor las cargas monotónicas y las cargas cíclicas que el depositado sobre substratos de cBN. Es va detectar la falla cohesiva del revestiment AlCrSiN quan es va dipositar sobre el substrat WC-Co, sense embargo, es va observar la falla adhesiva quan es va dipositar sobre el substrat cBN. La diferencia en el rendimiento mecánico del recubrimiento de AlCrSiN dipositat en diferents dureses del substrat depèn tant de la força d'adhesió com del rendiment mecánico del substrat.

Finalment, es va investigar l'efecte de la implantació d'ions Zr/Ta en les propietats mecàniques del recobriment d'AlCrSiN dipositat sobre substrat WC-Co. Els resultats mostraron una degradació de la duresa i el mòdul elàstic després de la implantació d'ions, però la força d'adhesió entre el recubriment i el substrat millorat. A més, l'enllaç metàl·lic d'Al-Al i Cr-Cr es va transformar en l'enllaç químic de nitruro metàl·lic Al-N i Cr-N respectivament després de la implantació d'ions, i s'ha mantingut una solució sòlida de (Cr,Al)N en la estructura cristalina del recubrimiento de AlCrSiN. La implantación de iones de Ta tuvo un mejor desempeño en la mejora de la fuerza de adhesión que la implantación de iones de Zr.

En resumen, l'estudi comparatiu i l'anàlisi de la implantació d'ions mostren que la duresa, el mòdul elástico i la força de adhesión son factors importants a considerar en la selecció del substrat i en la millora del rendiment mecànic del recobriment d'AlCrSiN. A més, la implantació d'ions pot ser una tècnica efectiva per millorar l'adhesió del recubriment al substrat.

Contents

Glossary

Symbol / acronym	Description
Al	Alunium
Cr	Chromium
CVD	Chemical vapour deposition
CrN	Chromium nitride
E	Elastic modulus
E_{eff}	Effective elastic modulus
FESEM	Field emission scanning electron microscope
FIB	Focus ion beam
Eq	equation
h	Penetration depth
h_f	Residual penetration depth
h_{max}	Maximum penetration depth
h_s	Surface depth
h_c	Contact depth
H	Hardness
HSS	High speed steel
ITT	Instrumented indentation technique
ISE	Indentation size effect
K_{IC}	Fracture toughness
P	Applied load
P_{max}	Maximum applied load
PVD	Physical vapor deposition
σ_y	Yield strength
S	stiffness
Si	Silicon
TiN	Titanium nitride
ε	Strain

1 Introduction

Nowadays, several industries, including aerospace, marine, oil and gas, and medical, are expanding rapidly, and their operations significantly impact diverse domains of human life and global economy. The manufacturing processes of these industries heavily rely on machinery, and machining operations assume a pivotal role in different stages of production [1, 2]. In recent decades, Europe has been at the forefront of tooling technology, striving to reduce the environmental impact of industrial production, enhance productivity, and minimize the dependence on critical raw materials. Consequently, current research efforts not only concentrate on developing novel materials but also emphasize augmenting the service life and reliability of tool materials. Among various machining techniques, metal cutting represents the most fundamental and widely employed method in several machining operations [3].

Cutting tool is the key factor to support and promote the development of machining process and its properties critically affects the quality and efficiency of cutting process [4, 5]. The ideal condition for cutting tool materials should simultaneously be high hardness, fracture toughness chemical inertness and thermal stability and wear resistance, however, reaching an equilibrium between these properties is not an easy task [4]. Therefore, hard materials for tool are generally aim to achieve high hardness and a relatively high fracture toughness [6, 7] at the sam time, a topic that has been researched extensively [8-11].

The primary materials employed in cutting tools can be broadly categorized into three groups: high speed steels, cermet and ceramic and superhard materials such as diamond and cubic boron nitride (cBN) [12]. The cermet play a critical role in the machining application, **Figure 1-1** provides a relationship of between hardness and fracture toughness of different cermet.

High speed steel (HSS) possesses a relatively lower hardness than cemented carbides and superhard materials. However, due to its superior process performance, strength and toughness, HSS finds significant applications in manufacturing complex thin blades, compact resistant metal cutting tools, as well as high-temperature bearings [13, 14]. However, its limited hardness renders it unsuitable for demanding operations.

Cemented carbide is the most widely applied materials in industry [15]. The main phase is ceramic (WC), which have excellent mechanical performance for instance high hardness, excellent wear resistance and stiffness. A metallic second phase, which generally is cobalt but it can be other metals such as nickel or iron, provides the material with high fracture toughness and damage tolerance [16-19].

Cubic boron carbide (cBN), with a hardness level slightly below that of diamond, is one of the most durable materials known. It is utilized as a tool material because of its exceptional thermal stability and conductivity [20-22]. During high-speed cutting operations, cBN's low tendency to transform into hexagonal boron nitride (hBN) at high temperature is advantageous for the machining of ferrous compounds [23]. This thesis emphasize the importance of the substrate, and two types of High-Speed Steel (HSS), cemented carbide, and cBN were chosen as substrates.

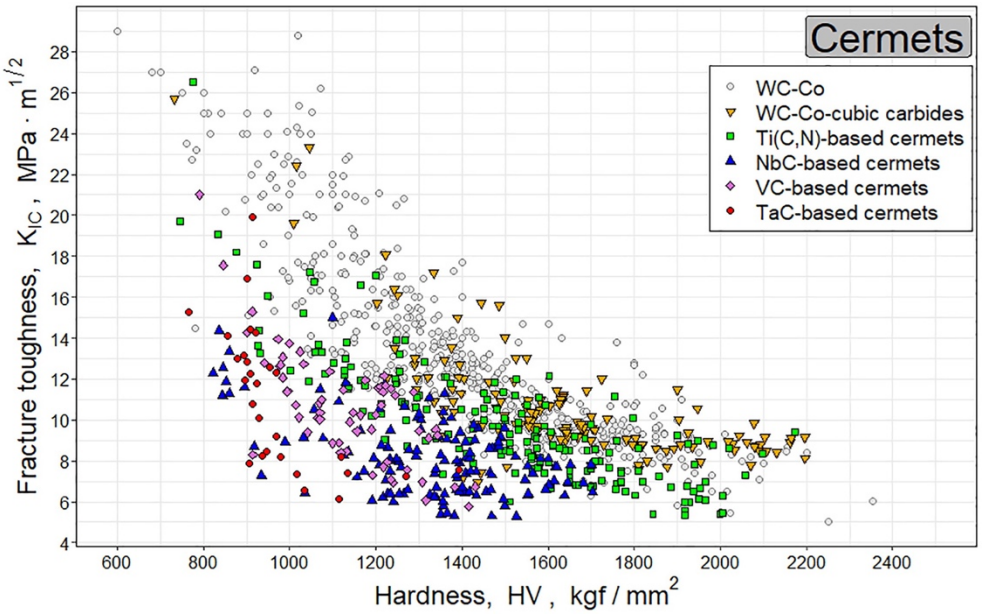

Figure 1-1. Hardness and fracture toughness of different cements [24].

Ceramic coatings are commonly employed to enhance the surface durability and tribological properties of hard materials such as tool steels, hard metals, alloys, and other sturdy materials [25]. Since ceramics exhibit relatively low fracture toughness and plastic deformation due to their microstructure at room temperature [26], coating systems made of ceramic materials are used to enhance the tribological behavior of the substrates [27]. The two primary methods of preparing ceramic coatings are physical vapor deposition (PVD) and chemical vapor deposition (CVD), both of which offer high performance based on their composition and the interface structure with

other components of the composite material [28, 29]. The interface is produced through the deposition process of various materials [30-32]. PVD and CVD are well-established surface modification technologies that are widely employed for coating hard substrates, providing high flexibility in terms of composition and structure of the coating. In this thesis, the focus is on the mechanical properties and response of the quaternary ceramic coating AlCrSiN, deposited on substrates of varying hardness, which is prepared through PVD.

From the viewpoint of coating or substrate itself, extensive researches have been focused on the mechanical properties, microstructure, high temperature properties, tribological properties and oxidation resistance [33-37]. However, it is important to understand that the performance of tool is not only governed by the coatings, but the substrates also play a critical role in the damage evolution during machining process. So, the synergic effect with substrate deserve to get more attention. The coating-substrate systems will undergo thermal cycles during operation and it is necessary to understand the evolution of the mechanical properties after thermal treatment. Although the evolution of hardness of quaternary coatings after thermal treatment has been reported [38-40] there are scarce reports on coating-substrate adhesion under similar condition [41, 42] [43]. Surface modification is other aspect to improve the mechanical performance of coating-substrate systems and ion implantation have been proven to be an effective method with a number of literature presenting enhance in properties [44, 45]. However, AlCrSiN quaternary coating deposited on WC-Co substrate reduce the enhance the mechanical performance [46], the effect of ion implantation has still not been studied. At the same time, the effects of different substrates on quaternary coatings has been explored but mainly on metallic substrates [47, 48]. However, they just studied one substrate and so the effect of different substrates in the mechanical response under contact is very interesting.

2 Hard coatings

2.1 Characteristics and deposition routes

Protective ceramic coatings are extensively used in tool industry owing to their superior mechanical performance. These coatings are a special form of inorganic multiphase materials with a single or multiple layers of ceramic or glassy material that are coated onto the surface of tool materials to enhance their durability and longevity [49]. Inorganic compounds, such as metal oxides and intermetallic compounds, are coated on various structural substrate using various methods to safeguard them from high temperature oxidation [50], corrosion and abrasion. Coatings can comprise at least one element from the group IV, V or VI of the periodic table and alumina, and can be combined with carbon, nitrogen and/or oxygen to create different compounds. From a microstructural standpoint these coatings consist of distinct phases [50].

Binary ceramic coatings such as CrN and TiN were initially the typical commercial ceramic coatings used [51-53]. However, over the past few decades, these binary structural ceramic coatings have been extensively studied and gained considerable attention [54-56]. In recent years, there has been an introduction of ternary systems,such as AlCrN and AlTiN, by incorporating alumina (Al) and silicon (Si) into the binary coating systems [57, 58]. Moreover, quaternary systems such as AlCrSiN and AlTiSiN have also been developed with improved mechanical properties, thermal stability and wear resistance [59, 60]. The fundamental reason for maintaining these capabilities is the stable crystalline structure and solid solution strengthening effect [33, 61-63]. The addition of Al aims to enhance the oxidation resistance and thermal stability of coatings by forming an oxide-rich top layers [64-66]. The role of Si introduced into quaternary coating systems is to produce an amorphous Si_3N_4 phase at the nanometer scale, inhibiting the sliding movement between neighboring grains, thus improving the hardness and thermal stability [67, 68]. However, when these coatings are used in harsh environments such as corrosive conditions, high temperatures, and rapid cutting operations, there is still enormous room for improvement. Coating materials should convert hardness into wear resistance, and the wear rate should remain low throughout the tool’s service life. However, hardness is

not the unique factor affecting the tool's lifespan and reliability. Other properties such as fracture toughness, surface finish, and Young's modulus also play an important in the coatings' performance and lifetime.

Among different deposition methods, Physical Vapor Deposition (PVD) is one of the most used and commercial in cutting tools [69]. PVD coating technology is a widely used method for creating hard coatings on various materials. PVD is a vacuum-based process that involves the deposition of thin films of materials onto the surface of a substrate using various techniques such as evaporation, sputtering, and arc deposition. The process takes place in a vacuum chamber where a target material is bombarded with high energy ions to release atoms or molecules that form a thin film on the substrate surface.

PVD technology is capable of producing hard coatings with exceptional wear resistance, corrosion resistance, and thermal stability, making them highly desirable for a wide range of applications. To create these coatings, materials such as nitrides, carbides, and oxides are deposited onto the surface of the substrate. These materials possess high melting points and are deposited at elevated temperatures, ensuring a strong bond between the coating and substrate.

PVD coating technology is versatile and can be applied to a wide range of materials, including metals, ceramic, and polymers. These coatings find application in various industries, including cutting tools, aerospace, automotive, medical devices, and electronics.

2.2 Intrinsic mechanical properties

While high hardness of ceramic coatings leads to improve tool life due to low wear rate, poor toughness is usually found [70, 71], which lead to high degree of crack propagation and further failure of coatings [72, 73].

Hardness is a fundamental property that characterizes a material's ability to resist deformation, such as indentation or penetration by a harder object [74]. In the mechanical field, hardness plays a crucial role in various applications, including cutting tools, mining and drilling equipment, where wear resistance is essential [75]. **Figure 2-1** illustrates that, in general, increasing the hardness of a material leads to a decrease in its wear rate.

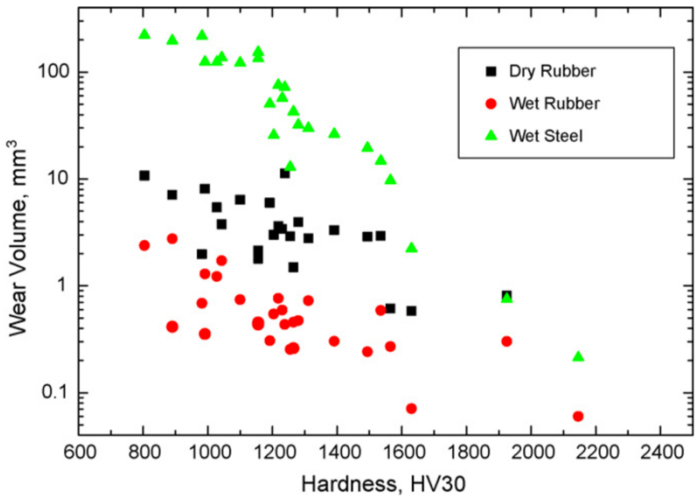

Figure 2-1. The relationship of wear volume and hardness on range of hardmetals with three wheel conditions as described in legend image taken from reference [76].

The elastic modulus is defined as the stress in a unidirectional stress state divided by the strain in that direction, which is used for evaluating the ability to resist elastic deformation. From the microscopic point, it is reflection of bounding strength between atoms, ions or molecules. The hardness to elastic modulus ratio (H/E) reflects the elastic deformation to failure and H^3/E^2 is generally adopted to present the resistance to plastic deformation [77-79].

The conventional method for measuring hardness involves pressing an indenter of a specific shape onto the surface of a sample using vertical force. The indentation area is subsequently determined based on the indentation area after unloading the indenter.

However, this measurement method is only appropriate for relatively large-sized samples. The advent of nanoindentation technology has addressed the limitations of traditional measurements. This technology, also referred to as depth-sensitive indentation, measures also at the same time the load and the penetration into the surface [80-82].

Figure 2-2 shows tan example of the hardness and elastic modulus of AlCrSiN quaternary coating deposited on WC-Co substrate via nanoindentation. The intrinsic hardness and elastic modulus could be extracted from the curve avoiding the effect of the substrate, as compared with traditional methods.

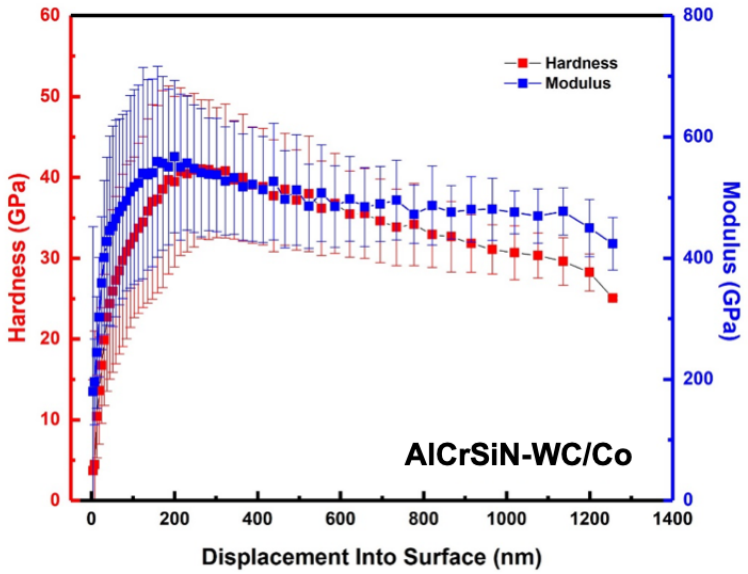

Figure 2-2. Mechanical properties for AlCrSiN quaternary coating deposited on WC-Co substrate as function of displacement into the surface. Hardness is left Y-axis and Elastic modulus is right Y-axis.

The thickness of a coating is an intrinsic property that significantly affects the performance of coating-substrate systems, and its impact on tribological performance has been widely investigated. Generally, thicker coatings exhibit better scratch resistance due to their higher load-carrying capacity, as compared to thinner coatings [83, 84]. However, for cutting tools, coating thickness plays a more complex role since its effects are magnified around the cutting edge [85]. Therefore, to ensure the reliability of mechanical performance assessment and testing, it is crucial to have uniform and consistent coating thickness.

3 Substrates

To gain a comprehensive understanding of the mechanical response coatings deposited on three substrates selected based on their hardness, this doctoral thesis employs various research methods and content based on their mechanical properties and application areas. The substrates comprise soft substrate of steel H13 (DIN 1.2344) and Inconel 718, a hard substrate of (WC-Co) and a superhard substrate of cubic boron nitride (cBN).

3.1 Soft substrate: steel H13 and Inconel 718

Steel H13 (DIN 1.2344) is a type of ferroalloy and widely used as hot work tool steel for extrusion and forging dies the processing of light metal. The steel's high hardness, good wear resistance and thermal stability at elevated temperature ensure its durability for high temperature application. The traditional thermo-mechanical process for fabricating dies using steel H13 involves homogenization, hot forging, annealing, machining, quenching, and double tempering [86, 87]. The surface working temperature of dies is approximately 550 °C, which is close to the tempering temperature of die tools. The high-temperature operation induces continuous evolution that can significantly affect the mechanical properties of tools [88]. The microstructure and mechanical properties are influenced by the final thermal treatment, quenching and double tempering. The annealed steel H13 comprise a ferrite matrix with approximately 5% (volume fraction) of alloy carbides [86], which may contain VC, Mo_2C, Fe_3C, Cr_7C_3 and $(Fe,Cr)_{26}C_6$ [89, 90]. The critical function of the alloy carbides is to prevent coarsening of crystal grains, leading to a fine microstructure after quenching [91].

Inconel 718 is a high-strength, corrosion-resistant, nickel-based superalloy that is widely used in high-temperature applications. It is composed of mainly nickel, chromium, and iron, with smaller amounts of other elements such as molybdenum, niobium, and titanium. This alloy was originally developed for use in the aerospace sector, energetic industries such as oil and gas, power generation, and chemical processing, among others. Inconel 718 exhibits excellent mechanical properties at high temperatures, including high tensile, creep, and rupture strength, It also has good

resistance to corrosion and oxidation, making it suitable for use in harsh environments. Additionally, Inconel 718 can be easily welded and fabricated, which further contributes to its versatility and wide range of application [92, 93]. For example, Inconel 718 has been used as components of aircrafts engine, such airfoils, supporting structures of fuselage and critical rotating parts which contains more one third of total weight of a modern aircraft engine [94]. For the complex parts, the manufacture is inhibited by the high hardness and low thermal conductivity of Inconel 718 when taking traditional machining process. The microstructure of Inconel 718 is composed of fcc γ'-Ni(Al,Ti, Nb), ordered tetragonal γ''-Ni_3Nb and fcc (Nb,Ti)(C,N), among which present a large number of strengthening carbide and intermetallic phases around an fcc γ-(Al) matrix [95]. Among of them, γ''-Ni_3Nb and γ'-Ni(Al,Ti, Nb) are the mainly strengthening phases which are coherent with the fcc matrix γ-(Al). A special thermal treatment processes is often applied to maximize the phase of γ''-Ni_3Nb and γ'-Ni(Al,Ti, Nb) at nano-scale with levels of 16% and 4%, respectively [94]. However, the high temperature would lead to form Laves phase due to Niobium segregation, which is detrimental to the mechanical properties of strength, fatigue resistance, and creep rupture, because it consumes the main element which is necessary for precipitation strengthening and helps the initiation and propagation of cracks [96, 97]. Some undersigned closed-packed phases also might be appeared in the microstructure of Inconel 718, like hexagonal Laves which is $(Ni,Fe,Cr)_2(Nb,Mo,Ti)$, orthorhombic δ-$Ni_3(Nb,Ti)$ and tetragonal σ-CrFe phases suffered thermal treatment [93], as shown in **Figure 3-1**.

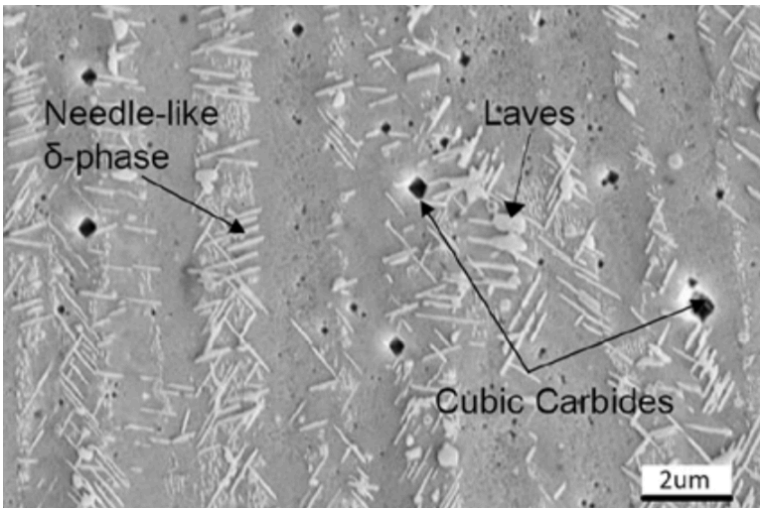

Figure 3-1. The main precipitation in Inconel 718 after selective laser melted (SLM) reproduced permission from [93].

Steel H13 and Inconel 718 are alloys with different base metals, namely Fe and Ni respectively. Given their applications, high-temperature performance is a critical factor, and there is still ample opportunity to improve their mechanical properties. Consequently, it is highly intriguing to investigate the evolution of the mechanical performance of the AlCrSiN quaternary coating deposited on them after thermal treatment. Such investigations could provide valuable insights into the efficacy of ceramic coatings in protecting these steels.

3.2 Hard substrate: cemented carbide (WC-Co)

Cemented carbide, also known as tungsten carbide, is a composite material consisting of tungsten carbide particles (WC) held together by a metallic binder, typically cobalt (Co), and sometimes additional elements like nickel (Ni). The tungsten carbide particles provide the material with high hardness, wear resistance, and strength, while the metallic binder helps to provide toughness and resistance to fracture. The combination of these properties makes cemented carbide a popular material for cutting tools, mining and drilling equipment, wear parts, and other applications that require high performance under extreme conditions [98, 99]. The production of cemented carbide involves powder metallurgy techniques, including mixing, compacting, sintering, and sometimes additional processing steps such as grinding or coating. The resulting material can be shaped into a wide range of forms, including insets, tips, rods and blanks, and can be used in various industries, including automotive, aerospace, and medical [18].

The microstructure of cemented carbides typically consists of tungsten carbide (WC) particles held together by a metallic binder phase, usually cobalt (Co). The tungsten carbide particles are typically in the form of hexagonal crystals and can have grain sizes ranging from a few nanometers to several microns. The metallic binder phase fills in the gap between the tungsten carbide particle provides toughness and resistance to fracture. The binder phase also contributes to the electrical and thermal conductivity of the material. Depending on the application, other elements may be added to the binder phase, such as nickel (Ni) or chromium (Cr), to enhance specific properties. An image of microstructure and 3dD tomography obtained by FIB/SEM is shown in **Figure 3-2**.

During the production of cemented carbides, the powder mixture of tungsten carbide and binder materials is compacted and then sintered at high temperature, typically in the range of 1300- 1500 °C. During the sintering process, the tungsten carbide particles bond with the metallic binder phase, resulting in a dense and homogeneous

microstructure [100]. The microstructure of cemented carbides can be further modified through additional processing steps, such as heat treatment or surface coating. For example, heat treatment can be used to enhance the grain growth of the tungsten carbide particles, resulting in improved wear resistance, A surface coating further improves hardness, wear resistance, and corrosion resistance of the material. The images of microstructure and 3D tomography obtained by FIB/SEM is shown in **Figure 3-2.**

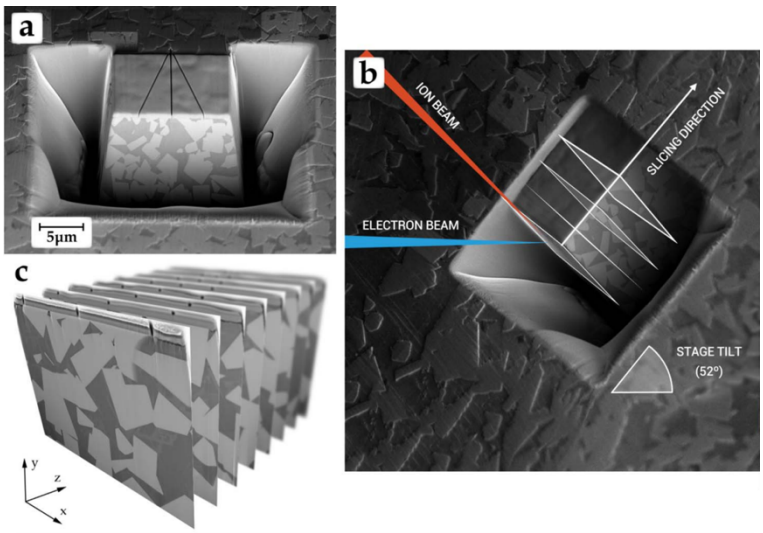

Figure 3-2. Images of typical microstructure of cemented carbide (WC-Co) by means of FIB/SEM 3D reconstruction. The light grey grain are tungsten carbide grains (WC) and the dark areas are cobalt binder (Co) reproduced with permission from [101].

Initially developed a century ago [102], cemented carbides have found increasingly widespread use in various fields [103, 104]. As shown in **Figure 3-3**,the areas where cemented carbides are extensively employed due to their high consumption have been analyzed. The analysis reveals that the largest area of consumption, approximately 36%, is for general wear parts. The oil and gas industry are the second-largest area of consumption, accounting for around 14%. The automotive and aerospace and defense sectors have similar shares of consumption, accounting for about 13%. In contrast, the consumption of cemented carbides in the mining, construction, and electronics sectors is relatively low, accounting for approximately 10% and 7%, respectively.

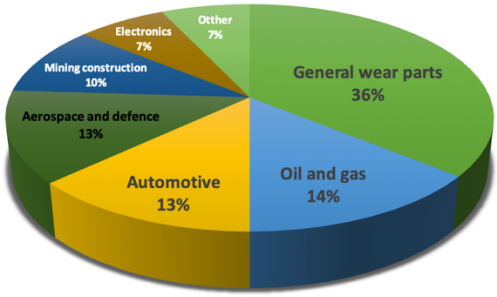

Figure 3-3. Distribution of applied areas of cemented carbide plotted after reference reproduced permission from [105].

The primary constituents of cemented carbide are WC grains and cobalt binder [106]. WC grains are the major composition of cemented carbides and contribute to their outstanding strength, hardness and wear resistance. Over 98% of cemented carbide grades contain WC, with tungsten monocarbide being the most important [16]. The grain size of WC particles ranges from several hundred nanometers to several micrometers, which significantly affect the mechanical properties of hardmetals and determine their application areas [18]. For instance, grain size less than 1μm are suitable for lighter roughing cuts due to their hardness, while sizes between 1μm and 6 μm are used for heavier rough cuts, owing to the tradeoff between hardness and toughness induced by larger grain size. When the grain size exceeds 6 μm, cemented carbide can be used as molding tools rather than cutting tools, because of their much higher toughness.

Cobalt is the most commonly used binder due to its strong chemical bonding with tungsten carbide, resulting in excellent adhesion and low interface energy at the solid solution boundary [107]. However, the high cost and negative effects on environment and health impact of cobalt necessitate the exploration of alternative metallic binders from the iron group, such as Fe and Ni, to overcome Co's limitations while maintaining good wettability with tungsten carbide particles. Substituting a portion of Co metal binder with Ni can improve the corrosion and oxidation resistance of cemented carbide [108]. However, a Fe-rich layer may result in higher hardness, wear resistance and toughness compared to pure Co binder of cemented carbide [109].

Various technologies have been developed to enhance the mechanical properties of WC-Co, an important material for cutting tools, such as coating it with AlCrSiN quaternary coatings. To serve different applications, coating-substrate systems require good adhesion, making surface modification a suitable approach to improve the properties of the interface.

3.3 Superhard substrate: cubic boron nitride (cBN)

Compared to diamond tools, polycrystalline cubic boron nitride (PcBN) are capable of machining hard steels and grey cast irons without chemical reactions occurring during machining process. PcBN materials are composed of cBN crystals together with a second phase. The properties of PcBN materials are determined by the synergy between cBN content and binder phase. PcBN tools are mostly employed for machining hardened steels and provide a more cost-effective alternative to traditional grinding procedure [43, 110, 111]. Hence, cBN is the preferred choice for the manufacture of cutting tools for hard materials, which are sintered at high temperature and pressure conditions to form complex compacts. Based on the amount of cBN phase, sintered cBN compacts are classified as "low" (50% cBN phase) or "high" (80-90% cBN phase). The different content of cBN grains in these compacts makes them suitable for various industrial applications. Low cBN compacts are used in turning tools to machine hardened steels and bearing steels, whereas high cBN compacts are used as cutting tools to process cast iron at high speeds [112].

High cBN compacts are typically made using hBN micron powders and binder powders. At a temperature of 2150 °C and pressure of 7.7 GPa, the hexagonal phase of boron nitride is transformed into the cubic phase to form translucent cBN [113]. This phase has a very small tendency to revert back to hBN even under high temperature, making it advantageous for using in cutting tools for machining ferrous materials [22]. Binders are often chosen from ceramic phases such as metal-carbide, metal-nitride and oxide, with titanium-based compounds like TiN and TiCN frequently used in combination with cBN. For example, a low cBN compact may be composed of 50% TiN binder and 50% cBN phase, along with a small amount of AlN and other aluminum-based compounds [112]. Other metal elements, such as Al, may be added into the raw mixture to increase sintering efficiency and react with excess oxygen at high temperature and pressures [22]. The SEM images of high and low cBN compacts are shown in **Figure 3-4**.

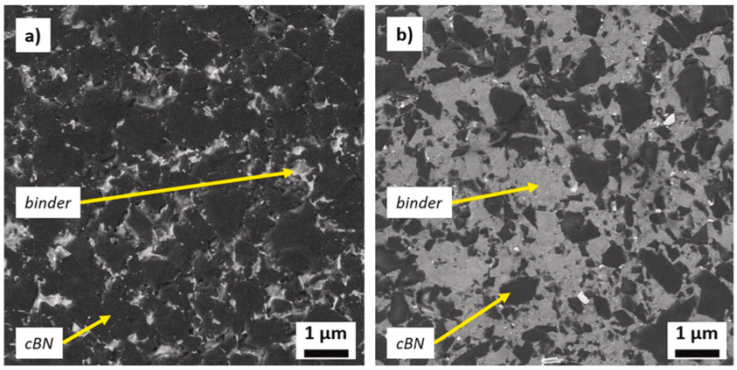

Figure 3-4. Micrographs of the structure of (a) high cBN compacts and (b) low cBN compacts reproduced permission from [43].

4 Ion implantation

4.1 Ion implantation

Ion implantation is a surface modification technique used to alter the physical and chemical properties of coatings. It involves the bombardment of a material surface with a beam of high-energy ions (typically from a plasma source) which penetrate the surface and embed themselves into the bulk material. The implanted ions can induce various effects, such as creating lattice defects, changing the material's composition, and altering its mechanical, electrical, or optical properties. This technique is widely used in various fields, such as semiconductor technology, materials science, and biomedical engineering, to improve the performance and functionality of materials, as well as hard ceramic coatings [44, 45].

The energies of ions are accelerated in the range of tens of kV and injected into a surface and stop at a profile with several hundred nanometers of depth, which is named as implanted zone (IZ) and is relatively shallow. In addition the implantation affected zone (IAZ) presents potentially beneficial work-hardening effects, which extend the depths of the order of microns and responsible of the long effect of ion implantation [44]. The work-hardening effects at IAZ are due to a dense and tangled dislocation network developed after ion implantation. However, in IZ, a structurally inhomogeneous and thin alloyed area is induced by ion implantation, and the elastic modulus and the work-hardening of materials is different from other areas. Therefore, in the interfacial area between the IZ and areas without ion implantation may exist residual stresses. Because of the less local stress of IAZ compared with the yield stress, dislocation are driven out into IAZ when the stress is up to the amplitude and overplus the local yield stress. Therefore, it produces a sublayer of IAZ containing a high density of dislocation and a work hardening zone [114, 115].

4.2 Ion implantation on hard coatings

Zirconium (Zr) ion implantation has been shown to improve the corrosion resistance of titanium nitride (TiN) coatings by forming a surface layer of ZrN and TiZrN detected

by X-ray photoelectron spectroscopy (XPS) chemical analysis [116]. The implanted Zr ions can partially or completely close pin-holes, inhibiting or delaying the arrival of electrolytes at the substrate, the enhancing the protection against corrosive medium. High energy titanium (Ti) ions were implantation into TiAlN coatings deposited on tungsten carbide-cobalt (WC-Co) substrate has also been investigated to improve adhesion strength and turning performance [117] . The improved performance is attributed to the formation of TiC alloy phase, which improves the hardness and resistance to plastic deformation. Additionally, a gradient layer was formed between coating and substrate, which reduced stress and eliminated the sharp interface. In another study, molybdenum and carbon ion implantation into CrAlSiN coatings resulted in an oxide top layer composed of MoO_2, Cr_2O_3, and Al_2O_3 that improved the high temperature wettability of the coatings [118]. This top layer effectively resisted interfacial diffusion between the coating and glass.

5 Objectives and thesis outline

Coatings are widely used in various industries, and with advancement of science and technology, the demands for the mechanical properties of materials have continued to rise. The improvement of both hardness and toughness, as well as the extension of service life and predictable lifespan, have become the focus of research in the field [68, 119, 120]. Inorganic multilayer coatings are widely applied in wear-resistant, hard, and metal materials [121, 122]. Recently, new quaternary AlCrSiN coatings have been developed with improved performance. Two main routes to improve mechanical performance are through the control of microstructure and gran size, and the use of multilayered coatings [123-125].

However, there is still a lack of understanding on the premature failure of coated hard materials. This is partly due to the fragmentation of research in the fields of coatings, hard materials, and numerical simulation. Often, the properties of the film itself are characterized without integrating the substrate in that characterization [123-125]. In actual operation, the performance of the tools is a direct consequence of the interaction between the coating and substrate under mechanical loads. Failure analysis based on the behaviour of bulk materials can also be problematic, as extrinsic flaws produced on the surface during use or modification of the material by coating deposition can be the cause of premature fracture. Moreover, it is necessary to understand the evolution of the mechanical properties after the material has undergone in-service use, particular after thermomechanical loads, as the microstructure of the coatings and substrate may have undergone relevant changes.

Based on the above motivation, the main objective of this thesis is to study the mechanical performance of PVD AlCrSiN coatings systems at micro-nano length scales on different substrates and under different ionic treatments.

Within this context, the main objectives of this doctoral thesis are:

1) To assess the mechanical properties of coatings by nanoindentation and to relate the obtained results with the microstructure of the coatings
2) To characterize the response of the coating/substrate systems by contact loads with different mode of monotonic and cyclic at different lengths. Special

attention will be devoted to the adhesion and the interaction between substrate and coating

3) To characterize the position and mode of fracture of coatings by micro-samples milled by FIB
4) To determine the possible change of mechanical properties of coatings after thermomechanical loadings (thermal shock and tribomechanical loads)

In order to understand the effect of the different substrates, the results of thesis have been divided in three chapters corresponding to three different papers (already published or in submission), with the aim of achieving the specific objectives of:

① To investigate the effect of thermal treatments on the mechanical properties of AlCrSiN and AlTiSiN coatings deposited on two different soft substrates, steel and Inconel.

② To compare the mechanical response of AlCrSiN quaternary coating deposited on two different hard substrates, WC-Co and cBN substrates, with objective of understanding the mechanical performance of the coated materials.

③ To investigate the effect of Zr and Ta ion implantation on the mechanics of AlCrSiN quaternary coating deposited on WC-Co substrate.

Samples had been provided by the Asociación Industrial Navarra (AIN) and ionic implantation will be done by EURECAT within the framework of the project "Enhanced performance (corrosion and mechanical integrity) of hard material substrates by means of PVD AlCrSiN coatings and ion implantation" PGC2018-096855-B-C41 sponsored by the Ministry of Science, Innovation and Universities. Samples will be coated on three substrates: Tool Steel, hard metal and cBN. Different deposition parameters will be tested to generate different microstructures. Both monolithic samples and multi-layered AlCrSiN/AlCrON coatings will be produced.

The layout of this doctoral thesis is schematically illustrated in **Figure 5-1**. According to it, the introduction of the doctoral thesis is in **Chapter 1**, a brief description of AlCrSiN quaternary coating and three different kinds of substrates is given in **Chapter 2** and **3** respectively. The technique of surface modification, ion implantation, is presented and reviewed separately in **Chapter 4**. **Chapter 5** describes the research objectives and scope. Experimental details and methodologies are presented in **Chapter 6**, including the parameter of the coating deformation, information of substrates, microstructure, analysis of chemical bonds and mechanical characterization techniques used for producing contact damages at micro and submicro length scales, and inspecting damages at surface and subsurface levels. The direct outcomes of this doctoral thesis are published or in process of being published as three papers which are

presented in **Chapter 7**, where the results and the discussion of them are presented. General conclusion of this thesis and expectations for future work are summarized in **Chapter 8**.

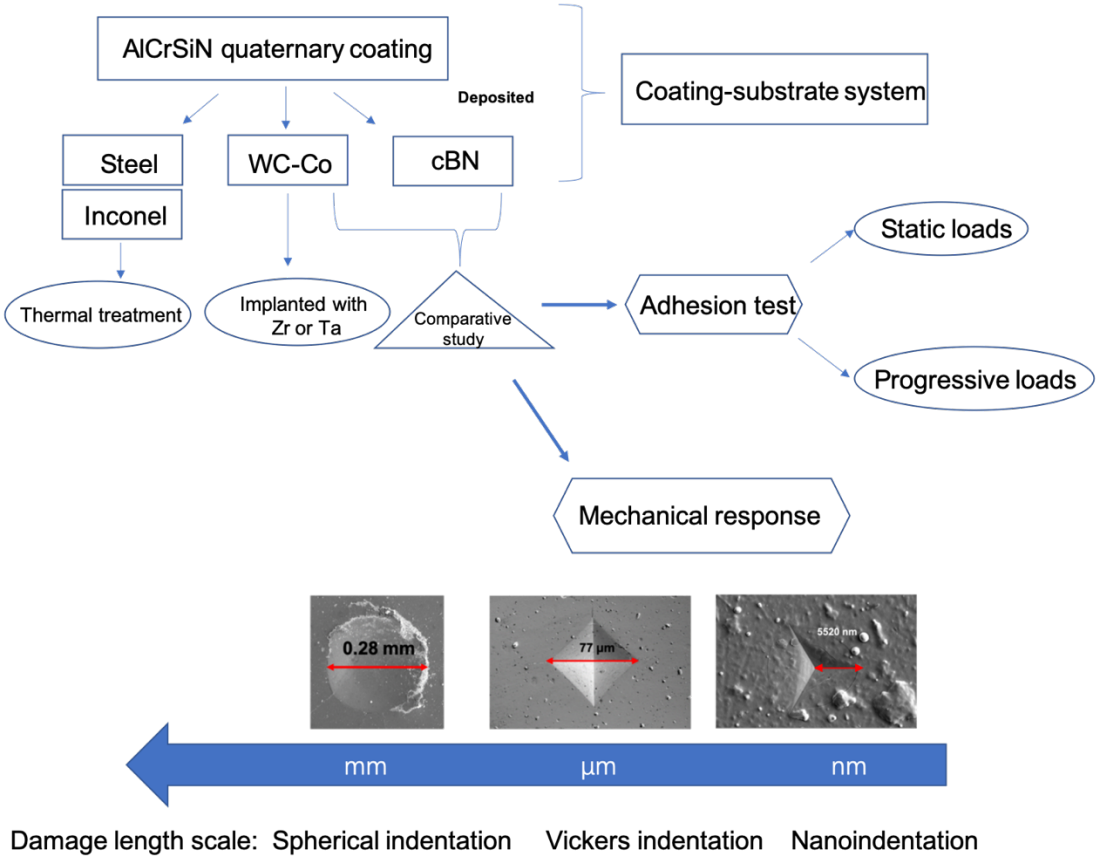

Figure 5-1. The schematic layout of this doctoral thesis.

6 Experimental techniques

6.1 X-ray diffraction (XRD)

X-ray diffraction technique (XRD) is a technique to study the crystalline structure of materials. It works by directing a beam of X-rays at a sample, which causes the atoms in the sample to diffract the X-rays in specific directions depending on their arrangement in the crystal lattice. By analyzing the pattern of diffracted X-rays, the crystal structure of the material, including information about its unit cell dimensions, symmetry, and orientation can be determined. XRD is a widely used analytical tool in materials science, chemistry, and physics for studying the properties of crystalline materials, such as minerals, metals, ceramics, and polymers.
The traditional θ - 2θ reflection geometry, as shown in **Figure 6-1 (a)**, consist in emiting X-rays from the device, whereby the incidence angle is equal to the scattered angle with the sample surface. The intensity of collected scattered X-ray is analyzed with specific software (like MDI JADE, SearchMatch) and plotted as a function of scatter angle. By comparing with the standard cards, the location, size, and intensity of the scattered angle are used to obtain the phase and structure of materials. However, conventional XRD typically incides at relative larger angle into the surface of samples, which can be several hundred micrometers, much greater than the thickness of thin coatings. Thus, conventional XRD is more suitable for analyzing bulk samples rather than shallow coatings [126].

Grazing incidence X-ray diffraction (GIXRD) has been developed to overcome the limitations of conventional XRD and improve the sensitivity to the near surface areas of samples while minimizing the effect of substrate on the diffraction response [127]. The main difference between GIXRD and conventional XRD is the use of "asymmetric diffraction", which allows for a small depth into the sample surface by changing the incidence angle. In GIXRD, a group of parallel X-ray beams is directed towards the sample surface at a fixed and low angle，α (usually smaller than 10°), and then the diffraction X-ray beams are only collected by the detector, as illustrated in **Figure 6-1 (b)** [126].

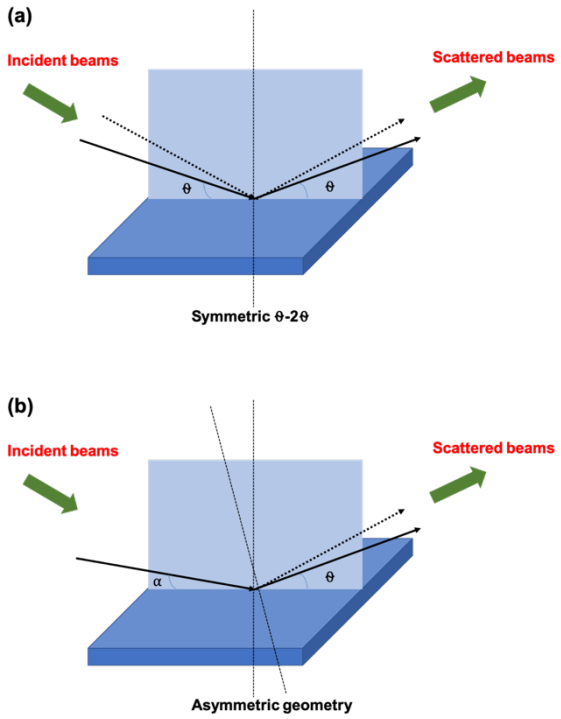

Figure 6-1. Scheme of (a) conventional XRD with symmetric θ - 2θ geometry and (b) grazing incidence XRD with asymmetric geometry.

6.2 X-ray photoelectron spectroscopy

X-ray photoelectron spectroscopy (XPS) is a surface-sensitive analytical technique used to identify and quantify the chemical composition of surfaces. In XPS, a material is exposed to a beam of X-rays which causes electrons from the material's surface to be ejected. The ejected electrons are then collected and analyzed by a detector to determine the kinetic energy and number of electrons ejected.

The kinetic energy of the ejected electrons is directly proportional to the binding energy of the electrons in the material. By measuring the kinetic energy of the ejected electrons, XPS can determine the binding energies of the electrons in the sample, which can be used to identify the elements present in the surface.

The number of electrons ejected from the surface is also related to the number of atoms of each element in the surface. Therefore, XPS can also provide quantitative information about the composition of the surface.

XPS can also provide information about the chemical state of the elements present on the surface. This is because different chemical states of an element will have different binding energies for their electrons. By measuring the binding energies of the ejected electrons, XPS can determine the chemical state of the elements in the surface.

XPS is a powerful tool for the analysis of surfaces because it can detect and quantify the elements present on the surface with a high level of sensitivity (down to about 0.1% atomic concentration), and it can provide information about the chemical state of the surface. XPS is commonly used in materials science, surface science, and other fields where the surface properties of materials are important.

An anode of Al or Mg, with 1253 eV and 1457 eV respectively, is often used [128-130]. The spectrum is plotted as the number of detected electrons per energy interval versus their kinetic energy and is unique for every element. The peaks of spectrum of the individual constituent were approximately summed up to form the spectrum of the mixture of elements. Due to the very small mean free path of electron in solid materials the electrons only can be detected originate from the few atoms of top layers, which lead to XPS be a surface sensitive technique for chemical analysis. Quantitative data could be analyzed by the heights and areas of peaks, and the determination of chemical bonding always is obtained from the exact position and deconvolution of peaks and also certain spectrum features.

6.3 Contact mechanics

Over the last few decades, various testing techniques have been prevalent in the assessment of the mechanical response of ceramic coatings on different substrates under contact loading [131-135].

Nanoindentation is widely used method for measuring the mechanical properties of ceramic coatings. It involves pressing a indenter tip of known geometry and size into the coating surface under a controlled load, and measuring thee resulting deformation. From this, various mechanical properties such as hardness, elastic modulus, and the fracture toughness can be calculated.

Scratching testing is another method used to evaluate the mechanical response of ceramic coatings. It involves dragging a sharp stylus across the coating surface under a constant load, and measuring the resulting damage, such as cracks or delamination. The

critical load at which failure occurs can be used to calculate the coating's adhesive strength.

Hertzian spherical indentation is a method that involves pressing a spherical indenter into the coating surface under a controlled load, and the measuring the resulting deformation. This method is particularly useful for evaluating the fracture toughness of brittle materials, as it allows for the calculation of the critical load required to initiate cracking.

6.3.1 Calowear

Calowear is an instrument utilized for measuring the wear rate of coatings with thickness on a micrometer scale. The apparatus involves a grinding ball with a precisely known radius that is rotated and exerts pressure on the coated sample. Throughout the test, the pressure applied and the relative position of the grinding ball to the sample is maintained constant. The interaction between the diamond particle slurry and relative motion of the grinding ball and the sample gradually wears away the surface of the sample, producing a spherical crown-shaped pit. Following this, the geometric parameters of the projected area of the coating and the base section of the wear pit are determined using metallographic microscopy observations. Using a simple geometric formula, the thickness (D) of the coating can be calculated once the length of X and Y are determined. The calowear instrument is widely utilized for testing the thickness of coatings with high accuracy [136].

6.3.2 Nanoindentation

Nanoindentation is a technique used to evaluate the mechanical properties of materials at the nanoscale. It involves using a small, sharp indenter (usually made of diamond) to apply a controlled force on the surface of a sample, and then measuring the resulting depth of indentation. By analyzing the load-displacement curve generated during the indentation process, various mechanical properties of the material such as hardness, elastic modulus, and toughness can be determined.

The basic principle of nanoindentation is similar to that of traditional indentation testing, but with much smaller forces and depths involve. The size of the indentation is typically on the order of nanometers, and the applied forces range from a few micro-Newtons to tens of mili-Newtons. The technique is especially useful for evaluating the mechanical

properties of thin films and coatings, where the thickness is comparable to or smaller than the size of the indenter used.

Nanoindentation has become a widely used tool in materials science, with applications ranging from fundamental research to industrial quality control. Some of the specific areas of research where nanoindentation is used include the study of deformation mechanisms in metals, characterization of biomaterials and soft matter, and evaluation of the mechanical properties of thin film and coatings [137].

The cross-section of an nanoindentation is shown in **Figure 6-2**, where the parameters used in after analysis can be easily defined.

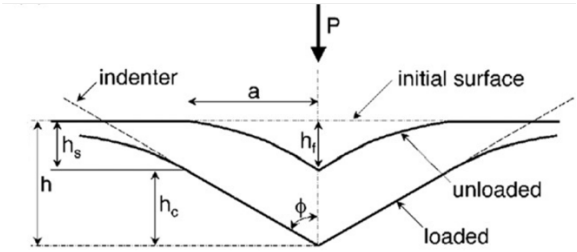

Figure 6-2. Scheme of the cross-section of nanoindentation [138].

The calculation of the mechanical properties of the material, such as hardness and elastic modulus can be conducted by analyzing the load (P)-displacement (h) curves based on the work of Oliver and Pharr [139, 140].
The method is based on calculating the elastic unloading stiffness after fitting the unloading curve with a power law relation:

$$P = \alpha(h - h_f)^m \qquad (1)$$

where α and m are fitting parameters, and h_f is the final depth. And S is stiffness which calculated by

$$S = \frac{dP}{dh}\Big| h_{max} \qquad (2)$$

In order to obtain h_c , the residual depth on the surface after loading (h_s) needs to be determined as shown in **Figure 6-2**, which varied geometry constant (ε) as,

$$h_c = h_{max} - \varepsilon \cdot \frac{P_{max}}{S} \qquad (3)$$

Where S is the stiffness.
When knowing the contact depth, the contact area *A(hc)* can be calculated. But it is not a universal or constant value and depends on the geometry of the indenter used. In nanoindentation testing of thesis doctoral thesis, a three-side Berkovich indenter was

used. Reason for this is because Berkovich indenter ends in a single point which avoids to possibly end in a vertex for four-side pyramids when suffered not perfectly manufactured and lend to not be at nanometric level. The hardness and Young's modulus are calculated as:

According to the $A(h_c)$, the hardness is calculated by:

$$H = \frac{P_{max}}{A(h_c)} \qquad (4).$$

It is possible to determine at the same time the elastic modulus (E), by using Nanoindentation technique, following the well know Oliver and Pharr method [139], following Equation (4).

$$E = \frac{\sqrt{\pi}}{2\beta} \cdot \frac{S}{\sqrt{A(h_c)}} \qquad (5)$$

where β is a correction factor (usually 1.034).

The assays of nanoindentation were conducted with a Berkovich diamond tip calibrated against a fused silica standard. The Oliver and Pharr method was used to calculated the hardness and elastic modulus using the load-displacement data recorded by the instrument, as shown in **Figure 6-3**.

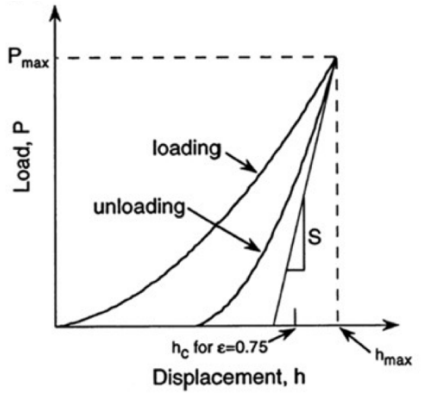

Figure 6-3. Scheme of a load-displacement curve and highlighting key experimental parameters reproduced permission from [138].

An MTS nanoindenter XP equipped with continuous stiffness measurement, as shown in **Figure 6-4** was used. Before nanoindentation, surfaces of all samples were smoothly polished by colloidal silica and then cleaned with acetone to reduce the effect of the roughness of coating during the measurement [140].

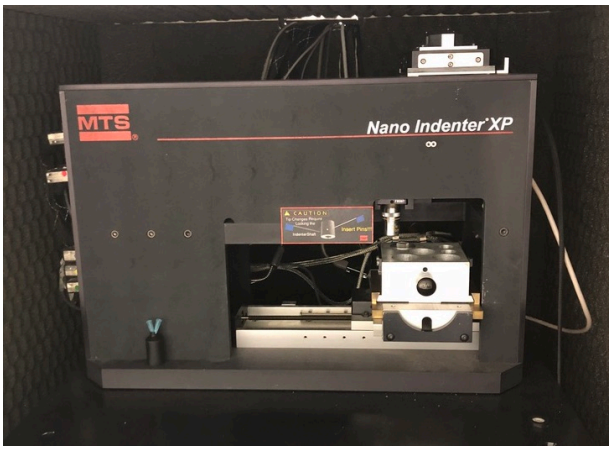

Figure 6-4. Picture of MTS nanoindenter XP.

6.3.3 Vickers indentation

Vickers indentation is a type of indentation hardness test that is commonly used to measure the hardness of materials [141]. It involves pressing a diamond pyramid-shaped indenter into the surface of a material and measuring the dimensions of the resulting indentation. The Vickers hardness value is then calculated based on the size of indentation and the applied load.

The Vickers indenter consists of a square-based pyramid with an angle of 136 degrees between opposite faces. A typical Vickers indentation test involves applying a load of between 1 kg and 120 kg for 10 to 15 seconds to the surface of the material being tested. The size of the resulting indentation is typically measured using a microscope or other optical imaging system. The Vickers hardness value is then calculated based on the area of the indentation.

Vickers indentation is often used to measure the hardness of ceramics, glasses, and other brittle materials that cannot be easily tested using other methods. It can also be used to measure the hardness of thin films and coatings, as well as the hardness of individual phases within a composite material.

In addition, Vickers (or other type of sharp indenters) can be used to estimate fracture toughness by the Indentation Microfracture Test (IMFT). Fracture toughness is a measure of a material's resistance to fracture when a crack is present. It is an important property in the design and analysis of materials used in various engineering applications. One common method of measuring fracture toughness is by using the indentation technique.

The indentation technique for measuring fracture toughness involves creating a small crack at the edge of an indentation made in the material's surface. The size and shape of the indentation are carefully controlled to ensure that the crack grows in a controlled manner. The size of the resulting crack is then measured, and the fracture toughness of the material can be calculated using mathematical models.

The indentation microfracture test has several advantages over traditional fracture toughness tests, such as the three-point bending test. It is faster, requires smaller samples, and can be used on a wider range of materials, including ceramics and brittle materials. However, there are also limitations to this technique, including the need for careful control of the indentation parameters and the assumptions made in the mathematical models. Consequently, this method can be used to estimate fracture toughness, but special care has to be taken to produce quantitative measurements [142-144].

In case of cemented carbides, the most widely used model for analyzing the indentation microfracture test is the Palmqvist crack model. The Palmqvist crack model assumes that the crack in the material is a penny-shaped crack with a semi-circular shape. By measuring the length of the crack, the geometry of the indentation, and the hardness of the material, the fracture toughness can be calculated using equations derived from the Palmquist model [142], as shown in **Figure 6-5**.

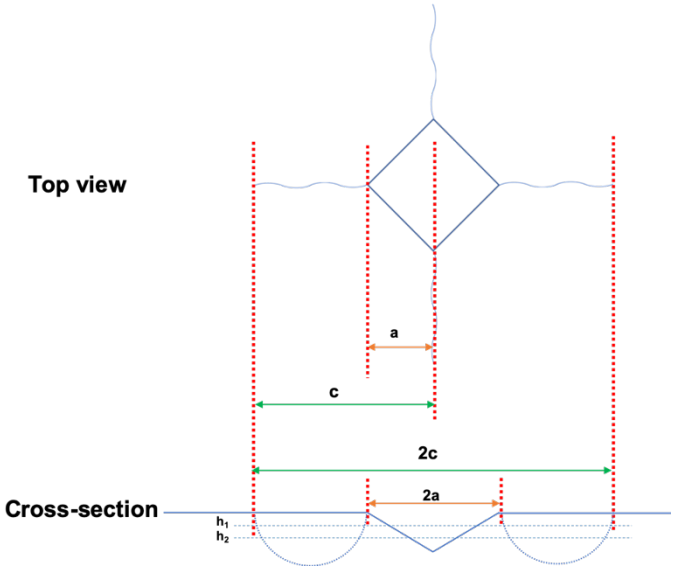

Figure 6-5. Schematically illustrating the Palmquist mode form the top view and the cross-section of contact damage induced by Vickers indenter reproduced permission from [145].

In this doctoral thesis, the Vickers Testwell FV-700 was applied to conducted the Vickers indentation.

6.3.4 Hertzian spherical indentation

Hertzian spherical indentation is a technique used to measure the mechanical properties of materials by applying a known force to a spherical indenter pressed onto the surface of a material. This method is based on the theory of Hertzian contact which describes the deformation of an elastic half-space by a spherical indenter.

In this technique, a spherical indenter of known radius is pressed onto the surface of the material under a known load. The resulting indentation is analyzed to determine the contact area, which is used to calculate the contact stress. These equations shown that, when a sphere of radius *R* is pressed against a flat solid, the relationship between the contact radius (*a*) and the load (*P*) was shown in Equations (6):

$$a^3 = \frac{3}{4} \cdot \frac{PR}{E_{eff}} \qquad (6)$$

Where E_{eff} is effective elastic modulus of the material can be calculated by:

$$\frac{1}{E_{eff}} = \frac{1-v^2}{E} + \frac{1+v_i^2}{E_i} \qquad (7)$$

Where *E* and υ denotes the elastic modulus and Poisson's ratio. The subindex *i* denotes the elastic mechanical properties of the diamond indenter, being 1141 GPa and 0.07 respectively [139].

$$E_{eff} = \frac{1}{1.034} \cdot S \cdot \frac{\sqrt{\pi}}{2} \cdot \frac{1}{\sqrt{A}} \qquad (8)$$

The mean pressure between the material and indenter (p_0)is plotted against a/R,

$$p_0 = \frac{P}{\pi a^2} = \frac{4E_{eff}}{3\pi}\left(\frac{a}{R}\right) \qquad (9)$$

The stress-strain contact relationship could be displayed, the maximum tensile stress (σ_m) is:

$$\sigma_m = \frac{1}{2}(1-2\upsilon)p_0 \qquad (10)$$

And the maximum shear stress is calculated by

$$\tau_m = 0.46p_0 \qquad (11)$$

The Hertzian spherical indentation technique has been widely used to measure the mechanical properties of a variety of materials, including metals, ceramics, polymers, and composites. It is a relatively simple and inexpensive method compared to other mechanical testing techniques, such as tensile and compression testing.

The experimental configuration of Hertzian spherical [146] indentation involves a polished and flat surface of studied AlCrSiN coating deposited on different substrates with a spherical hardmetal indenter at a series of given loads, as shown in **Figure 6-6**. The concentrated stresses induced during the process of spherical indentation are delivered and simulated the blunt conditions in actual service. Then, the mechanical response and integrity of coated materials would be evaluated based on the damage scenarios relative with the increasing loads and different modes of loading.

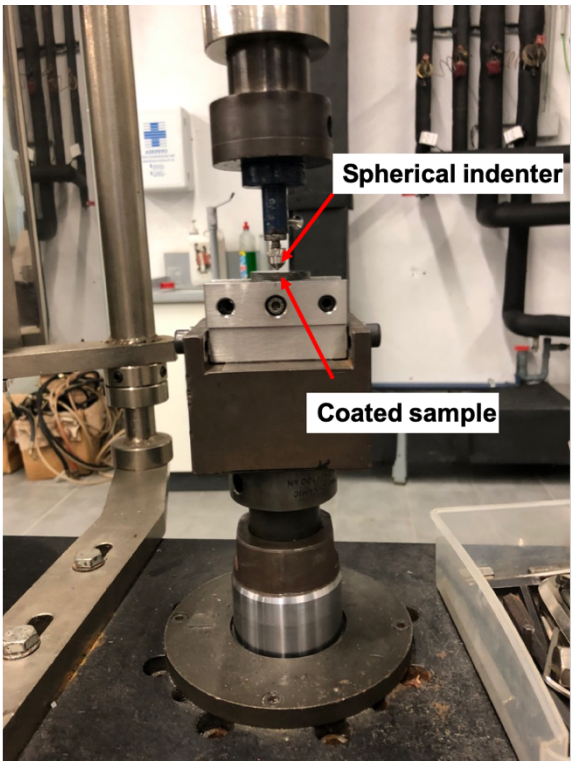

Figure 6-6. Typical configuration of a Hertzian spherical indentation (Instron 8500) on coated sample.

According to Hertzian theory test protocols have been adopted as a successful method for evaluating the mechanical response and damages induced by contact loadings of coated materials [147-150], which is based on the experimental methodology and analysis process induced and widely developed by B.R.Lawn for researching the contact damage of ceramic materials under spherical indentation [146, 151]. In these studies, cemented carbide sphere with millimeter length scale of curvature radius. Therefore, concentrated stresses induced by spherical indenter with monotonic normal contact loads are delivered to simulate the blunt shape impact in actual service conditions and the evolution of damage associated with increasing loads. Once the

plastic plow emerged in the substrate due to the normal loads, the coating have to deform along with the substrate [152].

For coated materials failure scenarios observed on the surface includes two different types: (i) irreversible plastic deformation presented “sink in state” under comparatively lower loads, (ii) ring and lateral cracks formed outside the elastic contact regions and around the edge of plastic deformation areas under the monotonic contact loads elevated to the certain value, which could appear three shapes along with the increasing loads, discontinuous or partial cracks, single full ring cracks and multiple cracks, as shown in **Figure 6-7**. The various types of ring cracks are stimulated by the tensile stress and strain with radial direction around the residual indentation [153].

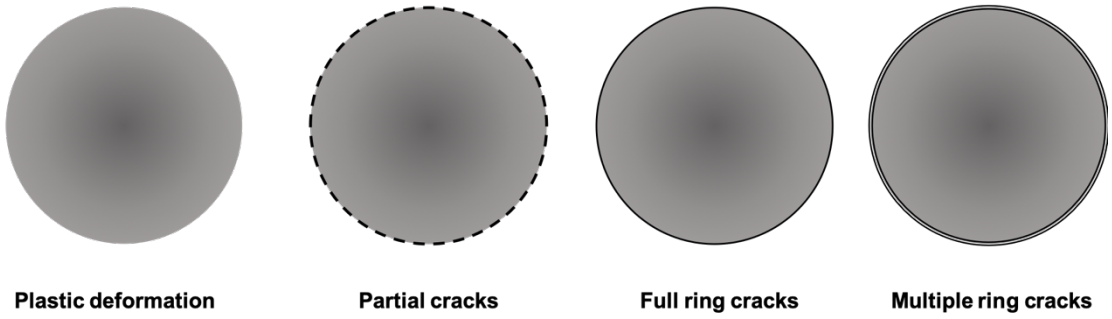

Figure 6-7. Scheme of contact damage of AlCrSiN coating deposited on hard substrates.

The generation of ring cracks extremely depend on the intrinsic properties of spherical indenter and coating, like the radius and the thickness respectively, together with the applied normal loads and the mechanical properties of both coating and substrate. The ring cracks appeared at the surface of coating mainly induced by tensile tresses, however, the reason for generation of lateral cracks is the plastic deformation of the substrate caused by normal loading and weak adhesion strength between coating and substrate [154-156]. Along with the increase of contact loading the removal of coatings like chipping would appear due to the generation of ring cracks caused by blunt indenter or spherical indenter. And another mechanism of removal is spallation of coatings induced by emergence of lateral cracks at the interface conducted by sharp indenter.

The mechanical response of coated materials under contact loading can be studied through two modes of loadings: monotonic and cyclic. Cyclic loading, also known as fatigue test, is necessary to meet the stringent tolerance of working conditions. The nature of cyclic contact loads play a critical role in the study of contact response. Therefore, the fatigue loading contact response can be extracted from indentation under monotonic contact loads, scratch parameters and established wear test techniques. This factor should be considered when designing, optimizing and selecting coating-substrate

systems [157]. Repetitive impacts on the surface of coated materials indicate the mechanical degradation. Typically, monotonic contact damage proceeds in three stages: initial plastic deformation, followed by cracking and chipping of coating or cohesive failure of coating, and finally spallation of coating or adhesive failure of coating at the interface between coating and substrate. The properties of both coating and substrate can affect the occurrence of degradation stages and fatigue susceptibility of relevant coating-substrate system.

Cyclic contact loading test are normally conducted with the critical monotonic contact load for full ring crack at the maximum cyclic load. The cyclic period of loading is executed by a sinusoidal waveform with a frequency of about 10 Hz as well as a corresponding load ratio of about 0.1. Choosing a range of values around below and above critical load as the maximum load of cyclic loading carried out fatigue test and the critical failure defined by the observation of full ring cracks. It is not same with the criteria of coating delamination which usually is used as a means for assessing the adhesion strength between coating and substrate of coated materials [158-160]. The main reason for choosing fracture of cohesive failures is because it is associated with the evolution damage under contact loading, therefore, it stands for the critical phenomenon from a design method according to “crack prevention” [161, 162].

Using spherical indenters with a blunt contact area is advantageous for studying the mechanical contact response of brittle coated materials, as it is well-suited for determining damage evolution at the micro scale and evaluating the fatigue susceptibility of coating-substrate systems. The properties of both the coating and substrate are critical in determining the contact response related to failure, and as such, different substrates have been coated with AlCrSiN quaternary coating in this doctoral thesis to study the fatigue susceptibility.

Contact damage tests were applied to determine the adhesion strength between coating and substrate under a series of constant normal loads, which prescribed by the VDI 3198 standard, and as a destructive quality method [163, 164]. A conical Rockwell C diamond indenter was pressed into the surface of coating-substrate system and then producing fracture and/or delamination of the coating and plastic deformation of the substrate. The scheme and principle of this test is shown in **Figure 6-8**. The mode of failure could be classified simply two categories: acceptable failure and unacceptable failure. The four different appearance of acceptable failure means the strong interfacial combination between coating and substrate namely good adhesion. On the other hand, the extensive delamination at the outer edge of indentation indicates a poor adhesion. The first sight of types and volumes of surface failure zone is the adhesion between

coating and substrate, and then the brittleness of coating [165]. The qualitative analysis of failure of coated materials is more effective under scanning electron microscopy than optical microscopy. In addition, radial cracks and small areas of delamination represent a strong adherent and brittle coating [166].

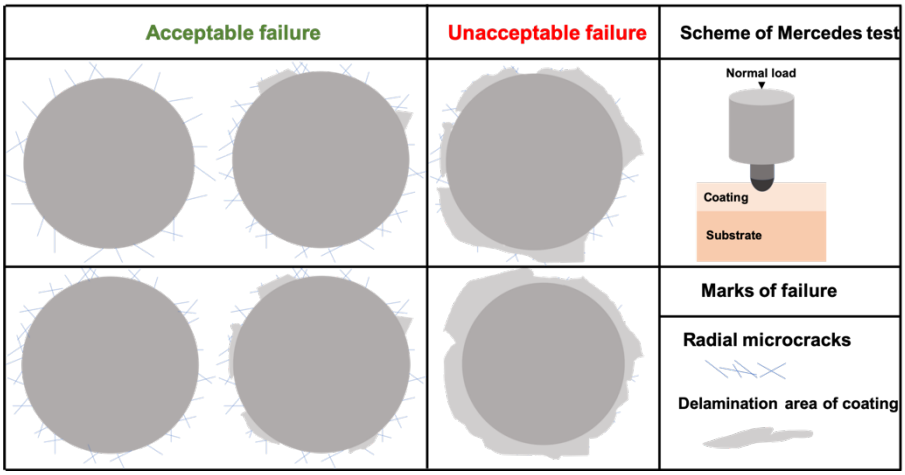

Figure 6-8. Scheme and principle of Mercedes test adapted from [164].

In this doctoral thesis, nine loads were chosen for different studies contents,9.8 N, 49 N, 98 N, 196 N, 294 N, 392 N, 498 N, 613 N and 980N to investigate the evolution of failure mode and further verify the adhesion strength between coating and substrate under different static normal loads.

6.3.5 Scratch test

Scratch tests are adopted to determine the practical adhesive strength and failure mode of hard and thin ceramic coatings deposited on metal and other hard substrates at room temperature. A diamond stylus with a defined geometry of Rockwell C is drawn across the surface of coated materials with a constant speed and a defined constant or progressive normal load through a defined length, which is a conical diamond tip with the apex angle of 120° and a spherical radius of 200 μm. The scheme of scratch test is shown in **Figure 6-9**. The contact damage along with the scratch track is evaluated as a function of the normal force applied under microscopy. Specific levels produced a specific level of damage on the surface of coatings are defined as a critical load. It also could provide the second test data, like tangential force and acoustic emission signals to determine different damage levels of coatings [167].

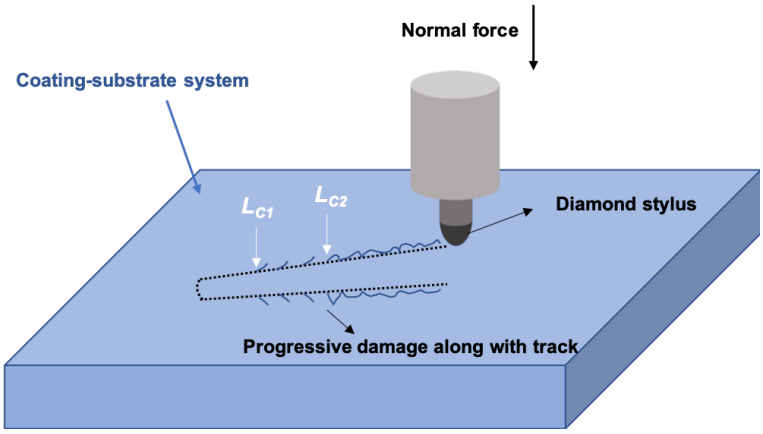

Figure 6-9. Scheme of scratch tests.

This test does not measure the fundamental adhesion strength between the coating and substrate, and just provide an engineering measurement of practical adhesion strength, which is determined by complicated interaction between the test parameters and the mechanical properties of coating-substrate systems. Therefore, it is very important to keep the same parameter, such as stylus geometry and properties, final loads, loading rate and displacement rate. In a comparative study, the thickness of all coatings is kept as consistent as possible.

In this doctoral thesis, scratch tests were performed in a CSM Revetest with progressive load from 0.9 N to 30 N, 120 N, 90 N for article I, article II and article III, at a constant loading rate of 10 N/min with a scratch length of 5 mm. The normal load is labelled as the first critical load (L_{C1}) which is caused the continuous cohesive failure of the coatings, like lateral cracks around the scratch track. And the second critical load is the normal load which induced the continuous and regular adhesive failure between coating and substrate, like spallation or delamination of coatings. Damage and failure induced by progressive loads were observed by Scanning electron microscopy (SEM) and further to make sure the position of emergence damage of the first and second critical loads.

6.4 Microscopy

Microscopy is a wide scope technical method to characterize the microstructure of samples and observe the features of deformation and damage scenarios suffered different modes of contact loads. In this doctoral thesis, optical microscopy, laser scanning confocal microscopy (LSCM) and field emission scanning electron

microscopy (SEM) together with a dual workstation of focused ion beam (FIB) to make the cross-section of interested areas were extensively employed.

6.4.1 Optical microscopy

An optical microscope is an optical instrument that uses optical principles to magnify and image small objects that cannot be distinguished by the human eye for people to extract more information of subtle structure, usually only seeing two-dimensional images.

The optical system of the microscope mainly includes four parts: an objective lens, an eyepiece, a mirror and a concentrator. From a broad scope speaking, illumination sources, filters, coverslips, and slides are also included.

6.4.2 Laser scanning confocal microscopy

The Confocal laser scanning microscope (CLSM) uses a laser as a scanning light source to scan the image point by point. When the focusing depth is different, images of different depth levels of the sample can be obtained. The image information is stored in the computer, and the three-dimensional structure of the cell sample can be displayed through computer analysis and simulation.The laser scanning confocal microscope can form a three-dimensional structure image of the sample by real-time scanning imaging of different layers of the same sample.

6.4.3 Field emission scanning electron microscopy (SEM) and focused ion beam (FIB)

Field emission scanning electron microscopy (FESEM) is a high-resolution imaging technique that uses an electron beam to produce images of a sample at a very high magnification. In contrast to conventional SEM, which uses a thermionic source to produce electrons, FESEM employs a field emission source that produces electrons by field-induced emission.

In an FESEM, the electron source consists of a sharp metal tip, typically made of tungsten or a similar material, that is held at a high electric potential. The tip is positioned very close to the sample, typically within a few millimetres, and a high voltage is applied between the tip and the sample. This electric field causes electrons

to be emitted from the tip, forming a beam that is focused onto the sample using electromagnetic lenses.

FESEM produces high-resolution images because the field emission source produce a very narrow electron beam with a small divergence angle. This allows for high spatial resolution and high magnification of the sample. The images produced by FESEM are also characterized by high contrast and high depth of field, allowing for the visualization of fine surface details and subsurface structures.

FESEM is used in a wide range of applications, including materials science, biology, and nanotechnology. It is commonly used to image and analyse surfaces and thin films, as well as to study the structure and composition of biological samples such as cells and tissues. FESEM can also be used in conjunction with other techniques, such as energy-dispersive X-ray spectroscopy (EDS), to analyse the elemental composition of a sample.

6.4.4 Focused ion beam (FIB)

A Focused Ion Beam (FIB) is a type of microscopy and nanofabrication technique that utilizes a beam of charges ions to remove, deposit or modify material at the nanoscale level.

In FIB, a beam of ions, typically gallium (Ga^+) or neon (Ne^+), is focused into a fine, high-energy stream and directed at the target material. The ion beam is focused using electromagnetic lenses and can be controlled with high precision, allowing for very precise and localized manipulation of the material.

One of the primary applications of FIB is in nanofabrication, by directing the ion beam to specific areas of a sample, material can be removed or deposited to create nanostructures or modify existing ones. This is useful in the fabrication of microchips and other electronic devices, where extremely precise feature are required. In addition to nanofabrication, FIB is also used extensively in materials science for imaging and analysis of materials at the nanoscale level. The high-energy ion beam can be used to sputter atoms from the surface of a sample, which can then be analyzed using techniques such as energy-dispersive X-ray spectroscopy (EDS) or secondary ion mass spectrometry (SIMS).

FIB can also be used in combination with other techniques, such as scanning electron microscopy (SEM), to create 3D images of materials with very high resolution. This is useful in fields such as biology and materials science, where understanding the structure and composition of materials at the nanoscale is important.

7 Results

The results are presented in three sections, corresponding three separate papers which stems from this doctoral thesis. The papers correspond to the mechanical response of AlCrSin quaternary coating:

(1) deposited on soft substrates of steel and Inconel compared with AlTiSiN quaternary coating. This paper is already published in “Materials”.
(2) deposited on two kinds of hard substrates of WC-Co and cBN comparatively. This paper is currently under submission.
(3) deposited on WC-Co hard substrate with Zr/Ta ion implantation. This paper is currently under submission.

7.1 Mechanical Performance of AlCrSiN and AlTiSiN Coatings on Inconel and Steel Substrates after Thermal Treatments

The objective of this study was to explore the mechanical properties of AlCrSiN and AlTiSiN coatings deposited on Inconel and steel substrates after thermal treatments of 500°C and 800°C. Nanoindentation was used to measure the hardness and elastic modulus of the coatings, and microindentation was used for observing the contact damage with Hertzian contact loadings. Microscratch and Mercedes tests were used to evaluate the adhesive strength between coating and substrate with both progressive and static loads, respectively. The surface damage was inspected by optical microscopy and scanning electron microscopy (SEM). Focus ion beams (FIB) were used to mill the cross-sections in order to detect the extent and mode of failure. The results show that AlCrSiN coatings and Inconel substrates exhibit better mechanical performance, even after thermal treatments.[1]

7.1.1 Introduction

Hard, protective coatings are frequently used in the tool industry due to their enhanced performance in wear and corrosion resistance. The first coatings used were TiN and CrN [53, 168-170], but the incorporation in their composition of other elements, such as Al and Si, has resulted in new ternary coatings demonstrating increased performance [171-173]. For example, the introduction of Si produces an amorphous Si_3N_4 phase at the nanometer scale, which inhibits the sliding movement between neighboring grains [67] and enhances hardness and thermal stability [174, 175]. However, tribocorrosion resistance is not optimal in these ternary coatings; therefore, the introduction of Al and Si to form quaternary coatings enhances the oxidation resistance and thermal stability of coatings via formation of an oxide-rich top layer [64-66]. Physical vapor deposition (PVD) for tool steel applied in various areas is a promising and effective technique to

[1] This chapter corresponds to the paper:

Liang, J., Almandoz, E., Ortiz-Membrado, L., Rodríguez, R., Fernández De Ara, J., Fuentes, G. G., Llanes, L., & Jiménez-Piqué, E. (2022). Mechanical Performance of AlCrSiN and AlTiSiN Coatings on Inconel and Steel Substrates after Thermal Treatments. *Materials*, *15*, 8605–8620. https://doi.org/10.3390/ma15238605

improve the mechanical performance and serving lives [68, 176-178]. These quaternary coatings consist of a metastable amorphous phase which is crystalized after thermal treatment into an fcc/wurtzite lattice with high atomic density, forming a coating with a columnar structure and high hardness [40, 179-182]. During operation, it is expected that these materials will suffer repetitive heating and cooling cycles with high temperatures reached in the coating of tool materials [183, 184]. Therefore, it is important to understand the evolution of the mechanical properties of these coatings with thermal cycles, similar to those suffered in service. Understanding the evolution of mechanical properties has direct implications in enhancing the reliability of coated tool materials.

However, it is also important to understand that the performance of the tools is not only governed by the coating; the substrate also plays a relevant role in the deformation and fracture of the surface. Currently, most of the literature on mechanical performance of the quaternary coatings and multilayers only concentrates on the coating itself, ignoring the synergic effect with the substrate [185-187]. The tribological performance, oxidation resistance, and thermal stability of quaternary coating have been studied in several prior studies [38, 123, 188-190]; however, there is scarce information on the evolution of mechanical properties with thermal treatments. It is worth mentioning that those coating/substrate systems will undergo thermal cycles during operation, and it is relevant to understand the evolution of the mechanical properties under such cycles. In this sense, Liu et al. [38] observed the evolution of hardness after the thermal treatment of AlCrSiN and AlTiSiN coatings on stainless steel, reporting a decrease in the values after thermal treatment of 600 °C [39, 40, 60]. However, they did not report any adhesion testing.

In summary, there is not much information on the mechanical evolution of these systems with thermal treatments, and there are no reports on coating–substrate adhesion. Scarce information is reported about the evolution of mechanical performance after thermal treatments when AlCrSiN and AlTiSiN quaternary coatings deposited on two kinds of cutting tool substrates. In this sense, adhesion and fracture is a combination of the mechanical performance of both the coating and the substrate under these special conditions. Although these tool materials are designed to work at intermediate temperatures (500 °C), they may suffer occasional high temperature peaks at critical work points. At high temperature, the mechanical properties of the substrates also change. Both steel and Inconel suffer softening, due to grain growth and change in the topology of the precipitates [191, 192]. In this sense, both types of materials usually

require surface treatments to complement their bulk properties to yield good performance in service. Due to the different natures of their chemical composition, and thus, metallographic structure, the response of each material is different when depositing a PVD coating. Basically, the differences affect adhesion, densification (hardness), corrosion/oxidation resistance, roughness, etc.

The present study investigated the effect of thermal treatments on the mechanical properties of AlCrSiN and AlTiSiN coatings deposited on two different soft substrates, steel and Inconel, with the aim of providing a novel sight to elucidate the mechanical performance of quaternary coatings on engineering substrate system, with special focus on not only studying the mechanics of the coating, but also the coating/substrate interface.

In doing so, nanoindentation, microindentation, microscratch, and Mercedes tests were used to characterize the mechanical response of coatings.

7.1.2 Experimental Procedure

7.1.2.1. Sample Preparation

Two different coatings (AlCrSiN and AlTiSiN) were deposited on two substrates (steel and Inconel), making four different coating–substrate systems: AlCrSiN/steel, AlCrSiN/Inconel, AlTiSiN/steel, and AlTiSiN/Inconel. The steel substrate was H13 (DIN 1.2344). Additionally, the Inconel was an aged Inconel 718. The chemical compositions of the two substrates are presented in **Tables 7-1 and 7-2.**

Table 7-1. Composition (% by weight) of steel H13 (DIN 1.2344).

	Composition (% by Weight)							
Name	**C**	**Si**	**Mn**	**Cr**	**Mo**	**V**	**P**	**S**
1.2344	0.37–0.43	0.90–1.20	0.30–0.50	4.80–5.50	1.20–1.50	0.90–1.10	0.030	0.030

Table 7-2. Composition (% by weight) of Inconel 718 used as a substrate.

	Composition (% by Weight)						
Name	**Ni**	**Cr**	**Nb**	**Mo**	**Ti**	**Al**	**Other Minor Elements**
Inconel	50–55	17–21	4.75–5.50	2.80–3.30	0.65–1.15	0.2–0.8	Balance

The coatings were produced by cathodic arc evaporation in a commercial METAPLAS MZR-323 PVD reactor able to reach a base pressure of $5 \cdot 10^{-4}$ Pa. The reactor was equipped with two opposing columns, each of them hosting three circular cathodes (6.3 cm diameter) aligned vertically. Both columns faced each other and left an effective volume of 0.5 m^3 available for the substrates. For the AlTiSiN coating, three cathodes of Ti (99.8% purity) and three cathodes of AlSi (80 at.% Al–20 at.% Si) were placed in an alternating arrangement (i.e., a Ti cathode faced an AlSi cathode). In the case of the AlCrSiN coating, the Ti cathodes were replaced by Cr cathodes (99.98% purity). The deposition parameter of the coatings is presented in **Table 7-3** and the process temperature for both cases is 400–450 °C. The AlTiSiN coating had a Ti bonding layer and the AlCrSiN had a Cr + CrN bonding layer.

Table 7-3. The deposition parameter of AlTiSiN and AlCrSiN coatings.

Coating	Step	Gas	Bias (V)	Total Pressure (mbar)	Rotating Speed (rpm)
AlTiSiN	Bonding layer	Ar	−60	1.2×10^{-2}	5
	AlTiSiN deposition	N_2	−60	4.0×10^{-2}	5
AlCrSiN	Bonding layer	Ar	−60	1.2×10^{-2}	5
		N_2	−60	1.2×10^{-2}	5
	AlCrSiN deposition	N_2	−60	4.0×10^{-2}	5

2.2. Coating Composition and Coating Thickness

Glow discharge optical emission spectroscopy (GDOES) was used to obtain the chemical composition of the coatings. The GDOES analyses were performed with a Jobin-Yvon JY 1000 RF optical spectrometer equipped with more than 40 channels and an optical monochromator. Coating thicknesses were measured by calowear tests, which were conducted specifically with a rotating a hard steel sphere of a known diameter to friction the surface of coating samples by continuously adding silica solution (30–50 weight percent) to increase the friction between sphere and samples. The solution may let the sphere abrade the coating and into the substrate, then form a spherical depression and seen from a plane the depression is rounded and followed Equation (1). By measuring the outer and inner edge radius of depression, the thickness of coating can be calculated as follows:

$$\boldsymbol{t = \frac{(R+r)(R-r)}{d}} \qquad (5)$$

Where t, the thickness of the coating (μm), R is the outer edge radius of depression, r is the inner edge radius of depression, and d is the diameter of the hard steel sphere.

7.1.2.3. Nanoindentation and Microindentation

The hardness and Young's modulus of coatings were measured with an MTS Nanoindenter XP equipped with continuous stiffness measurement. Prior to nanoindentation, all samples were polished by colloidal silica and cleaned with acetone to reduce the effect of the roughness of coatings on the measurements [140]. Nanoindentation assays were performed with a Berkovich tip calibrated against a fused silica standard. A matrix of 25 imprints was derived for each sample at a constant strain rate of 0.05 s^{-1}. The Oliver and Pharr method was used to calculate the hardness (H) and elastic modulus (E); the Poisson ratio was assumed to be $v = 0.25$ [139]. Hardness was measured at 10% penetration depth and Young's modulus of the coating was estimated by extrapolating the results to null thickness. The subscript f is used in the elastic modulus to indicate that it is the one of the coatings.

Micro contact damage tests were performed by Hertzian contact loading in a servo hydraulic test machine (Instron 8500) with a WC-Co sphere of 2.5 mm of diameter [193]. A trapezoidal wave was chosen as the loading curve with time, with a loading rate of 30 N/s rate, and maximum loads of 500 N or 750 N, held for 20 s.

Vickers tests on the substrates were performed with a Testwell FV-700 hardness tester under 10 kg load. The average and standard deviation for each sample under 10 kg load was obtained from five indentations.

7.1.2.4. Adhesion Test

Scratch tests and Damage contact tests were performed in order to measure the adhesion between coating and substrate. The reason for using two different tests was to induce different stress fields and damage scenarios at the interface by using different indenter tip geometries and loading conditions. Scratch tests were performed in a CSM Revetest with progressive loads from 0 to 30 N at a constant loading rate of 10 N/min with a Rockwell C diamond stylus of 200 μm radius and 120° apex angle, with a scratch length of 5 mm. Damage and failure were later observed by scanning electron microscopy (SEM).

To further characterize the contact damage of coated substrates, the adhesion was characterized by Damage contact test (Mercedes test) [163, 165]. In this test, a Rockwell C intender was pressed against the surface of coated substrates, producing

deformation and fracture. Four different loads were used: 98 N, 196 N, 392 N and 613 N in order to produce different amounts of damage.

7.1.2.5. Thermal Treatments

Two different temperatures were tested: 500 °C and 800 °C. Thermal treatments were conducted in an elevator furnace, starting from room temperature and heating at a 10 °C/min rate until the desired temperature. Samples were maintained at maximum temperature for 60 min, and then cooled down to room temperature.

7.1.2.6. Microscopy

In order to inspect the deformation and damage suffered by the coatings, Phenom XL SEM apparatus was used. The cross-section of the coatings was obtained with a Zeiss Neon 40 focus ion beam (FIB) [194], with a gallium source accelerated at 30 kV with a decreasing ion current down to a final polishing stage at 500 pA. To avoid the waterfall effect in the milling processing, a protective layer of platinum was deposited on the area of interest.

7.1.3 Results and discussions

7.1.3.1. Coating Composition and Coating Thickness

The coating thicknesses measured by the calowear tests are presented in **Table 7-4**. While all values are around 2 μm, the thickness of the coatings deposited on steel is slightly thicker than the ones deposited on Inconel. Reason for this may be attributed to the difference in the conductivity for the two substrates which results in different deposition rates. Composition of the coatings is presented in **Figure 7-1**.

Table 7-4. Thickness of coated samples.

Coating	**AlCrSiN**		**AlTiSiN**	
Substrate	Steel	Inconel	Steel	Inconel
Thickness (μm)	2.9	1.6	2.6	1.7

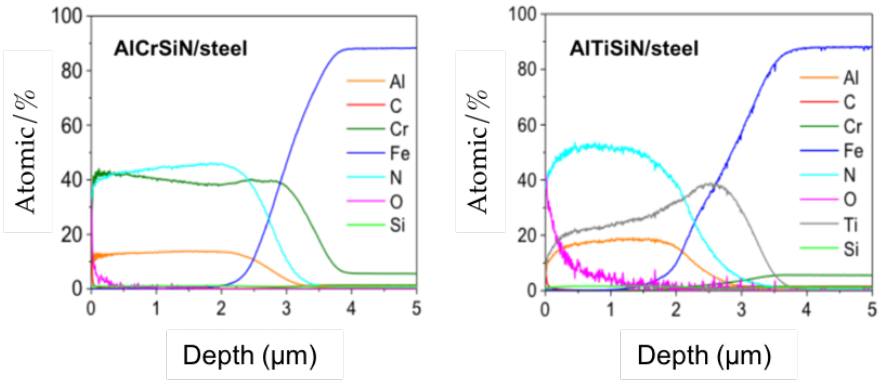

Figure 7-1. Composition (in atomic %) of the coatings vs. depth (µm) obtained by GDOES for AlCrSiN/steel (**left**) and AlTiSiN/steel (**right**).

7.1.3.2. Mechanical Properties of the Coated Materials

Nanoindentation results are presented in **Table 7-5** and **Figure 7-2**. The images of the nanoindentation imprints are presented in **Figure 7-3**. The hardness and elastic modulus ratio (H/E) was adopted to describe elastic deformation to failure and H^3/E^2 is the plasticity index to present the resistance to plastic deformation. Both are common parameters to characterize the mechanical performance and wear resistance of coatings [77, 78]. Based on **Table 7-2**, AlCrSiN coatings exhibited higher values of H^3/E^2 than AlTiSiN coatings when they all were deposited at the same substrate, indicating a better wear resistance response. It is elucidated that AlTiSiN coatings may present better wear resistance [195]. However, it should be considered that the performance of the tool materials is a combination of both the substrate and coating. In this respect, Vickers test results of the substrate are presented in **Table 7-6**.

Table 7-5. Mechanical properties of coated samples after thermal treatment.

Coating	**AlCrSiN**			**AlTiSiN**		
	Unheated	**500 °C**	**800 °C**	**Unheated**	**500 °C**	**800 °C**
Hardness (GPa)	28 ± 3	33 ± 4	22 ± 5	26 ± 3	30 ± 2	16 ± 2
Elastic Modulus (GPa)	369 ± 17	462 ± 46	280 ± 60	367 ± 42	476 ± 35	330 ± 16
H/E	0.075	0.071	0.077	0.072	0.063	0.047
H^3/E^2	0.158	0.168	0.128	0.137	0.117	0.034

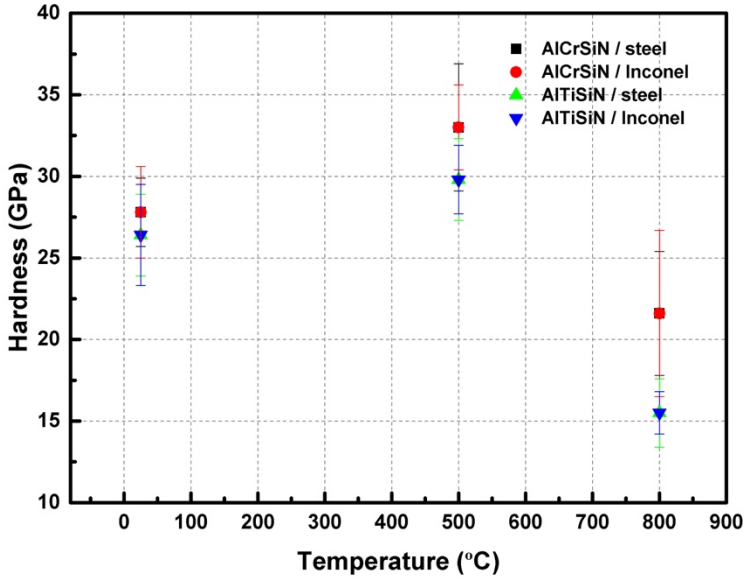

Figure 7-2. The relationship of the hardness of coatings with different thermal treatment.

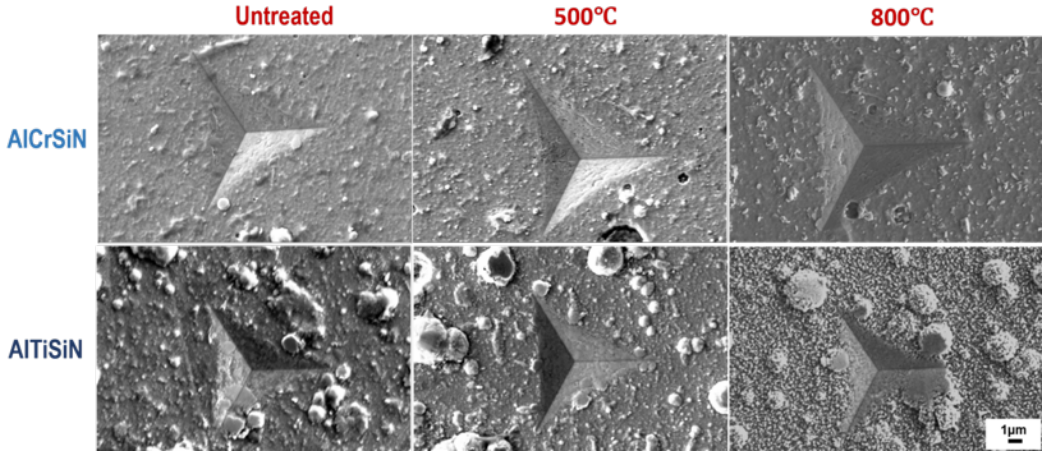

Figure 7-3. The SEM images of nanoindentation of AlCrSiN and AlTiSiN deposited on steel substrate after thermal treatment.

Table 7-6. Vickers hardness of the substrates.

Sample	Untreated	500 °C	800 °C
Steel	476 ± 4	479 ± 2	417 ± 4
Inconel	461 ± 3	454 ± 3	316 ± 7

It is seen how the samples that underwent a cycle of 500 °C presented an increase in the values of hardness, both for AlCrSiN and AlTiSiN coatings, regardless of the

substrate. At 800 °C, hardness decreased. This may be attributed to the densification of the microstructure at moderate temperatures and the phase transformation at high temperatures where the cubic nitride phase transforms into a hexagonal nitrides phase [33, 40].

Hardness of the substrates decreased in both cases, mainly after exposure at 800 °C. This is probably due to an increase in grain size and a modification of the precipitates [191, 192].

Images of the indented coatings (**Figure 7-3**) present droplets at the surface typical of the PVD process [196]. The thermal treatment at 500 °C did not produce relevant changes in the surface. However, after thermal treatment at 800 °C, there was a clear change in the surface, due to initial oxidation of the coatings. This oxidation is more evident in the case of the AlTiSiN coatings. This results in indentation imprints which deviates from the ideal shape, which gives rises to higher scattering in the mechanical values measured by this technique.

In **Figure 7-3**, it is also shown how, for AlCrSiN coatings, some ring cracks appear around the indentation, which may indicate a lower fracture toughness compared with AlTiSiN coatings [129].

7.1.3.3. Adhesion Tests

Figure 7-4 presents the critical loads for delamination of all the materials. **Figure 7-4** shows how the appearance of decohesion of the coating for the AlTiSiN coating is higher than AlCrSiN, independent of the substrate. However, after thermal treatments at 500 °C, the coatings deposited on Inconel presented a better adhesion than those deposited on steel. Furthermore, the AlCrSiN on Inconel coating thermally treated at 500 °C exhibited an enhanced scratch resistance compared with the samples without thermal treatment. This enhancement may be due to the higher thermomechanical stability of Inconel as compared with steel. For thermal treatments at 800 °C, all coatings present lower adhesion, due to degradation of the coating as well as softening of the substrates.

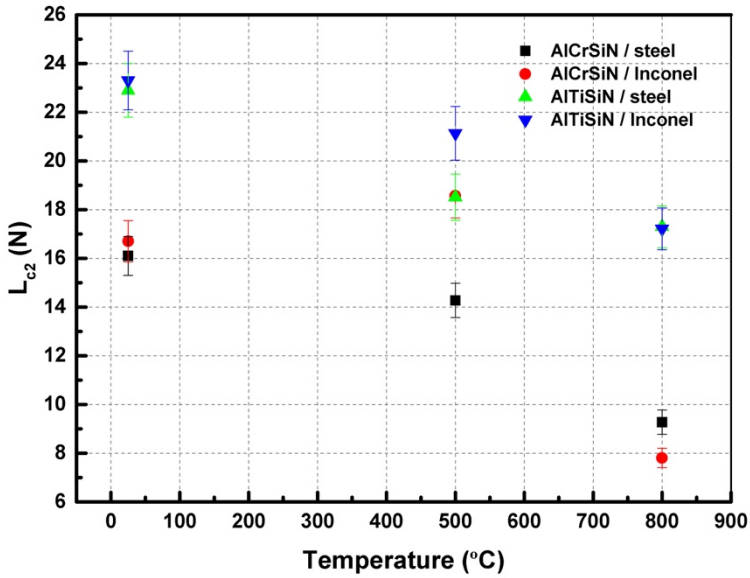

Figure 7-4. Critical load as a function of temperature of the thermal treatment.

Images obtained by optical microscopy; SEM of the scratch tracks are presented in from **Figure 7-5** to **Figure 7-8** for AlCrSiN/steel, AlCrSiN/Inconel, AlTiSiN/steel, and AlTiSiN/Inconel, respectively. The coating thickness affects the scratch loads for adhesion and the direct comparison of performance by scratch with different coating/substrate system could not be taken in account. Therefore, both coatings have comparable thicknesses for every substrate. In **Figures 7-5** and **7-6,** the scratch tracks of AlCrSiN on both substrates are presented. It is seen how plastic deformation, microcracking, and delamination are produced as load is increased. Stick–slip deformation induced by compressive stress appeared at the contour. External cracks in the scratch direction were formed as well. The load at which this failure appeared is labeled as critical load, L_{c1}. As the load increased, transverse cracks appeared, induced by tensile stress, until the detachment of the coatings: this load is defined as L_{c2}, which indicates failure of the interface of coated substrate.

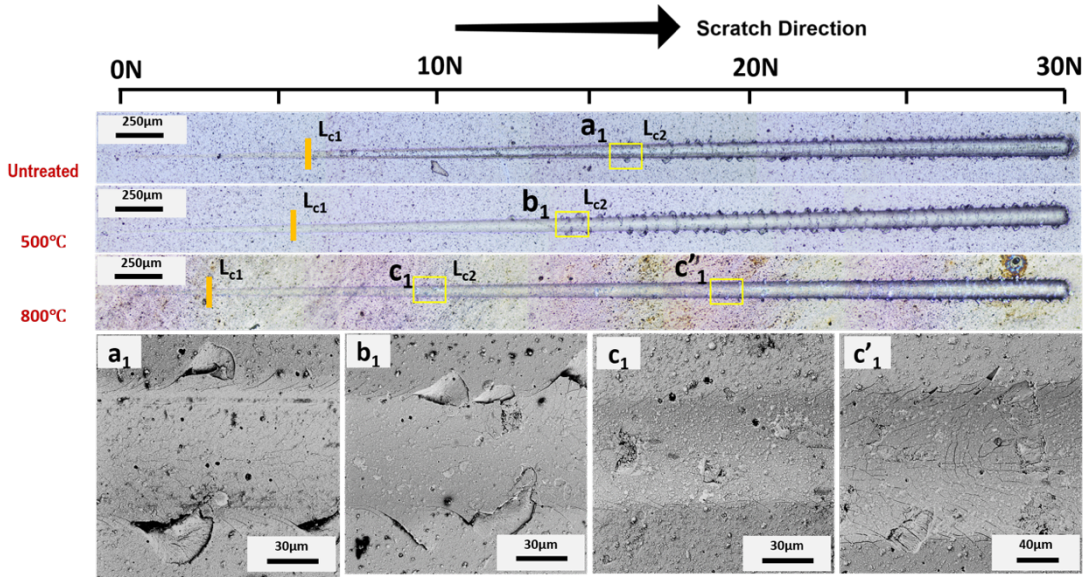

Figure 7-5. Adhesion optical profile of failure after microscratch tests of the AlCrSiN/steel sample. First (L_{C1}) and second (L_{C2}) critical loads are indicated. SEM magnification of selected areas (a_1,b_1,c_1 and c'_1) are also presented.

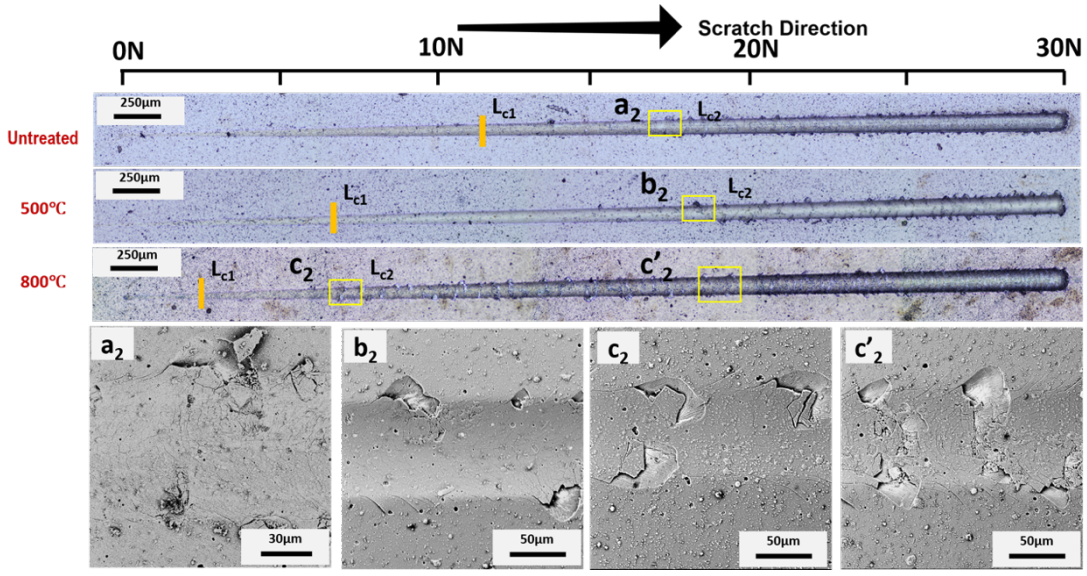

Figure 7-6. Adhesion optical profile of failure after microscratch tests of the AlCrSiN/Inconel sample. First (L_{C1}) and second (L_{C2}) critical loads are indicated. SEM magnification of selected areas (a_2, b_2, c_2 and c'_2) are also presented.

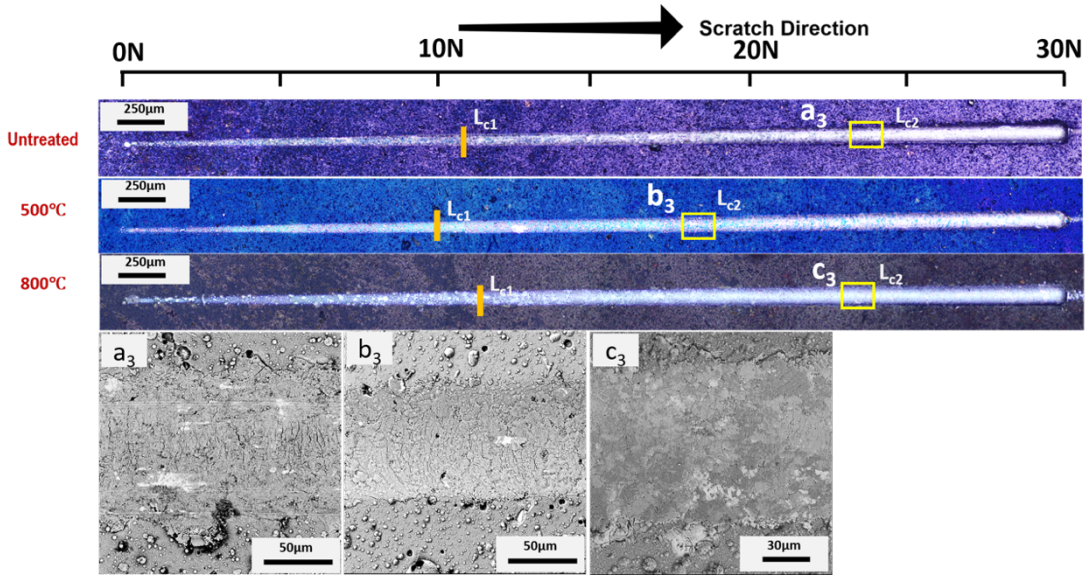

Figure 7-7. Adhesion optical profile of failure after microscratch tests of the AlTiSiN/steel sample. First (L_{C1}) and second (L_{C2}) critical loads are indicated. SEM magnification of selected areas (a_4, b_3 and c_3) are also presented.

After thermal treatment of the AlCrSiN coatings, critical loads were lower in the case of the steel substrate. In addition, the samples after thermal treatment at 800 °C presented a different type of damage, with more microcracking and less evident spalling. For the samples on the Inconel substrate, a slight improvement was appreciated for samples thermally treated at 500 °C, following the enhancement of mechanical properties observed previously. The mechanism for this enhancement may be the relaxation of the residual stress of AlCrSiN coating after 500 °C thermal treatment [197], whereas the decrease in adhesion may due to a phase transformation forming the fcc-CrN phase into h-Cr_2N [198].

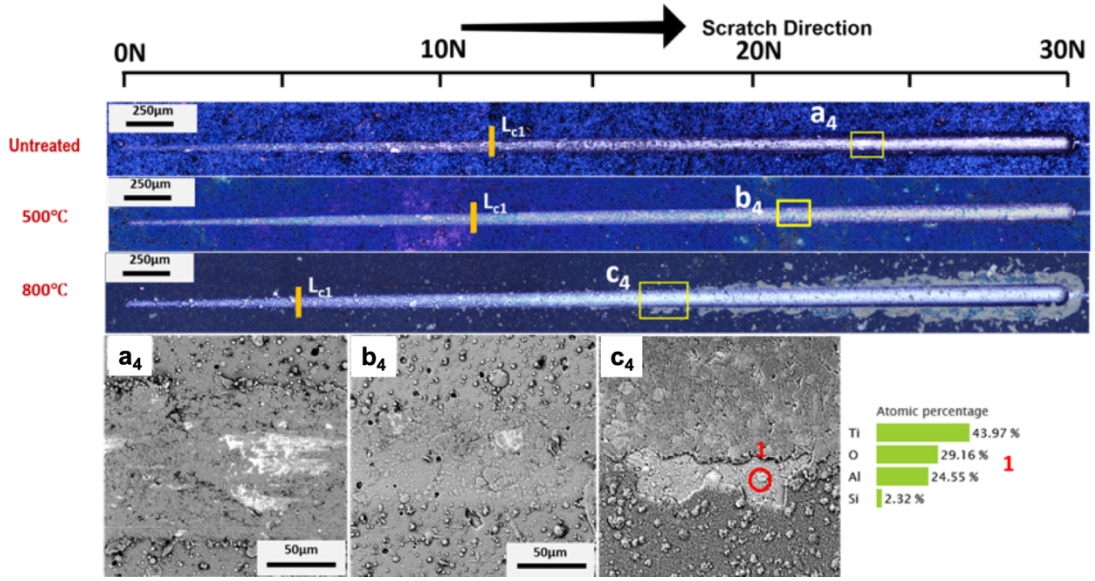

Figure 7-8. Adhesion optical profile and SEM images of failure after microscratch tests of the AlTiSiN/Inconel sample. First (L_{C1}) and second (L_{C2}) critical loads are indicated. SEM magnification of selected areas (a_4, b_4 and c_4) are also presented as well as the chemical composition by EDX of the indicated point.

In the case of AlTiSiN coatings, as presented in **Figures 7-7** and **7-8**, a small amount of deformation occurred at loads below 26 N [169]. As the loading increased, adhesive failure occurred for AlTiSiN coatings. The coatings spalled from the middle of the trace of the scratch. After thermal treatment, the amount of delamination diminished for both temperatures. The difference for AlTiSiN coatings deposited on Inconel after thermal treatment, especially at 800 °C, compared with steel as the substrate, is that part of coating was delaminated. A substantial area of the coatings peeled off. EDX was conducted at the delaminated area, showing that the elements were similar with AlTiSiN coatings, and indicating that a thin layer of the coating remained on the surface. Therefore, the failure may be considered cohesive failure and not coating delamination. The reason for this may be the fragile layer formed in the thermal treatment process as well as the evident softening of the substrate. This phenomenon could be explained by the phase transformation of fcc-AlN into hcp-AlN after 800 °C thermal treatment [199].

In **Figure 7-9**, FIB cross-sections of all four coatings and microstructures are presented. The images were taken at the same load (16 N) in order to compare the behaviors between coatings. **Figure 7-9** shows how that all cracks were arrested by interface, indicating a good structural integrity of the substrate. Both coatings had a dense microstructure and a bonding layer, as shown previously [34, 186].

Table 7-6. Critical load and adhesion energy of the coated systems after thermal treatment.

No.	Sample		G_c (J/m^2)		
	Coating	Substrate	Untreated	500 °C	800 °C
S1	AlCrSiN	steel	72 ± 7	56 ± 6	30 ± 3
S2	AlCrSiN	Inconel	87 ± 9	54 ± 5	23 ± 2
S3	AlTiSiN	steel	303 ± 30	105 ± 10	272.2 ± 27
S4	AlTiSiN	Inconel	322 ± 31	162 ± 16	117.0 ± 10

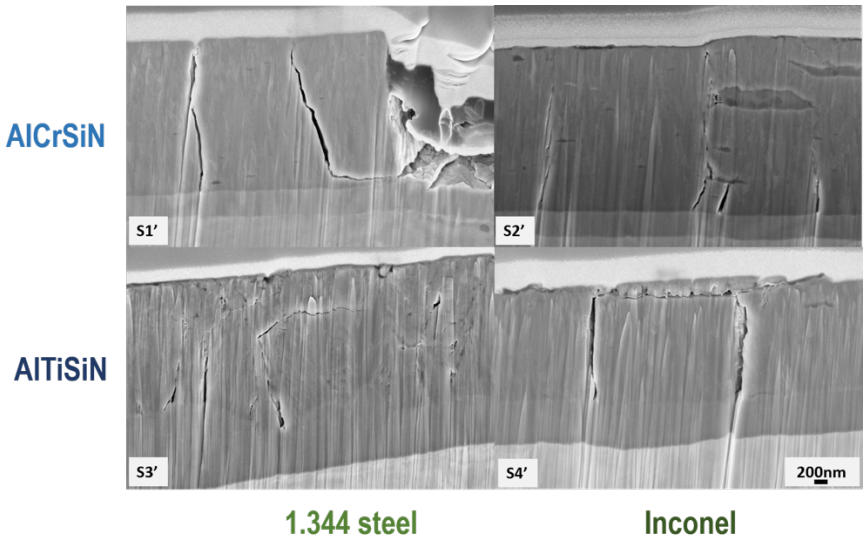

Figure 7-9. Cross-section SEM images at the same load (16 N) of scratch marked in from **Figure 7-5** to **Figure 7-8**.

In order to rationalize the scratch resistance of the coatings, the scratch crack propagation resistance (*CPR*) was calculated using Equation (6) [200].

$$CPRs = L_{C1}(L_{C2} - L_{C1}) \qquad (6)$$

where L_{C1} is the critical load of start of lateral crack, and L_{C1} is the critical load of the start of delamination or spallation; the results are presented in **Figure 7-10**.

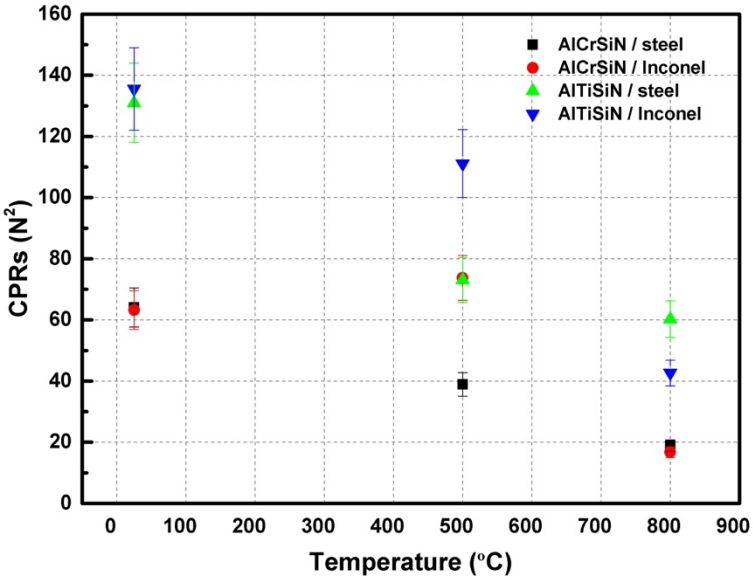

Figure 7-10. *CPR* of scratch tests after thermal treatment: AlCrSiN / steel, AlCrSiN / Inconel, AlTiSiN / steel, and AlTiSiN / Inconel.

The critical stress σ_c is calculated by,

$$\sigma_c = \left(\frac{2L_{c2}}{\pi d_c^2}\right)\left[\frac{(4+\nu_f)3\pi\mu}{8} - 1 + 2\nu_f\right) \qquad (7)$$

where d_c is the track width at L_{c2}, μ is the friction coefficient calculated by the friction force and ν_f is the Poisson rate of coatings. The surface energy of the interfacial crack known is defined by Equation (8) [201-203]:

$$G_c = \sigma_c^2 t \Big/ 2E_f \qquad (8)$$

where t and E_f are the thickness and the elastic modulus of coatings respectively. The values of E_f are experimentally determined from **Table 7-5**.

Crack propagation resistance (CPR) is presented in Figure 10, which shows how AlTiSiN coatings generally present higher CPRs than AlCrSiN coatings, independently of the substrate. After thermal treatments, the CPR degraded in all cases, with the exception of AlCrSiN on Inconel, which presented a similar CPR after thermal treatment at 500 °C.

The AlTiSiN/Inconel sample presented the highest value of G_c = 321.5 J/m^2, as seen in **Table 7-4**. The range of values was similar to those previously report by other researchers for similar hard coatings [204-206]. Of all the studied systems, AlTiSiN/steel presented the higher adhesion energy. This coating also exhibited the highest G_c after 800 °C thermal treatment. In comparison with AlTiSiN, AlCrSiN

presented lower values for critical stress and adhesion energy, which was consistent with the analysis of the CPR microstratch test.

Figure 11 presents the results of the Mercedes Test at a normal load of 613 N. In all cases, radial cracks and partial ring cracks appeared. However, in the AlCrSiN/steel and AlTiSiN/Inconel systems after 800 °C thermal treatment, the vicinity of the indentation appeared with a high area of delamination. This high degree of delamination was also a consequence of the softening of the substrate, which resulted in higher deformation under contact loading and larger differential strains between the coating and substrate.

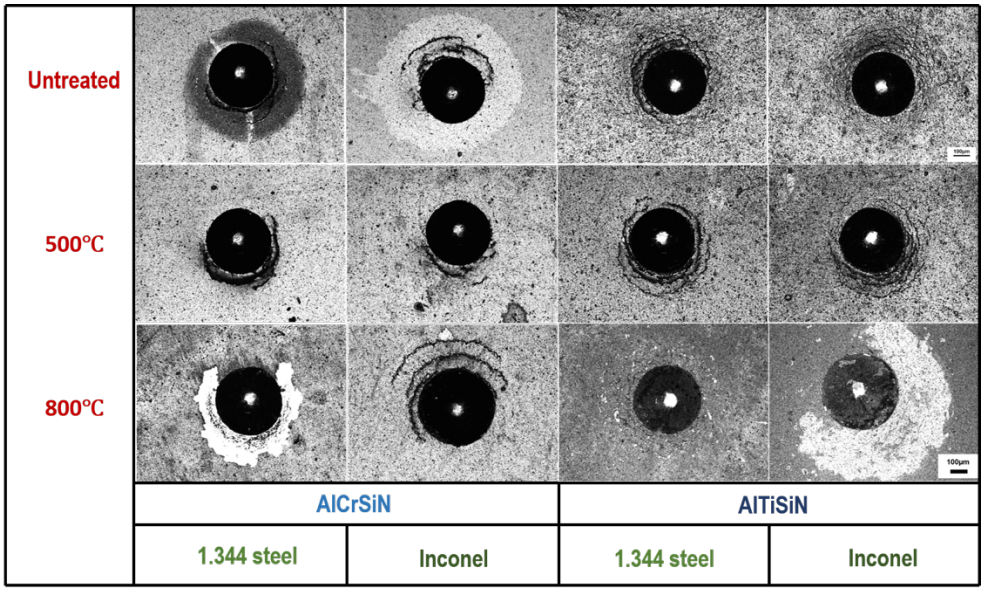

Figure 7-11. Confocal images of the Mercedes test at 613 N with a Rockwell C tip contrasted with different thermal treatments.

In the untreated AlCrSiN/Inconel sample, a similar phenomenon was noticed. In this case, delamination without spallation was observed, which indicated lower adhesion than after thermal treatment at 500 °C. This is coherent with the enhancement in CPR as observed in **Figure 7-10**.

In order to further explore the damage at 613 N after 800 °C, the particular area of indentation after Mercedes test was magnified by SEM, as shown in **Figure 7-12**, and EDX was performed to probe the elements of the delaminated area to ensure that the substrate was exposed. For AlCrSiN/steel, the exposed and light color area consisted of Cr and Fe. However, for AlTiSiN/Inconel, two contrasts appeared: shallow grey (circled as red 3) and white (circled as red 4). The SEM images demonstrate the delamination with large area of AlCrSiN/steel and AlTiSiN/Inconel at 613 N after

800 °C, but with traces of the coating still attached to the substrate. To further observe the internal de-formation mechanisms, a cross-section at the areas was indicate as S5'and S6', and is shown in **Figure 7-13**. In all cases, it was seen how the cracks were contained at the coating, without propagating into the substrate.

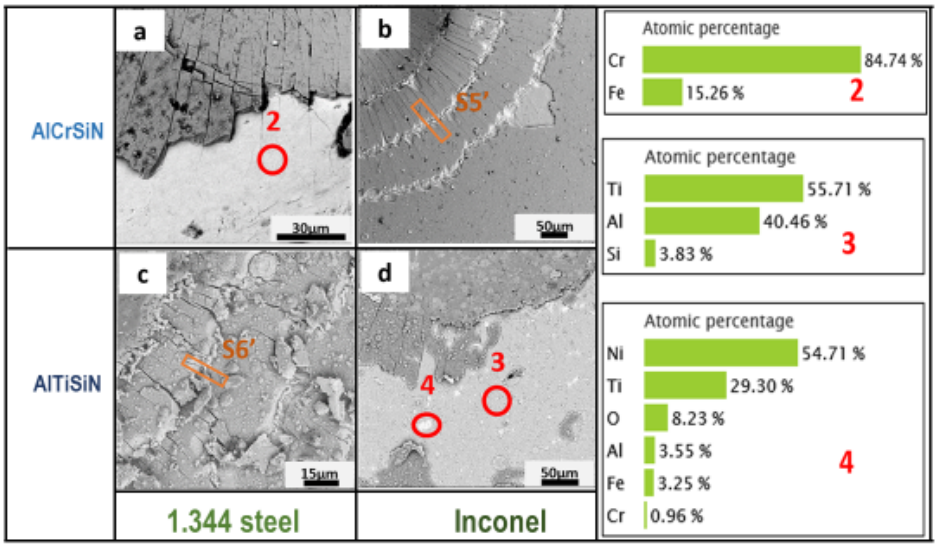

Figure 7-12. SEM images of the Mercedes test and EXS analysis at 613 N with a Rockwell C tip after 800 °C treatment: (a) AlCrSiN / steel, (b) AlCrSiN / Inconel, (c) AlTiSiN / steel, and (d) AlTiSiN / Inconel. Numbers 2, 3, and 4 indicate the chemical analysis by EDS. S5' and S6' indicate the FIB cross-sections as presented in **Figure 7-13**.

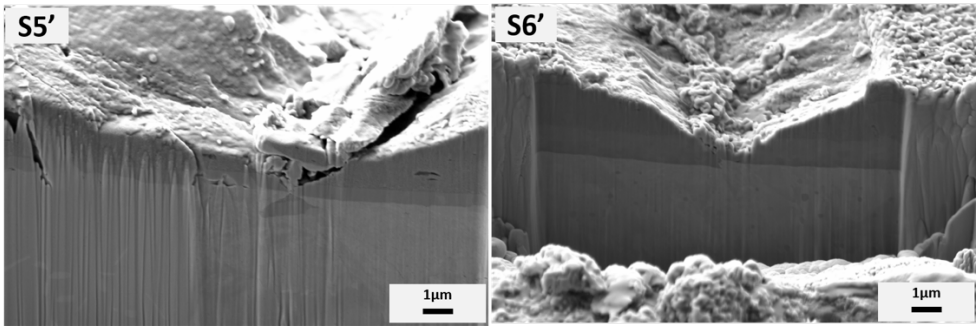

Figure 7-13. Cross-sectional SEM images with two magnifications of partial ring cracks at 613 N with a Rockwell C tip after 800 °C treatment marked in **Figure 7-12**.

7.1.3 Conclusions

The mechanical properties of AlCrSiN and AlTiSiN quaternary coatings deposited on Inconel and steel which underwent thermal treatments at 500 °C and 800 °C have been characterized. The conclusions can be summarized as:

① Nanoindentation results show values of hardness of 28 GPa and 26 GPa, and elastic modulus values of 369 GPa and 367 GPa for AlCrSiN and AlTiSiN coatings, respectively, before thermal treatment. After 500 °C, the hardness and elastic modu-lus increased for all samples. After the 800 °C thermal treatment, these properties decreased, indicating a degradation of the material.

② Through microscratch tests, the AlTiSiN samples presented better adhesion and AlCrSiN coating displayed lower adhesion for all thermal treatments. This is fur-ther evidenced by the Mercedes test, where AlCrSiN coatings presented a higher detached area. Through SEM and FIB observations, it was evidenced that the mode of failure was cohesive.

③ Regarding the substrates, coatings deposited on Inconel exhibited better performance, especially after thermal treatment at 500 °C, associated with the better performance of Inconel at high temperature. Thermal treatments at 800 °C resulted in a degradation of the mechanical performance, due to the microstructural changes in both the coating and the substrate, such as increases in the grain size and mod-ification of the precipitates. Based on the data of crack propagation resistance and surface energy of an interfacial crack, it is observed that the AlTiSiN coating pre-sented better adhesion than the AlCrSiN coating, even after thermal treatments.

7.2 Comparative study of mechanical performance of AlCrSiN coating deposited on WC-Co and cBN hard substrates

The objective of this study is to explore and compare the mechanical response of AlCrSiN coating deposited on two different substrates, namely, WC-Co and cBN. Nanoindentation was used to measure the hardness and elastic modulus of the coating and microindentation was used for observing the contact damage under Hertzian contact with monotonic and cyclic (fatigue) loads. Microscratch and Mercedes tests were also used to evaluate the strength of adhesion between AlCrSiN coating and two substrates under progressive and constant loads respectively. The surface damages induced by different mechanical tests were observed by scanning electron microscopy (SEM). Focus ion beam (FIB) was used to produce cross-section of coating-substrate system in order to further detect the mode and extent of failure induced. The results show that AlCrSiN coating deposited on WC-Co substrate perform better adhesion strength and contact damage response than deposited on cBN substrate attributed to the lower plasticity of the cBN substrate as well as its lower adhesion to the coating. [2]

7.2.1 Introduction

Hard protective coatings are frequently used in the tool industry to improve wear and corrosion resistance [53, 169]. Based on traditional binary metal nitride ceramic coatings (like CrN, TiN), aluminum (Al) and silicon (Si) are introduced to formed quaternary coating systems (AlCrSiN and AlTiSiN) with enhanced mechanical properties, thermal stability and wear resistance [59, 207]. By adding Al and Si an oxide rich layer is formed on top, contributing to the improvement of the oxidation resistance and the thermal stability of coating [64, 66]. In addition, the amorphous Si_3N_4 phase formed in the grain boundary inhibit the neighboring grains sliding, which results in higher hardness and thermal stability [67, 174, 175]. These coatings are normally deposited by physical vapor deposition (PVD) [68, 177]. The crystalline phase

[2] This chapter corresponds to the paper:

Comparative study of mechanical performance of AlCrSiN coating deposited on WC-Co and cBN hard substrates. J. Liang1, *, M. Serra1, S. Gordon1, J. Fernández de Ara3,E. Almandoz L. Llanes1,2 ,E. Jimenez-Piqué1,2, Currently under review.

coatings consist of a face-centered cubic lattice with high atomic density formed by the crystallization of a metastable amorphous phase after thermal treatment, producing a coating with a columnar structure [46, 139, 165].

Although the mechanical properties of these coatings have been studied before [46], information about the mechanical behavior when the coating is deposited in different substrates is scarce. Performance of tool materials is governed by both the coating and the substrate, which may result in very different performance even for the same coating if the substrate is different. The two most used hard substrates in the coating industry are hardmetals (also known as cemented carbides) and cubic boron nitride.

Hardmetals are composed by a hard WC phase bonded together with a metal, usually Cobalt (WC-Co), presenting an outstanding combination of mechanical properties of hardness, fracture toughness and wear resistance [208, 209]. Cubic boron nitride (cBN) is a superhard material consisting in cBN particles bonded with a ceramic, with hardness only second to diamond, with an extremely high hardness and wear resistance, together with exceptional thermal and chemical properties [42, 43, 210-214]

There are some examples of works exploring the effects of different substrates on quaternary coatings, but mainly on metallic substrates. For example, Gao et al. focused on the effect of the structure of AlCrSiN coating protecting the high speed steel (HSS) [48], Tuchid et al. were attracted by the thermal oxidation on HastelloyX substrate [47]. These papers studied just one substrate, so it is interesting to study the effect of different substrates in the mechanical response of TiAlSiN coatings under contact loads. Similar works on other type of coatings exist for other type of coatings Sveen et al [215] studied the scatch adhesion of TIAlN on three different substrates (high speed steel, cBN and cemented carbides, but no evidence still exist on quaternary AlCrSiN coatings.

Therefore, the present study focusses on comparing the mechanical response of AlCrSiN quaternary coating deposited on two different hard substrates: WC-Co and cBN with the objective of understanding the mechanical performance of the coated materials.

7.2.2 Experimental Procedure

7.2.2.1. Sample Preparation

AlCrSiN coating was deposited on two different commercially available hard substrates of cemented carbide (WC-Co) and cubic boron nitride (cBN), making two different coating-substrate systems: AlCrSiN / WC-Co and AlCrSiN / cBN. The WC-Co material consisted in WC grains with 0.9 ± 0.4 μm grain size and 10 % of cobalt content, while the cBN was a low cBN content with an average grain size of 1.5 microns and a TiC ceramic binder.

Cathodic arc evaporation was used to deposit the AlCrSiN coating. The process was carried out using the industrial equipment Platit p80, in a vacuum chamber with an argon atmosphere at 0.8-2 Pa and a negative bias voltage of -65 V. Cr and Al+Si cathodes were used as material source. The deposition process of the AlCrSiN coating with adhesion Cr layer can be found in [216].

The thickness of coatings was measured by Calowear test, and calculation of the coating thickness was done after Equation (9).

$$t = \frac{(R+r)(R-r)}{d} \quad (1)$$

Where t is the thickness of coating, and d is the diameter of the hard steel sphere. R is the outer edge radius of the ring depression and r is the inner edge radius of depression, which were measured under the microscopy.

7.2.2.2. Characterization of structure and composition

The crystallographic phase of the coating was characterized by glancing incident angle X-ray diffraction (GIXRD) with Cu X-ray tube radiation (D8 advance. Bruker), the test voltage and current were up to 40 kV and 40 mA. The incident angle was fixed at 1 °. The scan speed was 10 s per step and 0.01 ° scan size performed from 20 °- 70 °.

7.2.2.3. Nanoindentation and microindentation

The hardness and elastic modulus were measured with an MTS Nanoindenter XP with a continuous stiffness measurement. All surfaces of coatings were slightly polished by colloidal silica and cleaned by acetone to lessen the effect caused by the roughness of coating during the measurement [140]. Nanoindentation tests were performed with a Berkovich diamond tip calibrated against a fused silica standard. An array of 25 imprints was made for each sample with a constant strain rate of 0.05 s^{-1}. All indentations were done up to 2000 nm maximum penetration depth. The calculation of the hardness (H) and elastic modulus (E) was obtained by the Oliver and Pharr

method and the Poisson ratio was assumed to be ν=0.25 [139]. The hardness was measured at 10 % penetration depth and the elastic modulus was estimated by extrapolating the results to null thickness.

The spherical contact response was assessed by means of spherical microindentation with both monotonic and cyclic loads. Hertzian tests were carried out by a servo hydraulic test machine (Instron 8500) using a cemented carbide sphere with a radius of 5 mm. Monotonic loads were conducted following a trapezoidal waveform, at a loading rate of 500 N/s and holding 10 seconds at maximum load, under seven equally spaced loads: 2000 N, 3000 N, 4000 N, 5000 N, 6000 N, 7000 N and 8000 N. The same loading waveform was applied for the cyclic loading with the frequency of 3 Hz and 10^3 circles. At least three indentations were made at each load and loading mode.

7.2.2.4. Adhesion test

Adhesion strength between coating and substrate was evaluated with scratch and Contact damagetest. Scratch tests were conducted by a CSM Revetest with a progressive load from 0 N to 90 N at a constant loading rate of 10 N/min with a Rockwell C tip of radius and 120 ° apex angle and through a length of 5 mm. Contact damagetests were performed by a same tip geometry [163]: a Rockwell C indenter was pressed against the surface of samples to generate deformation and cracking. Nine loads were used for the two coated systems:9.8 N, 49 N, 98 N, 196 N, 294 N, 392 N, 490 N and 613 N with the intention of producing different type of damage. Failure and damage produced by scratch and Contact damagetest were observed through scanning electron microscopy (SEM).

7.2.2.5. Microscopy

A Phenom XL SEM and a Zeiss Neon 40 SEM-FIB coupled with an energy dispersive X-ray detector (EDX) were used to observe the samples. The cross-section by FIB of the coated systems was done by using gallium ions accelerated up to 30 kV with a decreasing ion current down to 500 pA. A protective layer of platinum was deposited on the area of interest to avoid the waterfall effect.

7.2.3 Results and discussion

7.2.3.1. Coating composition and coating thickness

To confirm the crystallographic structure and phase composition, XRD patterns were done and are presented in **Figure 7-14** and **Table 7-7**. The phase detected for the coating on both substrates was (Cr,Al)N solid solution, which was the main phase of AlCrSiN coating. The (111), (200) and (220) of peaks were shifted about 0.2 degrees due to the lattice expansion produced by the substitution of Cr atoms by Al atoms [217, 218]. The WC-Co substrate was also detected, as shown in **Figure 7-14 (a)**. In **Figure 7-14 (b)**, indexing of the cBN substrate is also presented. The binder phase TiN of the cBN substrate is clearly identified as a cubic phase. The diffraction peak at 42.6 degrees was assigned to the face-centered cubic cBN [219].

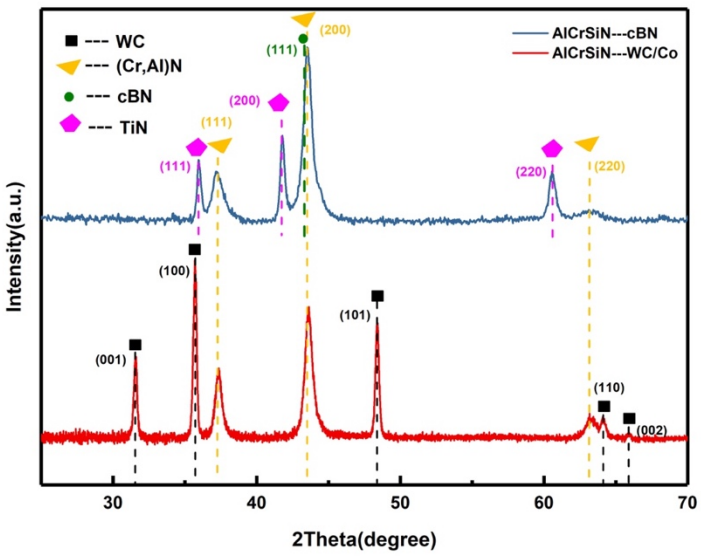

Figure 7-14. XRD patterns of AlCrSiN coatings deposited on WC-Co and cBN substrates. The coating presents a (Cr,Al)N crystallographic phase.

The deposited AlCrSiN coating was uniform and dense both on WC-Co and cBN substrates, as seen in **Figure 7-15 (a)** and **(b)**. Based on the EDX composition maps, elements of chromium (Cr), aluminum (Al) and nitrogen (N) were detected in the coating. Elements of Wolfram (W), Cobalt (Co), Titanium (Ti), Boron (B) and Nitrogen (N) were detected on the substrates. The results are consistent with the composition of coatings and substrates.

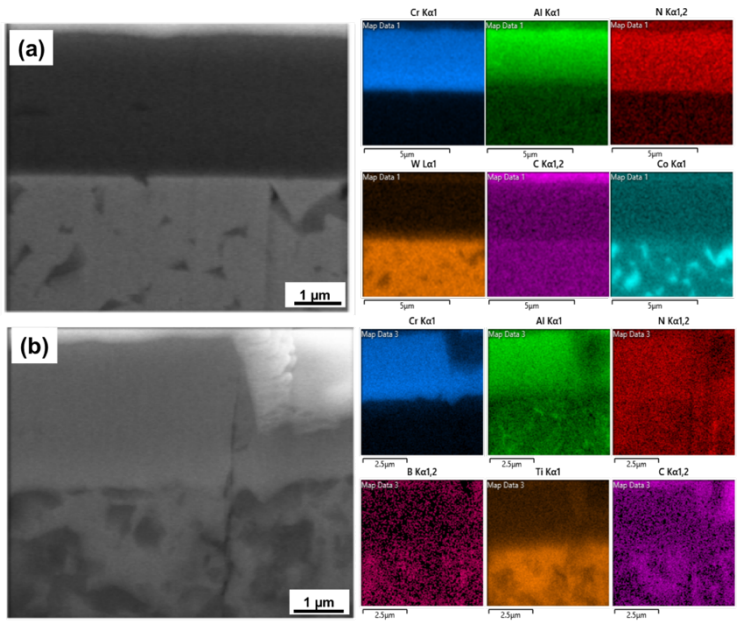

Figure 7-15. SEM micrograph of the cross-section and the EDX composition maps for corresponding areas. (a) AlCrSiN coating deposited on WC-Co substrate, (b) AlCrSiN coating deposited on cBN substrate.

Table 7-7. Elements concentration of AlCrSiN coatings deposited on WC-Co substrate

Element	Al	Cr	Si	N
Concentration	41	13	8	38

The measured thickness of coatings is presented **Table 7-7**, showing similar values for both substrates. Consequently, the geometry is similar, and the results of the mechanical testing can be compared for both substrates.

Table 7-8. Thickness of coating-substrate systems

Coating	AlCrSiN	
Substrate	WC-Co	cBN
Thickness(µm)	3.6 ± 0.4	3.5 ± 0.3

7.2.3.2. Mechanical properties of the coating-substrate systems

The results of nanoindentation are presented in **Table 7-8** and the images of nanoindentation imprints are presented in Figure **7-16**. According to **Table 7-8**, AlCrSiN coating exhibited similar values when deposited on different substrates WC-Co and cBN, which means the mechanical properties of the coating were not altered by the substrate. Some circumferential cracks, showed in **Figure 7-16 (c)**, appeared at the

inner edge of nanoindentation and indicated that the cracking resistance of AlCrSiN coating deposited on cBN substrate maybe lower than the sample with the WC-Co substrate, probably due to the higher stiffness of the substrate.

Table 7-9. Mechanical Properties of coating-substrate systems.

	Material	Hardness (GPa)	Elastic modulus (GPa)	H/E	H^3/E^2
Coating	AlCrSiN on WC-Co	40±5	553±60	0.073	0.211
	AlCrSiN on cBN	39±4	508±52	0.076	0.225
Substrate	WC-Co	31±3	574±54	0.054	0.091
	cBN	36±5	510±90	0.071	0.179

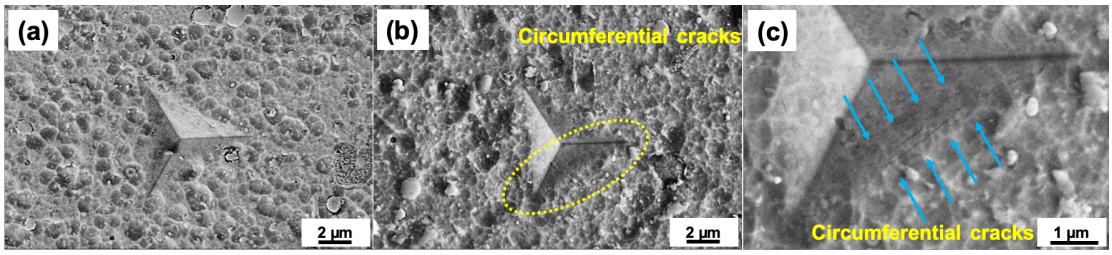

Figure 7-16. SEM images of nanoindentation, (a) AlCrSiN coating deposited on WC-Co substrate, (b) AlCrSiN coating deposited on cBN substrate, (c) magnification of the circumferential cracks highlighted with dotted circle on the image (b).

7.2.3.3. Adhesion test

Figure 7-17 presents the scratch tracks of the two coating-substrate systems obtained by optical microscopy together with the magnification of failure events by SEM. It is seen how plastic deformation, microcracking and delamination are produced as the load is increased. First cracking of the coating (indicated as L_{C1}) is present in both samples. For the WC-Co substrate, stick-slip deformation was induced by compressive stress and appeared at the contour. Along with the load increased, transverse cracks which were induced by tensile stress, until the spallation of the coating; this load is defined as the second critical load (L_{C2}), implying failure of the interface of coating and substrate [220]. Interfacial failure occurred much earlier in the cBN substrate (seen in **Figure 7-17 (b)** and **(c)**) with clear spallation of the coating [167] [221]. Fracture features were also different, with more substrate exposure in the case of cBN.

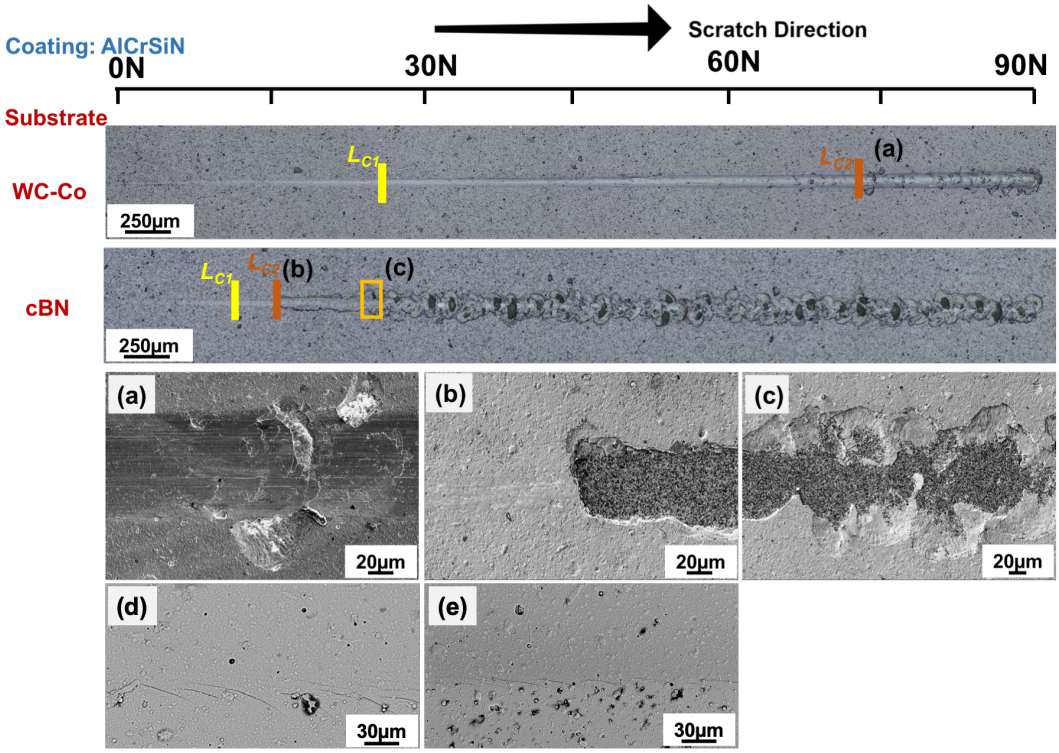

Figure 7-17. The optical profile and SEM images of failure after scratch tests of AlCrSiN coating deposited on WC-Co and cBN two different substrates. The second critical loads (L_{C2}) are magnified at the images of (a) and (b), respectively. (c) was showed the scenario of cBN substrate exposed totally after more the second critical load. The first critical loads (L_{C1}) are magnified at the images of (d) and (e), respectively.

The scratch crack propagation resistance (*CPR*) was calculated to rationalize the scratch resistance of the coatings in the coating-substrate systems, calculated by Equation (10).

$$CPRs = L_{c1}\ (L_{c2} - L_{c1}) \quad (10)$$

where L_{C1} is the first critical load and the start of lateral crack, and L_{C2} is the second critical load and the start of the coating delamination or spallation. The results are presented in **Figure 7-17**.

The critical stress σ_c was calculated by Equation (11) ,

$$\sigma_c = \left(\frac{2L_{c2}}{\pi d_c^2}\right)\left[\frac{(4+\nu_f)3\pi\mu}{8} - 1 + 2\nu_f\right] \quad (11)$$

Where d_c is the track width at L_{C2}, μ is the friction coefficient calculated by the friction force and ν_f is the Poisson ratio of the coatings [222]. The surface energy of the known interfacial crack (adhesion energy) is then defined by Equation (12) [201, 203, 222, 223].

$$G_c = {\sigma_c^2 t}/{2E} \quad (12)$$

Where t and E are the thickness and elastic modulus of coatings, respectively. The values of t and E were experimentally presented from **Table 7-8** and **Table 7-9**, respectively.

The results of *CPRs* and adhesion energy are presented in **Table 7-10**. AlCrSiN coating deposited on WC-Co substrate present higher values of the *CPRs*, which means better scratch resistance. The adhesion energy between AlCrSiN coating and WC-Co substrate was higher than cBN substrate, which illustrate better adhesion strength between the coating and WC-Co substrate. The method of calculation of adhesion energy was followed the previous study of Bull etc. and the values of G_c were similar to previous researches of similar coatings such as CrAlN and AlCrSiN [203, 206, 220, 224].

Table 7-10. Scratch crack propagation resistance and adhesion energy of both coated samples.

Coating	Substrate	CPR (N^2)	G_C (J/m^2)
AlCrSiN	WC-Co	1244±87	357±36
	cBN	48±7	210±20

Figure 7-18 presents the SEM images after Contact damagetest at a series of normal loads of 98 N, 196 N and 294 N. For the sample of AlCrSiN coating deposited on WC-Co substrate, the coating does not show any cracking. At loads of 196 N and higher radial cracking and delamination can be observed. In the case of the cBN substrate, delamination is clearly present even for the smaller loads. As the load increases, more spalling of the coating is observed, similar to previous works in similar materials [41, 225].

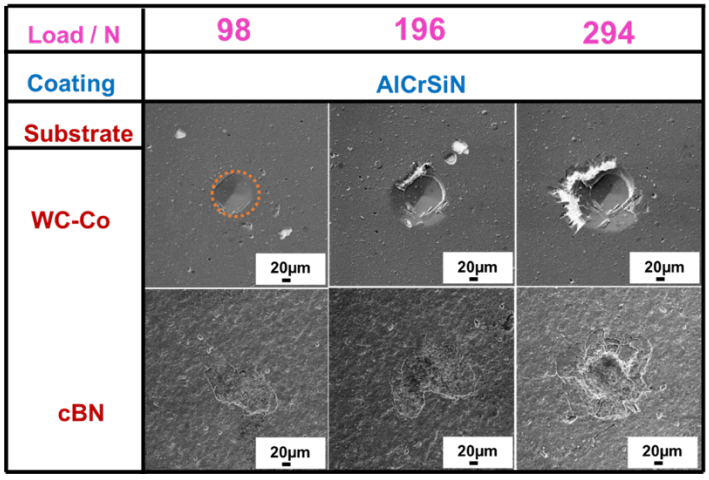

Figure 7-18. SEM images of the Contact damagetest of AlCrSiN coatings at 98 N, 196 N and 294 N with a Rockwell C tip for both substrates. Contact area of the coating on WC-Co for 98 N is indicated.

In order to further inspect the mechanisms of this delamination, lower loads of 9.8 N and 29.4 N were conducted on the cBN substrate sample, and the surface was observed by SEM, as presented in **Figure 7-19**. Under lower normal load, the delamination of AlCrSiN coating appeared on the surface. Cohesive failure of the coating was evident by normal load of 9.8 N, as seen in **Figure 7-19 (a_2)**, where it can be seen that the coating has fractured, without exposing the substrate. However, when the normal load was increased to 29.4 N, the coating was delaminated totally from the cBN substrate, as seen in **Figure 7-19 (b_2)**. The exposure of the cBN substrate indicates that adhesion failure between the AlCrSiN coating and cBN substrate was produced at that load. In any case, this illustrates worse mechanical performance as compared to the WC-Co substrate.

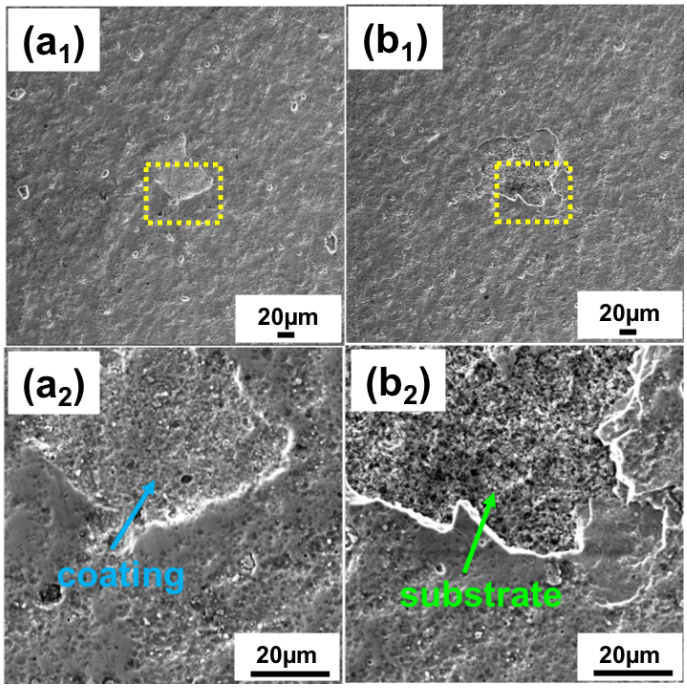

Figure 7-19. SEM images of the Contact damagetest of AlCrSiN coating deposited on cBN substrate with a Rockwell C tip. The failure in (a_1) and (a_2) were under 9.8 N and in (b_1) and (b_2) were at 29.4 N.

7.2.3.4. Mechanical response under contact loading

Both materials were indented by a spherical indenter with monotonic load and cyclic load to investigate the contact mechanical response under different conditions [157, 161, 226]. **Figure 7-20** shows the SEM images of the damage failure induced by

spherical indentation under monotonic loads. The surface of the sample of the cBN substrate presented discontinuous cracks under the monotonic loads of 2000 N. When the load increased up to 3000 N the edge of indentation formed a complete crack circle. However, for the sample deposited on WC-Co, the discontinuous crack and complete ring cracks appeared at larger loads of 5000 N and 6000 N, respectively, which show the form and shape of the cracks over the load of the first damage. In agreement with previous results, the contact resistance of the coating deposited on WC-Co is larger than the coating deposited on the cBN substrate.

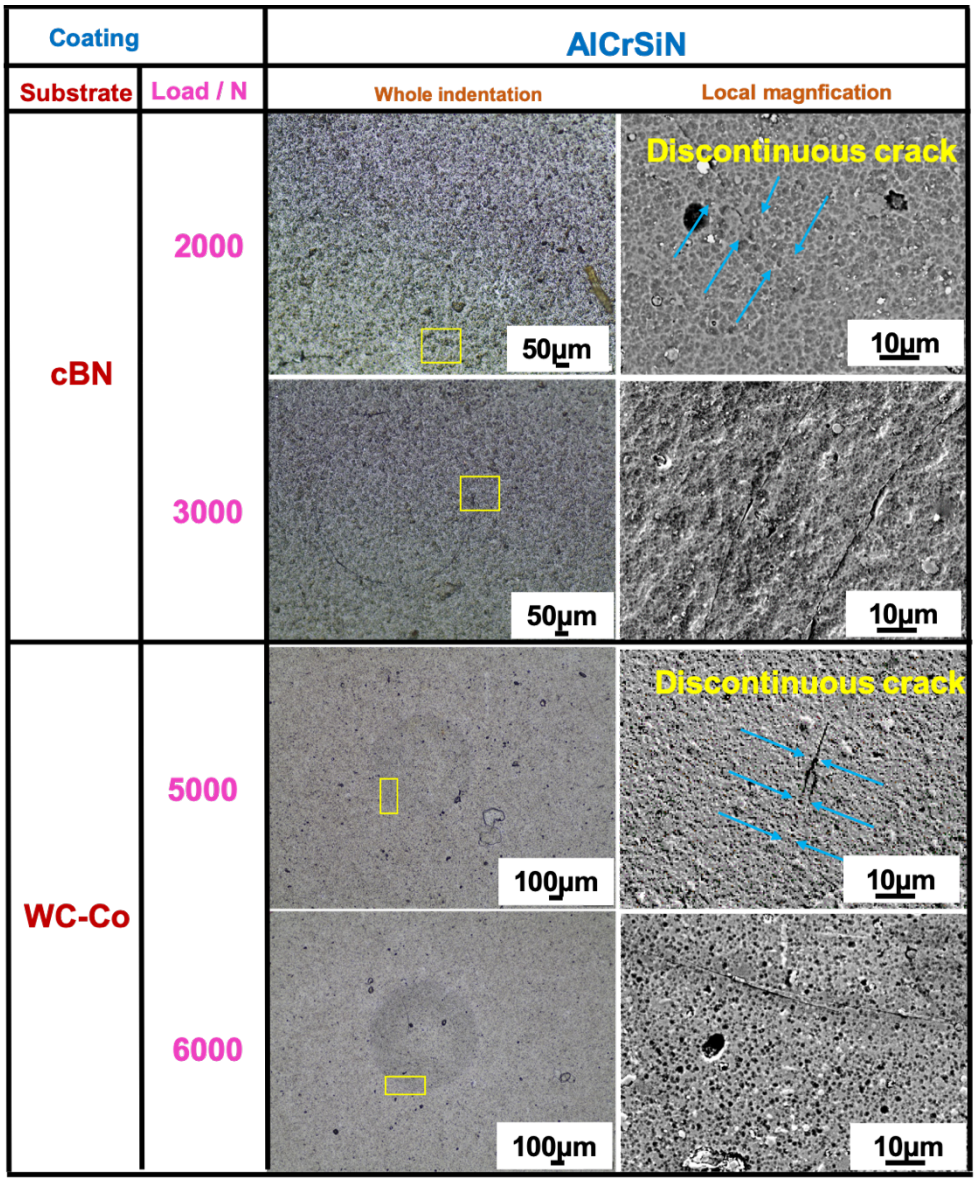

Figure 7-20. SEM images of damage feature of AlCrSiN coating deposited on WC-Co and cBN substrates induced by spherical indentation under different loads (2000 N, 3000 N, 5000 N and 6000 N).

Based on the results, fatigue tests were conducted at the loads causing first damage, that is 5000 N and 2000 N for the sample on WC-Co and cBN substrates respectively, as presented in **Figure 7-21**. For the cBN substrate, the ring crack was fully developed and partial delamination could be observed, as seen in **Figure 7-21 (b_1)**. However, for the WC-Co substrate, the ring crack was not fully developed, even after 10^3 cycles under 5000 N, the same load for appearance of first damage under, as seen in **Figure 7-21 (a_1)**. The results indicate that AlCrSiN coating deposited on WC-Co substrate performed better under contact fatigue than the same coating deposited on cBN substrate.

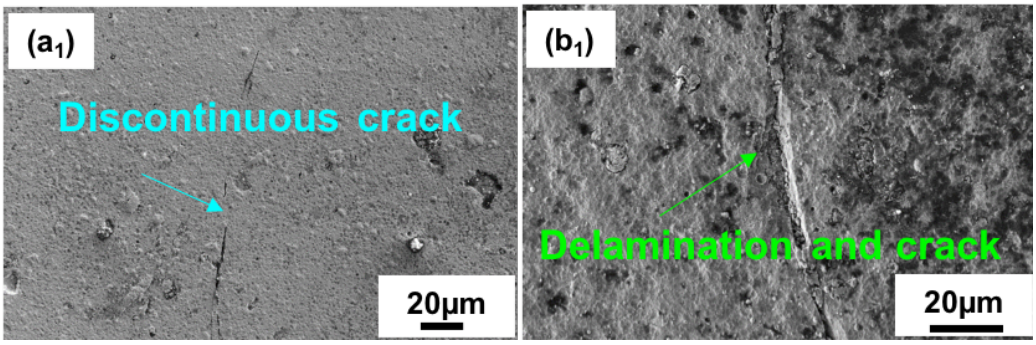

Figure 7-21. SEM images of spherical indentation cyclic loads with 10^3 cycles. (a_1) AlCrSiN coating deposited on WC-Co substrate under the load of 5000 N; (b_1) AlCrSiN coating deposited on cBN substrate under the load of 2000 N.

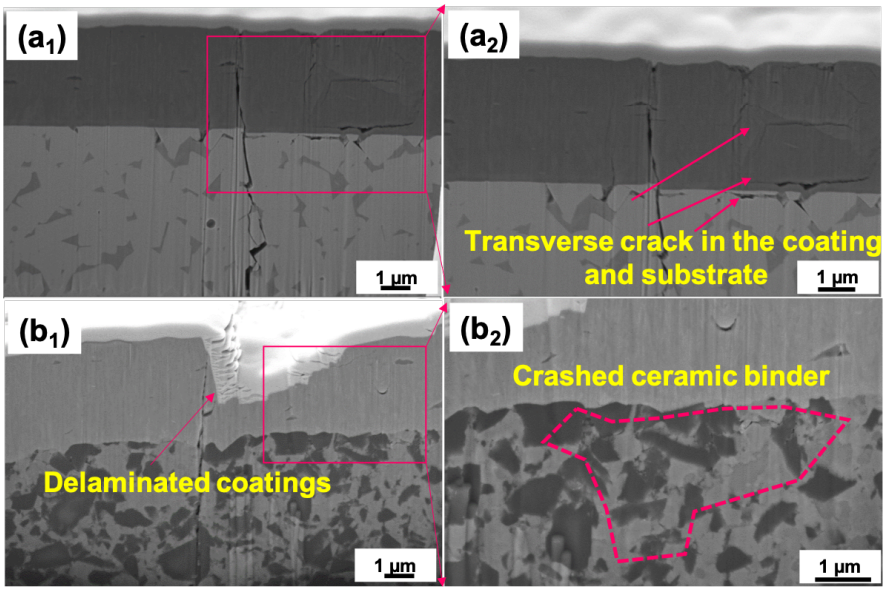

Figure 7-22. Cross-section SEM images of indentations and morphologies of fatigue cracks. (a_1) and (a_2) were presented the sample of AlCrSiN coating deposited on WC-Co substrate under the cyclic load of 6000 N with 10^3 cycles, (b_1) and (b_2) were presented the sample of AlCrSiN coating deposited on cBN substrate under the cyclic

load of 3000 N with 10^3 cycles. (a_2) and (b_2) were the enlarged views of the corresponding areas in the (a_1) and (b_1), respectively.

In order to further explore the direction of crack development caused by fatigue tests, the cross-section at the complete circle crack were done by FIB, as shown in **Figure 7-22**. The ring cracks of the surface penetrated both the AlCrSiN coating and both substrates. For the cBN substrate, a part of the coatings was removed from the surface, as seen in **Figure 7-22 (b_1)**, a delaminated area of coating formed a valley shape. However, as seen in **Figure 7-21 (b_1)**, the coatings were spalled from the cBN substrate completely, indicating that cohesive and adhesive failure of the coating coexisted under contact fatigue loading. As seen in **Figure 7-22 (b_2)**, the ceramic binder of cBN substrate suffered by microcracking due to the cyclic loads. For the sample deposited on WC-Co substrate, only some transverse cracks appeared in the coating and substrate which kept the original morphologies, as seen in **Figure 7-22 (a_1)** and **(a_2)**, the overall shape of coating-substrate system remained intact and transverse cracks only appeared inside the coating but not the interface. Another interesting phenomenon can be observed in **Figure 7-22 (b_1)** and **(b_2)**, the interface between AlCrSiN coating and cBN substrate was not flat and kept the tortuous morphology of the surface of cBN substrate. Multiple cracks were observed in the ceramic binder of the cBN substrate, and the substrate appeared to be crushed along with the periphery of the boron nitride particles.

7.2.4 Discussion

From the above presented results, it is clear that coatings deposited on cBN, have a lower mechanical performance as compared with the same coatings deposited on WC-Co substrates. Adhesion strength, as measured by scratch testing, is lower, implying that the coating delamination is easier in this substrate. In addition, different fracture features are evident for both substrates.

This lower adhesion can be partially attributed to the difference in chemical nature of both substrates. However, it is also seen that the structure integrity of the coating is also more affected when deposited on cBN substrate under contact loadings, albeit having the same composition and intrinsic mechanical properties such as hardness and elastic modulus. In this sense, the difference in mechanical properties of the two substrates induce different contact damage response and damage evolution with increasing loads (as seen in **Figure 7-20** and **7-21**). As seen in **Table 7-8**, cBN is harder than the WC-Co. If the contact loading is done at relative high loads (such as the Contact damageand

scratch tests) deformation will be a combined response of both coating and substrate. Because of its higher hardness of cBN substrate, the deformation will be concentrated close to the surface, which will lead to a larger amount of microcracking in order to accommodate the deformation [227]. This results are in agreement with Sveen et al. [215], who also observed much lower scratch resistance and different damage mechanisms for the cBN substrate. In the case of contact loads, the results are also in agreement with works of S.Gordon et al. [215] who studied TiN/TiAlN coated cBN under contact loads, the failure appear near the interface between AlCrSiN coating and the cBN substrate. In **Figure 7-22** it is seen in the FIB cross section the existence of microcracking of the substrate, which can explain the failure of the substrate observed by these authors and in this work as well.

From the above results, it is clear that the contact resistance of coated hard materials is a multifaceted issue, in which the microstructure of both coating and substrate, as well as the interfacial adhesion play a key role.

7.2.5 Conclusions

The mechanical performance of AlCrSiN coating deposited on WC-Co and cBN two different substrates have been characterized comparatively. Main conclusions could be summarized as:

(1) Nanoindentation results show the same value of mechanical properties and thickness of the coatings when deposited on both substrates as well as chemical compostion. The crystal structure of AlCrSiN coating deposited on different substrates was mainly (Cr,Al)N solid solution. Si was not detected by XRD due to its small amounts relatively or the formation of an amorphous phase. Therefore the coating structure is not affected by the substrate.

(2) Through microscratch tests, AlCrSiN coating deposited on WC-Co substrate presented better adhesion than deposited on cBN substrate. This is further evidenced by the Contact damage tests, where a part of AlCrSiN coating detached totally from the cBN substrate at 29.4 N but the delamination of AlCrSiN coating on the cBN substrate appeared at 294 N.

(3) The results of mechanical response under contact Hertzian loads were presented that AlCrSiN coating deposited on WC-Co substrate perform better resistance of

monotonic loads and cyclic loads than deposited on cBN substrate. Through SEM and FIB, cohesive and adhesive failure of AlCrSiN coating were observed under cyclic loads when deposited on WC-Co and cBN substrate, respectively.

(4) The difference in mechanical performance of the same coating deposited on different substrates depend on both the adhesion strength and the distinct mechanical properties of the substrate.

7.3 Assessment of the mechanical performance of AlCrSiN coating implanted with Zr and Ta ions

The aim of this study was to investigate the mechanical properties of AlCrSiN quaternary coating deposited on WC-Co cermet hard substrate, with surface modification by Zr/Ta ion implantation. Nanoindentation was utilized to measure the intrinsic hardness and elastic modulus of the coatings, while microindentation with a Vickers indenter was employed to observe the evolution of contact damage and measure the Vickers hardness of coating-substrate systems. Adhesive strength between coating and substrate was determined using both scratch and Contact damage tests with progressive and static normal loads, respectively. Scanning electron microscopy (SEM) and optical microscopy were employed to inspect the surface damage induced by different mechanical contacts. The mode and extent of failure were detected by producing cross-sections of coating-substrate system using focus ion beam (FIB) techniques. The results indicate that Zr/Ta ion implantation of AlCrSiN coating leads to the improved mechanical performance and structure integrity under loading conditions that are similar to the service. [3]

7.3.1 Introduction

Hardmetals are materials composed by a hard WC phase, bonded by a metal alloy, generally cobalt and are widely used in industrial tools like forming, cutting and milling due to their exceptional mechanical properties, exhibiting high hardness and high fracture toughness, which result in a high wear resistance [6, 209, 228] and mechanical reliability [229-231]. High-performance cutting tools make then full use of the advantageous properties of hard metals increasing the wear machining and manufacturing could be done by depositing a hard ceramic coatings increasing the lifetime of cutting tools [220, 232].

[3] This chapter corresponds to the paper:

Assessment of the mechanical performance of AlCrSiN coating implanted with Zr and Ta ions. J. Liang[1,*], L. Ortiz-Membrado[1], J. Orrit-Prat [3], R. Bonet [3], J. Caro [3], J. Fernández de Ara[4], E. Almandoz[4,5], Q.D. Ruan[6], R.K.Y. Fu[6], P.K. Chu[6], L. Llanes[1,2] E. Jiménez-Piqué [1,2] , Currently under submission.

Quaternary coating system, like AlCrSiN AlTiSiN AlCrBN, are based on traditional metal nitride ceramic coatings (like CrN, TiN) with the introduction of other element to enhance the mechanical properties, especially hardness, thermal stability, oxidation resistance and wear resistance [59, 60, 233]. AlCrSiN coating is one of the most used coatings to protect cutting tools and further to expand the service life under severe working conditions [234]. The structure of AlCrSiN coating is generally columnar with columns of (Al,Cr)N with a small amount of amorphous SiN_x at the column boundaries which inhibit the growth of crystalline (Al,Cr)N and promotes the enhancement of the hardness of the coating [235, 236].

Ion implantation has been proven to be an effective technique for enhancing the mechanical properties of cemented carbide materials and PVD hard coatings deposited on them. For example, in a study by Shum et al. [117], TiAlN coatings were deposited on Ti-implanted WC-Co substrates that had undergone pretreatment. The formation of TiC alloy phase resulted in an increase in the hardness of the implanted substrate, leading to the improved adhesion and mechanical support for the TiAlN coating, and better performance in a turning test. Similarly, in another study by Fu et al. [237], N, Mo and Mo&W implantation was applied to ternary carbide WC-TiC-Co materials, resulting in the improved hardness and the wear resistance. This was achieved through the formation of tungsten nitride, titanium nitride and molybdenum carbide in the WC-TiC grains in a solid-state precipitate phase or nanoclusters. In addition, Ortiz et al. [238] also studied the effect of ion implantation in hard substrates. As a result, the treated cermets were better able to absorb the impact energy of external loads.

Ion implantation has been extensively applied on TiN PVD hard coatings. Early work of Mitsuo et al. demonstrated the improvement of high-temperature oxidation resistance of TiN coatings by Al implantation due to the formation of Al oxides [239]. Wang et al. [240] have demonstrated that AlN and/or ternary TiAlN are formed as result of Al ion implantation or TiN. Carbon implantation of TiN has been found to increase the hardness in the near-surface region, owing to the formation of TiC and TiCN. Additionally, the friction coefficient is considerably reduced by the formation of a carbonaceous layer on the surface, which serves as a solid lubricant [241]. In a study by Deng et al. [242] similar results were observed with the Nb and C implantation of TiN, where the formation of NbN, Nb_2O_5, and TiC phases resulted in an increase in hardness due to strain hardening effect caused by lattice mismatch. Similarly, vanadium implantation of TiN coatings led to the generation of hard VN and TiVN compounds [243]. Zr implantation, on the other hand, has been shown to enhance the corrosion

resistance of TiN in saline environments [116]. This protection is attributed to the closure of existing pinholes and the formation of various nitrides, oxides and oxynitrides of Ti and Zr. Finally, recent work by Tian et al. [244] has shown that high-doses W implantation of TiN induces a remarkably decrease of the friction coefficient, due to the formation of lubricious tungsten and titanium oxides.

CrN coatings have also been the subject of considerable interest. Weng investigated the effects of C and V implantation on CrN coatings and found that compared to unimplanted samples, ion implantation led to densification of the film, increased compressive residual stress, and hardness, resulting in improved wear and corrosion resistance [245, 246]. Furthermore, Nb, Zr and Cr implantation has been shown to enhance the corrosion resistance of CrN coatings by promoting the formation of different binary and ternary nitrides, oxides, and oxynitrides at the surface [247-249].

The investigation of ion implantation on ternary nitride hard coatings is limited. Boron implantation into TiAlN, for instance, enhances the tribological properties of the coating by producing TiB_2 and BN phases [250]. The improved wear resistance is attributed to the hardening effect of TiB_2, while the lubricious effect of BN leads to a decrease in the friction coefficient. Similarly, Nb implantation on TiAlN coatings improves the wear resistance due to the formation of an amorphous and nanocrystalline structure [251]. Moreover, Nb implantation in TiAlN/CrN nanomultilayer coatings produces NbN and Nb_2O_5, and a small amount of niobium oxynitride in the implanted zone [252]. This results in an increase in hardness and a decrease in friction coefficient due to the amorphous top layer on the surface that acts as solid lubricant during wear sliding.

In contrast, there is a dearth of research on ion implantation of quaternary nitride hard physical vapor deposition (PVD) coatings. However, Chang et al. reported the advantages of Mo and C implantation of CrAlSiN coatings in high temperature wettability by molten glass [118]. Mo carbides were found in the implanted layer of CrAlSiN, while the compressive stress increased by more than two times. The wettability of the implanted films by molten glass at 500ºC decreases due to the presence of an oxide layer consisting of molybdenum, chromium and aluminum oxides on the surface. This makes the films resistant to inter-diffusion between the glass and the coating.

Despite the fact it has been demonstrated that AlCrSiN coatings deposited on WC-Co substrate improve mechanical performance, the impact of ion implantation has not yet been studied [46]. Therefore, this study focus on the mechanics of AlCrSiN quaternary coatings with Zr and Ta ion implantation.

7.3.2 Experimental Procedure

7.3.2.1. Sample Preparation

Zr and Ta were implanted in AlCrSiN coatings by means of MEVVA ion implantation technique. Zr and Ta cathodes (99.95% purity) were evaporated using a pulsed metal cathodic vacuum arc source (MEVVA50, Plasma Technology Limited). In all the processes, the vacuum chamber was pumped down a pressure below $5 \cdot 10^{-4}$ Pa before conducting the ion implantation. The samples were placed on a water cooled and grounded substrate holder. The acceleration ion implantation voltage was 50 kV and the mean beam current was about 5 mA. The treatment time was 4 hours. Taking into account that sample holder area was 20 cm^2, the incident ion dose was estimated to be $2.5 \cdot 10^{17}$ ions/cm^2.

7.3.2.2. Characterization of structure and composition

The crystallographic phase of the coating and interface was characterized by glancing incident angle X-ray diffraction (GIXRD) with Cu X-ray tube (up to 40 kv and 40 mA) radiation (D8 Advance, Bruker) in Bragg-Brentano configuration for grazing incidence. A scintillation detector with some soller mirrors to converge the diffracted rays onto the detector was used. A fixed incident angle was adopted as 1° scan size from 20° to 70°.

The chemical bond of coatings was determined by X-ray photoelectron spectroscopy (XPS) using a SPECS system equipped with a XR-50 high intensity X-ray source with a twin anode of Al or Mg, with 1253 eV and 1457 eV respectively. The Al anode was selected a 150W and using a Phoibos 150 MCD-9 XP detector (SPWCS, Berlin). C 1s peak (284.5 eV) was chosen as a calibration for all spectra. The plot of Cr 2p and Al 2p elements were deconvoluted after the measurement.

7.3.2.3. Nanoindentation and microindentation

An MTS nanoindenter XP equipped with a continuous stiffness measurement module was used to perform indentations at a constant rate strain (0.05 s^{-1}) with a Berkovich

tip calibrated against fused silica. 25 indentations were conducted on the surface of all samples with a maximum penetration depth of 2000nm. The separation distance was kept 50 μm to avoid the overlap between neighboring indentations. The results were analyzed by Oliver and Pharr Method [139].
Vickers hardness was measured by Vickers Testwell FV-700. The average and standard deviation for each sample under five different loads (9.8 N, 49 N, 98 N, 196 N and 294 N) and calculated by Equation (13):

$$H_V = 1.854P/d^2 \qquad (13)$$

Where P is the applied load and d is the diagonal of projection of the imprints.

7.3.2.4. Adhesion

Adhesion strength was evaluated by scratch testing and contact damage test. For a scratch test, a Rockwell C diamond was used, with a scratch length of 5 mm and an increasing load from 0.9 N to 120 N, at a constant rate of 10 N/min . The first appearance of failure was cohesive failure, labelled (L_{c1}), and the second was adhesive failure, labelled (L_{c2}), following the standard ASTM-C1624 [167]. Damage was observed by SEM.

For the Contact damage test, a Rockwell C tip applied on surface with a constant load in order to see deformation, cracks and spallation [165]. Five loads were used: 98 N, 196 N, 392 N, 613 N, and 980 N so as to create different damage scenarios.

7.3.2.5. Microscopy

Images were obtained by an optical microscopy and SEM microscopy, using a PhenonXL and a ZeissNeon 40 SEM/FIB. Cross sections were obtained by Focus Ion Beam (FIB) using decreasing currents for milling down to 500pA as the final polishing procedure. A Platinum layer was deposited on the position of interest to prevent waterfall effect during milling processing.

7.3.3 Results and discussions

7.3.3.1. Characterization and mechanical properties of the coated materials

Zr The thickness of coating was measured by the SEM images of cross section after FIB and the roughness of the surface was measured by the confocal microscope, as presented in **Table 7-11**. *RSa* is the arithmetical mean height of surface and *RSz* is the maximum height of surface.

The hardness of AlCrSiN coatings with ion implantation present lower values (around 22 GPa) than the samples without ion implantation (around 34 GPa). The hardness value of the coating is obtained by measuring the hardness at a penetration depth around 1/10 of the thickness of the coating [253-255]. Elastic The elastic modulus was calculated by extrapolating the results to zero depth, as recommended by IOS 14577. The trend of hardness through ion implantation is consistent with the conclusion of previous studies that hardness is generally lowered by implantation, attributed to the formation of other crystalline phases the surface of the material after ion implantation [45, 256].Elastic modulus of sample without ion implantation is 553 GPa but the values of elastic modulus after ion implantation are significantly less than those of the non-implanted sample.

Table 7-11. Thickness and roughness of coated samples.

No.	Coating: AlCrSiN		Thickness (μm)	Roughness(μm)	
	Substrate	Element implanted		RSa	RSz
S1	WC-Co	--	0.88 ± 0.10	0.048 ± 0.003	4.9±0.6
S2	WC-Co	Zr	0.72 ± 0.07	0.035 ± 0.003	2.6±0.7
S3	WC-Co	Ta	0.92 ± 0.08	0.044 ± 0.002	3.5±0.2

Table 7-12. Mechanical Properties of coated samples.

No.	Coating: AlCrSiN		Hardness (GPa)	Elastic Modulus (GPa)	H/E	H^3/E^2
	Substrate	Element implanted				
S1	WC-Co	--	34.0 ± 5.0	553 ± 55	0.061	0.129
S2	WC-Co	Zr	21.0 ± 0.5	492 ± 64	0.043	0.038
S3	WC-Co	Ta	22.5 ± 0.4	461 ± 82	0.048	0.052

The Vickers hardness of AlCrSiN coatings deposited on WC-Co without ion implantation was about 21 ± 1 GPa. For the sample with Ta ion implantation the value was GPa and for the case of the Zr ion implantation was 18 ± 1 GPa measured at 1 kg. It has to be taken into account that the deformation under the Vickers loads will be also governed by the substrates. In **Figure 7-23**, details of the indentation imprints produced by Vickers indentation are presented. It is seen how, the sample without ion implantation produce spalling of the coating, while the indentations on the samples with ion implantation only show a small amount microcracking.

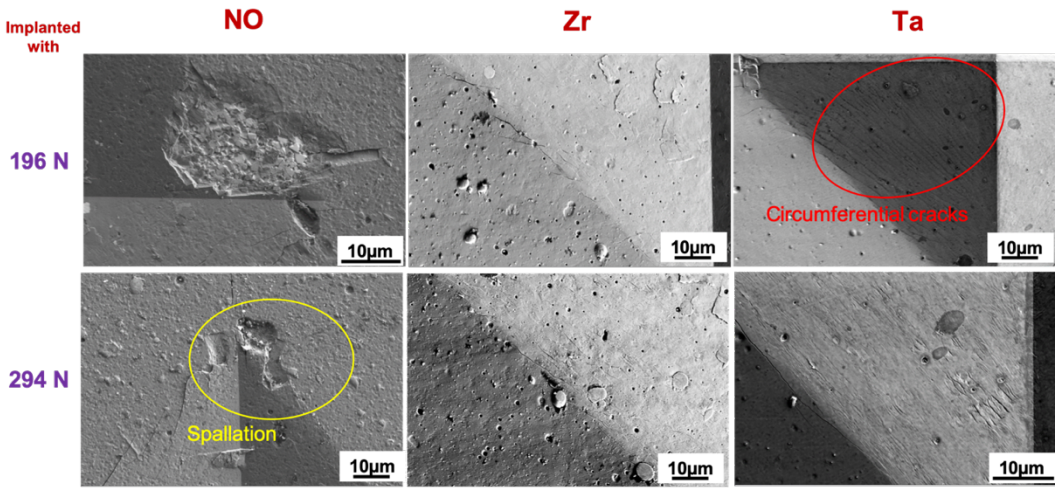

Figure 7-23. Details of the Vickers imprints of the different materials at 196 N and 294 N. Spallation is clearly seen on the reference materials, while the ion implanted coatings only present narrow microcracking.

The XRD spectra of the materials are presented in **Figure 7-24**. The detected phases for all samples were (Cr,Al)N solid solution (JCPDS 76-2494 and JCPDS 25-1495) and WC (JCPDS 72-0097). The (111), (200) and (220) peaks of (Cr,Al)N are shifted about 0.2 degrees due to the substitution of Cr atoms by Al atoms [218] which induce lattice parameter expansion [217]. For the coating with Zr ion implantation, partial formation of zinc-blende(zb)-AlN is also detected (JCPDS 80-0010) [257]. The width of the (200) peak without ion implantation is wider than with Zr or Ta ion implantation, as shown in **Figure 7-24 (b)**, which is induced by the (110) orientation of Cr grain. Because of the relative low amount of silicon (less than 5%) present in the coatings no associated crystalline phases associated with this element were detected.

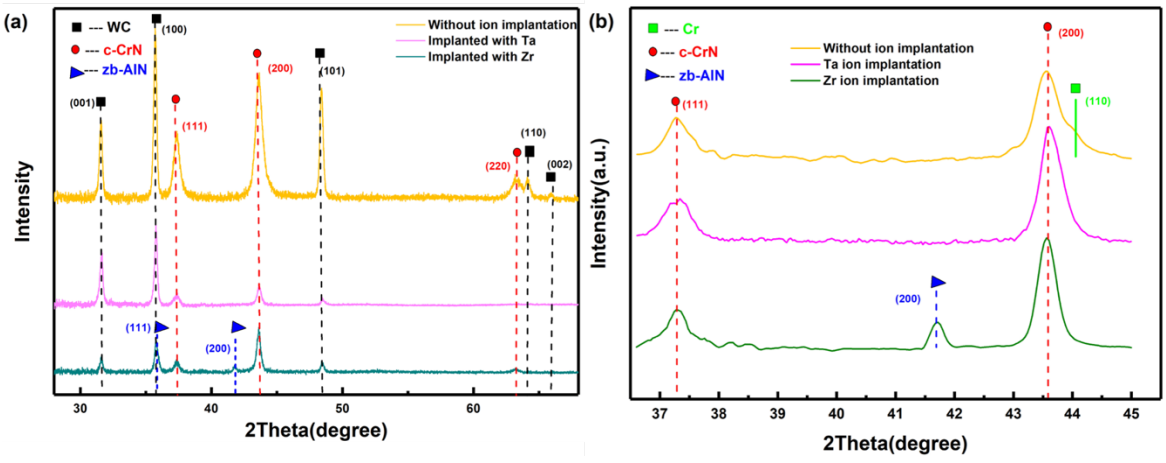

Figure 7-24. XRD patterns of AlCrSiN coatings deposited on WC-Co substrates with Zr or Ta ion implantation (a) and the detailed peaks range from 37°to 45°(b).

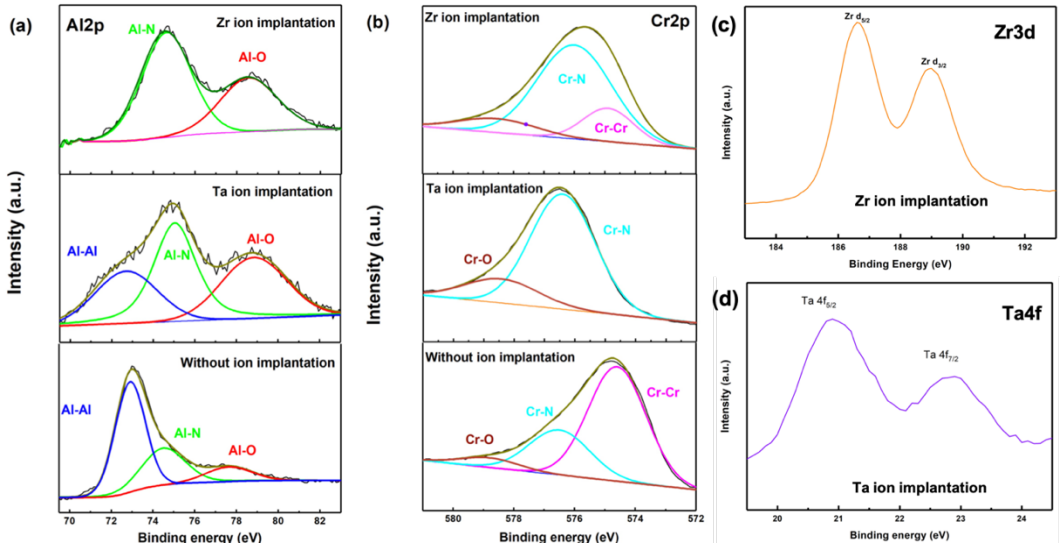

Figure 7-25. XPS wide scan for AlCiSiN coatings deposited on WC-Co substrate with various ion implantation and high-resolution elemental analysis of (a) Al 2p and (b) Cr 2p (c) Zr 3d (d)Ta 4f.

Chemical bonding analysis and the elemental concentration determination were performed using X-ray photoelectron spectroscopy (XPS), as illustrated in **Figure 7-25** and **Table 7-13**. Deconvolution of the Al 2p and Cr 2p resulted in three compositions: Al-Al at 72.3 eV, Al-N at 73.8 eV, Al-O 74.8 at eV, Cr-Cr at position 574.3 eV, Cr-N at 576.3eV and Cr-O at 578.5 eV respectively [128]. The proportion of Al-N and Cr-N bonds increased after Zr or Ta ion implantation, as inferred from the sub-peak of Al 2p and Cr 2p, suggesting that the pure metal bonds, both for Al-Al and Cr-Cr phase, were transformed into metal-nitride bonds. The relatively high amount of Cr-Cr bonds in the unimplanted samples is consistent with the results of the X-ray diffraction (XRD) results. Ta ion implantation reduced the Al / Cr ratio [129], as shown in **Table 7-13**, leading to the formation of h-AlN, facilitating the formation of (Cr,Al)N solid solution and the crystal structure of coatings. The concentration of carbon in the unimplaned sample was very high (arrived at 52%), exceeding that in the sample after ion implantation both Zr and Ta, indicating that surface etching was not performed to eliminate the physically adsorbed carbon, which is a common practice in XPS measurements. Zr and Ta ions were bound to oxygen and nitride, respectively, as revealed by XPS analysis of the Zr 3d and Ta 4f spectra (**Figure 7-25 (c)** and **(d)**), Zr-O at 187eV [258] and Ta-N at 23 eV [259], respectively.

Table 7-13. Element concentration of AlCrSiN coatings with various ion implantation.

Sample	Element concentration (at.%)								
	Al	Cr	Si	N	O	Co	Zr	Ta	C
Without ion implantation	13.33	3.82	2.98	11.85	15.37	0.4	---	---	52.25
Implanted with Zr	12.59	8.1	0.55	2.18	29.47	0.22	8.3	---	38.6
Implanted with Ta	14.06	5.32	1.29	11.44	26.04	0.24	---	7.56	34.04

7.3.3.2. Adhesion

The optical images of the scratch tracks and magnified failure events as observed by SEM for the three materials as shown in **Figure 7-26**. The critical loads, L_{c1} and L_{c2}, are also indicated in the figure . L_{c1} is the first critical load and corresponds to cohesive failure characterized by the formation of ring cracks on the coatings. At higher loads, the second critical load, L_{c2}, is reached. This critical load corresponds to adhesive failure of the coating, resulting in spalling and delamination. The failure mode for samples implanted with Zr and Ta showed similar failure loads and fracture surfaces. In both cases, the loads were significantly higher than the sample without ion implantation, indicating that samples with ion implantation exhibited better resistance under a progressive sliding normal load. Additionally, the spalling of the sample without ion implantation was more severe than the samples with ion implantation, suggesting better fracture resistance. Among the ion implanted samples, the Ta-implanted sample showed the highest resistance to scratch.

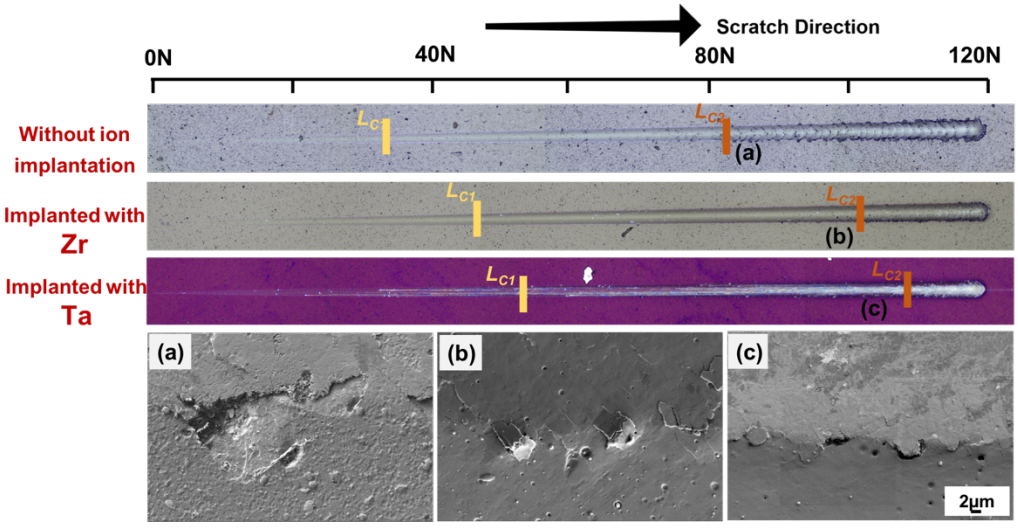

Figure 7-26. Adhesion optical profile and SEM image of failure of AlCrSiN coatings after microscratch tests.

FIB cross sections were conducted to observe the damage resulting from scratch testing at the location where a load of 90N was applied, inducing damage for all samples. **Figure 7-27** shows the SEM images of the cross section. The reference coating exhibited extensive cracking in both the coating and substrate, along with evident delamination. In contrast, the Zr-implanted coating displayed some cracking in the substrate, but the coating surface did not exhibit cracking, and incipient delamination was observed. Furthermore, in the case of the Ta-implanted coating, very minimal damage was appreciated in the substrate, and the coating maintained its structural integrity. As a result, the AlCrSiN coating implanted with Ta, deposited on WC-Co substrate, demonstrated a better adhesion.

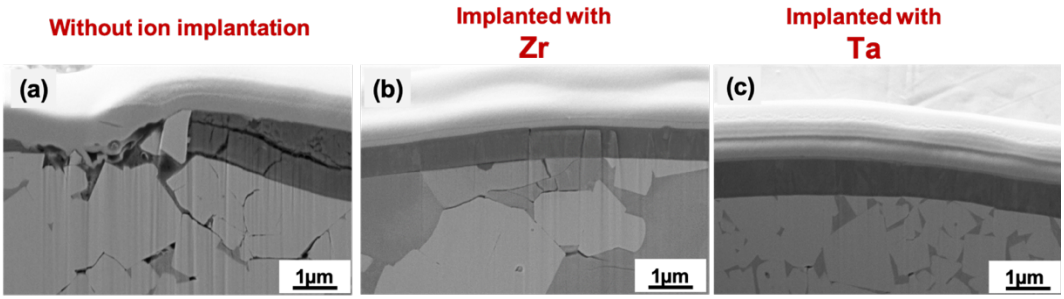

Figure 7-27. Cross-section SEM images of scratch about 90N of AlCrSiN coating (a) without implanted (b) implanted with Zr (c) ion implantation with Ta deposited on WC-Co substrate.

Contact damage test was also done to confirm the improved adhesion of the ion implanted materials. **Figure 7-28** shows the results of the test, where the untreated material exhibited delamination starting at a load of 196N. On the other hand, the coatings with ion implantation did not show apparent damage at that load for the sample with Ta ion implantation. However, for the sample with Zr ion implantation, a small area of coating delamination was observed to the right of the footprint, which was much smaller compared to the sample without ion implantation under the same loading conditions. The delamination for both ion treatments started at higher loads and the area was much smaller. In the case of Ta ions, delamination was only observed at 980 N and with a very small surface. These results are consistent with the previous result of the scratch test. Additionally, in all the images and samples, chipping phenomena of the coating were formed on the right side of the tracks, which would indicate a possible misalignment of the indenter with respect to the sample.

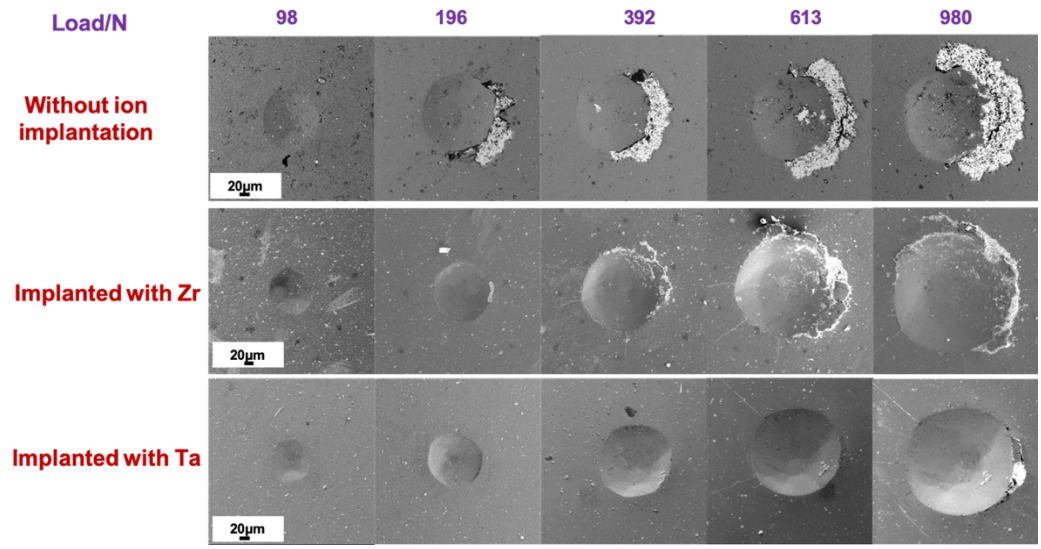

Figure 7-28. SEM of Contact damage test at different load with Rockwell C tip of AlCrSiN coatings deposited on WC-Co substrates with Zr or Ta ion implantation and no ion implantation.

To further observe the failure after 980 N, images obtained by SEM are presented in **Figure 7-29**. The WC-Co substrate was exposed for all samples but the coating remained more adhered for the samples with ion implantation, meaning that the coating presents a better adhesive strength after ion implantation.

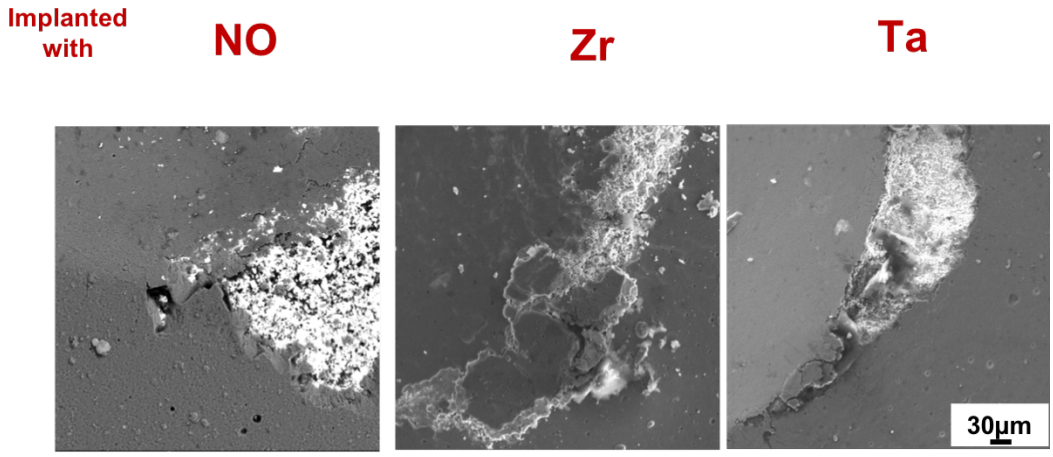

Figure 7-29. SEM of Contact damage test at 980N with Rockwell C tip of AlCrSiN coatings deposited on WC-Co substrates with Zr or Ta ion implantation and no ion implantation.

Using the results of the scratch of the scratch testing, the critical stress for spallation σ_c was calculated by [201, 203] Equation (14).

$$\sigma_c = \left(\frac{2L_{c2}}{\pi d_c^2}\right)\left[\frac{(4+\nu_f)3\pi\mu}{8} - 1 + 2\nu_f\right] \qquad (14)$$

where d_c is the width of track at L_{c2}, μ is the friction coefficient was obtained from the scratch test and ν_f is the Poisson rate of coatings, equal to 0.25 followed by [188, 220]. The surface energy of the interfacial crack known is defined by Equation (15):

$$G_c = {\sigma_c^2 t}\Big/{2E_f} \qquad (15)$$

where t is the thickness of the coating, and the E_f is the elastic modulus of coatings .

Table 7-14. Critical load and adhesion energy of coated system.

No.	Coating: AlCrSiN		L_{c1} (N)	L_{c2} (N)	σ_c (GPa)	Gc (J/m^2)
	Substrate	Element implanted				
S1	WC-Co	--	33	81	3.04	69 ± 6
S2	WC-Co	Zr	46	102	3.03	67 ± 7
S3	WC-Co	Ta	52	109	5.01	247 ± 24

Table 7-14 displays the value of critical load L_{c1} *and* L_{c2} obtained from the optical images as well as the critical stress (σ_c) of coatings delaminated or spalled from the substrate and interfacial fracture energy (G_c). The sample of AlCrSiN implanted with Ta sample exhibits the highest adhesive energy with a value of G_c =247 J/m^2 and a critical stress of σ_c = 5.01 GPa, which is in agreement with the results obtained from the CPRs microstratch test.

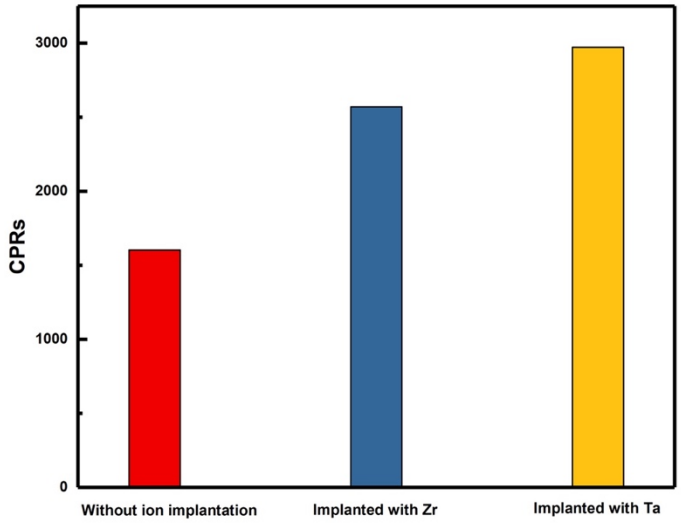

Figure 7-30. Plot of CPRs of scratch tests.

The scratch Crack Propagation Resistance (*CPRs*) was calculated by L_{c1} and L_{c2} is [200]:

$$CPRs = L_{c1}(L_{c2} - L_{c1}) \quad (4)$$

where L_{c1} is the lower critical load, and L_{c2} is the higher critical load.

Figure 7-30 illustrates that the sample with ion implantation exhibited superior results compared to those without ion implantation. Specially, the sample implanted with Ta showed significantly better crack resistance than the one implanted with Zr. This enhanced performance can be attributed to the softening of the material, which allows for better accommodation of deformation under contact loading and scratch testing. In contrast, untreated material must accommodate deformation through cracking and spalling of the coating.

In terms of the coating's crystalline structure, Zr or Ta ion implantation altered the width of the (200) peak of (Cr,Al)N solid solution, leading to the formation of a new phase of zb-AlN as observed through XRD analysis. The diffraction peaks of (Cr,Al)N solid solution shifted towards higher angles by about 0.2 degrees due to residual stress after Zr or Ta ion implantation [260]. Further analysis of the chemical bonds of the AlCrSiN coating showed that Zr or Ta ion implantation facilitates the transfer of metal bonds into metal–nitride bonds and promote the formation (Cr,Al)N solid solution [129]. These structural changes are responsible for the improved mechanical performance after Zr or Ta ion implantation.

7.3.1 Conclusions

In this study, the effect of Zr and Ta ion implantation on AlCrSiN coating deposited on WC-Co substrate was investigated. The following conclusions were drawn:

(1) Nanoindentation tests revealed that the values of coating hardness and elastic modulus decreased after ion implantation, with the values being 21.0 ± 0.5 GPa and 492 ± 64 GPa for Zr, 22.5 ± 0.4 GPa and 461 ±82 GPa for Ta, and 34.0 ± 5.0 GPa and 553 ± 55 GPa for no ion implantation. This result is consistent with previous studies that have reported a degradation of mechanical properties after ion implantation.

(2) The crystal structure AlCrSiN coating remained mostly (Cr,Al)N solid solution regardless of ion implantation, but Zr ion implantation resulted in the formation of a small amount of zb-AlN. The XPS analysis showed that ion implantation transformed the metal bonding of Al-Al and Cr-Cr into Al-N and Cr-N metal-nitride chemical bonding, respectively.

(3) Microscratch and contact damage tests demonstrated that AlCrSiN coating with Zr or Ta ion implantation exhibited better adhesion, with Ta ion implantation showing the best performance. SEM and FIB observations confirmed that the samples without ion implantation suffered more severe damage.

In summary, the ion implantation treatment of AlCrSiN quaternary coatings improved their mechanical performance and structure integrity under loading conditions, such as scratch and contact loading, that are commonly encountered in service.

8 General conclusions

8.1 Summary of results

This doctoral thesis is devoted to investigate the mechanical response of AlCrSiN quaternary coating deposited on different substrates in micro and submicro length scales after thermal treatments or ion implantation on different substrates. The microstructure of AlCrSiN quaternary coating, the adhesion strength between coating and substrate, deformation and damage scenarios under different mode of contact loading and intrinsic mechanical properties are studied. They have been constructed into three parts and the main discoveries are summarized as:

(1) Mechanical properties and contact response of AlCrSiN and AlTiSiN coatings deposited on steel and Inconel have been investigated under thermal treatments at 500 °C and 800 °C. The mechanical properties of coatings were measured at nanometer scale lengths and contact response were documented and analyzed. The information gathered is expected to aid in understanding the evolution of coating-substrate system under thermal treatments.

(2) AlCrSiN and AlTiSiN coatings exhibit better mechanical performance when deposited on Inconel substrate, especially after 500 °C thermal treatment. Adhesion strength is better for AlTiSiN coatings deposited on both steel and Inconel substrates than AlCrSiN coatings. The mechanical performance of all samples was degraded after thermal treatment at 800 °C due changes in microstructure of coatings and substrates.

(3) A comparative study of AlCrSiN coatings deposited on WC-Co and cBN substrates was conducted to characterize and analyze their mechanical performance and response with contact loading. Intrinsic mechanical properties and structure of the coating are nor affected by the substrate. Adhesion strength is better for AlCrSiN coatings deposited on WC-Co substrate than on cBN substrate.

(4) Zr and Ta ion implantation on AlCrSiN coatings deposited on WC-Co substrate have been studied to determine their effect on mechanical properties, microstructure,

and contact response with different loading modes. Ion implantation leads to a degradation of hardness and elastic modulus of the coating, but better adhesion strength with WC-Co substrate. XPS analysis demonstrated the transformation of metal bonding into metal-nitride bonding, influenced by ion implantation

8.2 Future work

The doctoral thesis focused on exploring the mechanical performance and response of AlCrSiN quaternary coating on substrates with different hardness in micro and submicro length scales, with the application of various treatments. The study investigated the evolution of AlCrSiN quaternary coating under different loads in blunt or sharp contact geometry, along with the substrate. The research included the simulation of service-like conditions, which provided valuable insights into desigining and modifying coated materials beyond the coating and substrate interface.

The thesis began with the examination of AlCrSiN quaternary coating on softer substrates, including steel and Inconel, under two temperature thermal treatments. The mechanical performance of AlCrSiN coating was compared to AlTiSiN quaternary coating. In addition, the effect of substrate mechanical properties on the mechanical response of coating-susbtrate system was explored by comparing AlCrSiN quaternary coating hard substrates of WC-Co and cBN. The ion implantation technique was used to modify the interface between coating and substrate, Zr and TA ion implantation were found to improve the mechanical performance of AlCrSiN coating deposited on WC-Co hard substrate.

Future research should consider both the coating and substrate by addressing the following aspects:

① Investigate the properties and response of both hard quaternary coatings and hard substrates under various and complex applied environments, such as high temperature and corrosion during high-speed cutting operations, in order to explore the mechanism that affect the combination of the coating and the substrate.

② Apply the ion implantation method of Zr/Ta to the cBN substrate in order to enhance the mechanical properties of the AlCrSiN quaternary coating and substrate system, as has been done to improve the mechanical strength between AlCrSiN quaternary coating and WC-CO substrate.

③ Introduce other elements, such as Ni and Ti, into AlCrSiN coating deposited on substrates of different hardness to modify the interface between the coating and substrate.

9 References

[1] F. Nabhani, Machining of aerospace titanium alloys, Robotics and Computer-Integrated Manufacturing, 17 (2001) 99-106.
[2] K. Gupta, A review on green machining techniques, Procedia Manufacturing, 51 (2020) 1730-1736.
[3] I. Mukherjee, P.K. Ray, A review of optimization techniques in metal cutting processes, Computers & Industrial Engineering, 50 (2006) 15-34.
[4] J. Niu, C. Huang, C. Li, B. Zou, L. Xu, J. Wang, Z. Liu, A comprehensive method for selecting cutting tool materials, The International Journal of Advanced Manufacturing Technology, 110 (2020) 229-240.
[5] D. Zhou, X. Dai, A granulation analysis method for cutting tool material selection using granular computing, Proceedings of the Institution of Mechanical Engineers, Part C: Journal of Mechanical Engineering Science, 230 (2016) 2323-2336.
[6] D. Mari, L. Miguel, C. Nebel, Comprehensive hard materials, Newnes2014.
[7] Z.Z. Fang, X. Wang, T. Ryu, K.S. Hwang, H. Sohn, Synthesis, sintering, and mechanical properties of nanocrystalline cemented tungsten carbide–a review, International Journal of Refractory Metals and Hard Materials, 27 (2009) 288-299.
[8] J.P. Womack, D.T. Jones, D. Roos, The machine that changed the world: The story of lean production--Toyota's secret weapon in the global car wars that is now revolutionizing world industry, Simon and Schuster2007.
[9] J.P. Davim, Machining of hard materials, Springer Science & Business Media2011.
[10] G. Bartarya, S. Choudhury, State of the art in hard turning, International Journal of Machine Tools and Manufacture, 53 (2012) 1-14.
[11] J. Lima, R. Avila, A. Abrao, M. Faustino, J.P. Davim, Hard turning: AISI 4340 high strength low alloy steel and AISI D2 cold work tool steel, Journal of Materials Processing Technology, 169 (2005) 388-395.
[12] B. Mills, Recent developments in cutting tool materials, Journal of Materials Processing Technology, 56 (1996) 16-23.
[13] M. Hashimoto, What' s New in Roll Technologies of the World?, The Iron and Steel Institute of Japan, Tokyo, Japan, (1995) 59-66.
[14] J.W. Park, H.C. Lee, S. Lee, Composition, microstructure, hardness, and wear properties of high-speed steel rolls, Metallurgical and Materials Transactions A, 30 (1999) 399-409.
[15] L. Liu, Z. Zhao, S. Zhang, T. Yu, G. Yang, Tetragonal Structure BC4 as a Superhard Material, The Journal of Physical Chemistry C, 121 (2017) 10119-10123.
[16] H. Exner, Physical and chemical nature of cemented carbides, International metals reviews, 24 (1979) 149-173.
[17] J. Gurland, New scientific approaches to development of tool materials, International Materials Reviews, 33 (1988) 151-166.
[18] L. Prakash, Fundamentals and general applications of hardmetals, (2014).
[19] H.F. Fischmeister, Conference key note paper development and present status of the science

and technology of hard materials, Science of hard materials, (1983) 1-45.
[20] R. De Vries, Cubic Boron Nitride: Handbook of Properties, Rep. 72CRD178, General Electric Company, Schenectady, NY, 1972.
[21] D. Herzog, Cutting tools with COMPAX diamond and BZN compact inserts slash production time and lower part cost, Cutting Tool Engineering, 29 (1977) 64-66.
[22] J. Angseryd, M. Elfwing, E. Olsson, H.-O. Andrén, Detailed microstructure of a cBN based cutting tool material, International Journal of Refractory Metals and Hard Materials, 27 (2009) 249-255.
[23] P.J. Heath, Properties and uses of amborite[polycrystalline cBN], Industrial diamond review, 46 (1986) 120-127.
[24] A. Chychko, J. Garcia, V.C. Cipres, E. Holmström, A. Blomqvist, HV-KIC property charts of cemented carbides: A comprehensive data collection, International Journal of Refractory Metals and Hard Materials, 103 (2022) 105763.
[25] W.D. Münz, Titanium aluminum nitride films: A new alternative to TiN coatings, Journal of Vacuum Science & Technology A: Vacuum, Surfaces, and Films, 4 (1986) 2717-2725.
[26] H. Awaji, S.-M. Choi, E. Yagi, Mechanisms of toughening and strengthening in ceramic-based nanocomposites, Mechanics of Materials, 34 (2002) 411-422.
[27] S.-Y. Zhang, C.-X. Fang, Y.-P. Tian, K.-R. Zhu, B.-K. Jin, Y.-H. Shen, J.-X. Yang, Synthesis and characterization of hexagonal CuSe nanotubes by templating against trigonal Se nanotubes, Crystal growth & design, 6 (2006) 2809-2813.
[28] I. Jawahir, E. Brinksmeier, R. M'saoubi, D. Aspinwall, J. Outeiro, D. Meyer, D. Umbrello, A. Jayal, Surface integrity in material removal processes: Recent advances, CIRP annals, 60 (2011) 603-626.
[29] R. Sun, T. Tisone, P. Cruzan, The origin of internal stress in low— voltage sputtered tungsten films, Journal of Applied Physics, 46 (1975) 112-117.
[30] D. Bahr, J. Robach, J. Wright, L. Francis, W. Gerberich, Mechanical deformation of PZT thin films for MEMS applications, Materials Science and Engineering: A, 259 (1999) 126-131.
[31] X. Zheng, Y. Zhou, J. Liu, A. Li, Use of nanomechanical fracture-testing for determining the interfacial adhesion of PZT ferroelectric thin films, Surface and Coatings Technology, 176 (2003) 67-74.
[32] E. Klokholm, B. Berry, Intrinsic stress in evaporated metal films, Journal of The Electrochemical Society, 115 (1968) 823.
[33] T. Polcar, A. Cavaleiro, High temperature properties of CrAlN, CrAlSiN and AlCrSiN coatings–Structure and oxidation, Materials Chemistry and Physics, 129 (2011) 195-201.
[34] R. Wang, H. Mei, R. Li, T. Zhang, Q. Wang, Influence of V addition on the microstructure, mechanical, oxidation and tribological properties of AlCrSiN coatings, Surface and Coatings Technology, 407 (2021) 126767.
[35] A. Molinari, M. Pellizzari, S. Gialanella, G. Straffelini, K. Stiasny, Effect of deep cryogenic treatment on the mechanical properties of tool steels, Journal of materials processing technology, 118 (2001) 350-355.
[36] R.M. Raihanuzzaman, Z. Xie, S.J. Hong, R. Ghomashchi, Powder refinement, consolidation and mechanical properties of cemented carbides—An overview, Powder Technology, 261 (2014) 1-13.
[37] A. McKie, J. Winzer, I. Sigalas, M. Herrmann, L. Weiler, J. Rödel, N. Can, Mechanical properties of cBN–Al composite materials, Ceramics International, 37 (2011) 1-8.
[38] K. Drozd, M. Walczak, M. Szala, K. Gancarczyk, Tribological behavior of AlCrSiN-coated tool

steel K340 versus popular tool steel grades, Materials, 13 (2020) 4895.
[39] S.-H. Lee, B.-S. Son, G.-T. Park, J.-S. Ryu, H. Lee, Investigation of short-term, high-temperature oxidation of AlCrN coating on WC substrate, Applied Surface Science, 505 (2020) 144587.
[40] Y. Liu, H.d. Liu, Q. Wan, Y. Cai, H. Chen, Y.m. Chen, J.l. Guo, B. Yang, High-temperature oxidation behaviour of AlTiSiN and AlCrSiN coatings, Surface Engineering, 35 (2019) 652-660.
[41] J. Yang, M. Odén, M.P. Johansson-Jõesaar, L. Llanes, Influence of substrate microstructure and surface finish on cracking and delamination response of TiN-coated cemented carbides, Wear, 352 (2016) 102-111.
[42] S. Gordon, H. Besharatloo, J. Wheeler, T. Rodriguez-Suarez, J. Roa, E. Jiménez-Piqué, L. Llanes, Micromechanical mapping of polycrystalline cubic boron nitride composites by means of high-speed nanoindentation: Assessment of microstructural assemblage effects, Journal of the European Ceramic Society, (2022).
[43] S. Gordon, F. García-Marro, T. Rodriguez-Suarez, J. Roa, E. Jiménez-Piqué, L. Llanes, Spherical indentation of polycrystalline cubic boron nitride (PcBN): Contact damage evolution with increasing load and microstructural effects, International Journal of Refractory Metals and Hard Materials, (2023) 106115.
[44] A.J. Perry, R.R. Manory, L.P. Ward, P.P. Kavuri, The effects of metal ion post-implantation on the near surface properties of TiN deposited by CVD, Surface and Coatings Technology, 133 (2000) 203-207.
[45] R. Manory, C. Li, C. Fountzoulas, J. Demaree, J. Hirvonen, R. Nowak, Effect of nitrogen ion-implantation on the tribological properties and hardness of TiN films, Materials Science and Engineering: A, 253 (1998) 319-327.
[46] S.K. Mishra, S. Ghosh, S. Aravindan, Investigations into friction and wear behavior of AlTiN and AlCrN coatings deposited on laser textured WC/Co using novel open tribometer tests, Surface and Coatings Technology, 387 (2020) 125513.
[47] K. Tuchida, K. Wathanyu, S. Surinphong, Thermal oxidation behavior of TiAlCrSiN and AlCrTiN films on hastelloyX, Advanced materials research, Trans Tech Publ, 2012, pp. 400-405.
[48] Y. Gao, F. Cai, X. Lu, W. Xu, C. Zhang, J. Zhang, X. Qu, Design of cycle structure on microstructure, mechanical properties and tribology behavior of AlCrN/AlCrSiN coatings, Ceramics International, 48 (2022) 12255-12270.
[49] P. Sidky, M. Hocking, Review of inorganic coatings and coating processes for reducing wear and corrosion, British Corrosion Journal, 34 (1999) 171-183.
[50] D. Hong, K. Bae, S.-P. Hong, J.H. Park, I.S. Choi, W.K. Cho, Mussel-inspired, perfluorinated polydopamine for self-cleaning coating on various substrates, Chemical communications, 50 (2014) 11649-11652.
[51] R. Buhl, H. Pulker, E. Moll, TiN coatings on steel, Thin Solid Films, 80 (1981) 265-270.
[52] S. Bhowmick, A. Kale, V. Jayaram, S. Biswas, Contact damage in TiN coatings on steel, Thin Solid Films, 436 (2003) 250-258.
[53] M. Fellah, L. Aissani, A. Zairi, M. Abdul Samad, C. Nouveau, M.Z. Touhami, H. Djebaili, A. Montagne, A. Iost, Thermal treatment effect on structural and mechanical properties of Cr–C coatings, Transactions of the IMF, 96 (2018) 79-85.
[54] Z. Huang, Y. Sun, T. Bell, Friction behaviour of TiN, CrN and (TiAl) N coatings, Wear, 173 (1994) 13-20.

[55] C. Liu, Q. Bi, A. Matthews, EIS comparison on corrosion performance of PVD TiN and CrN coated mild steel in 0.5 N NaCl aqueous solution, Corrosion Science, 43 (2001) 1953-1961.
[56] A. Friedrich, B. Winkler, E.A. Juarez-Arellano, L. Bayarjargal, Synthesis of binary transition metal nitrides, carbides and borides from the elements in the laser-heated diamond anvil cell and their structure-property relations, Materials, 4 (2011) 1648-1692.
[57] J. Mo, M. Zhu, Tribological oxidation behaviour of PVD hard coatings, Tribology International, 42 (2009) 1758-1764.
[58] G. Fox-Rabinovich, B. Beake, J. Endrino, S. Veldhuis, R. Parkinson, L. Shuster, M. Migranov, Effect of mechanical properties measured at room and elevated temperatures on the wear resistance of cutting tools with TiAlN and AlCrN coatings, Surface and coatings technology, 200 (2006) 5738-5742.
[59] S. Spor, N. Jäger, M. Meindlhumer, H. Hruby, M. Burghammer, F. Nahif, C. Mitterer, J. Keckes, R. Daniel, Evolution of structure, residual stress, thermal stability and wear resistance of nanocrystalline multilayered Al0. 7Cr0. 3N-Al0. 67Ti0. 33N coatings, Surface and Coatings Technology, 425 (2021) 127712.
[60] N. Jäger, M. Meindlhumer, M. Zitek, S. Spor, H. Hruby, F. Nahif, J. Julin, M. Rosenthal, J. Keckes, C. Mitterer, Impact of Si on the high-temperature oxidation of AlCr (Si) N coatings, Journal of Materials Science & Technology, 100 (2022) 91-100.
[61] K.-D. Bouzakis, G. Skordaris, S. Gerardis, G. Katirtzoglou, S. Makrimallakis, M. Pappa, E. Lill, R. M'Saoubi, Ambient and elevated temperature properties of TiN, TiAlN and TiSiN PVD films and their impact on the cutting performance of coated carbide tools, Surface and Coatings Technology, 204 (2009) 1061-1065.
[62] K. Kutschej, P.H. Mayrhofer, M. Kathrein, P. Polcik, R. Tessadri, C. Mitterer, Structure, mechanical and tribological properties of sputtered Ti1−xAlxN coatings with 0.5≤ x≤ 0.75, Surface and Coatings Technology, 200 (2005) 2358-2365.
[63] D. Holec, R. Rachbauer, L. Chen, L. Wang, D. Luef, P.H. Mayrhofer, Phase stability and alloy-related trends in Ti–Al–N, Zr–Al–N and Hf–Al–N systems from first principles, Surface and Coatings Technology, 206 (2011) 1698-1704.
[64] D. McIntyre, J. Greene, G. Håkansson, J.E. Sundgren, W.D. Münz, Oxidation of metastable single-phase polycrystalline Ti0. 5Al0. 5N films: Kinetics and mechanisms, Journal of Applied Physics, 67 (1990) 1542-1553.
[65] L. Chen, J. Paulitsch, Y. Du, P.H. Mayrhofer, Thermal stability and oxidation resistance of Ti–Al–N coatings, Surface and Coatings Technology, 206 (2012) 2954-2960.
[66] L. Chen, B. Yang, Y. Xu, F. Pei, L. Zhou, Y. Du, Improved thermal stability and oxidation resistance of Al–Ti–N coating by Si addition, Thin Solid Films, 556 (2014) 369-375.
[67] J.H. Park, W.S. Chung, Y.-R. Cho, K.H. Kim, Synthesis and mechanical properties of Cr–Si–N coatings deposited by a hybrid system of arc ion plating and sputtering techniques, Surface and Coatings Technology, 188 (2004) 425-430.
[68] A. Baptista, F. Silva, J. Porteiro, J. Míguez, G. Pinto, Sputtering physical vapour deposition (PVD) coatings: A critical review on process improvement and market trend demands, Coatings, 8 (2018) 402.
[69] E. Le Bourhis, P. Goudeau, M. Staia, E. Carrasquero, E. Puchi-Cabrera, Mechanical properties of hard AlCrN-based coated substrates, Surface and Coatings Technology, 203 (2009) 2961-2968.
[70] W.J. Clegg, Controlling cracks in ceramics, Science, 286 (1999) 1097-1099.

[71] Y.X. Wang, S. Zhang, Toward hard yet tough ceramic coatings, Surface and Coatings Technology, 258 (2014) 1-16.
[72] C. Baudin, A. Sayir, M.-H. Berger, Mechanical behaviour of directionally solidified alumina/aluminium titanate ceramics, Acta materialia, 54 (2006) 3835-3841.
[73] P. Liu, J. Zheng, Recent developments on damage modeling and finite element analysis for composite laminates: A review, Materials & Design, 31 (2010) 3825-3834.
[74] G. Sundararajan, M. Roy, Hardness testing, Encyclopedia of Materials: Science and Technology, (2011) 3728-3736.
[75] M. Gee, A. Gant, B. Roebuck, Wear mechanisms in abrasion and erosion of WC/Co and related hardmetals, Wear, 263 (2007) 137-148.
[76] M. Gee, A. Gant, W. Byrne, B. Roebuck, Abrasion and reciprocating wear of hardmetals and ceramics, (1999).
[77] Y. Bao, W. Wang, Y. Zhou, Investigation of the relationship between elastic modulus and hardness based on depth-sensing indentation measurements, Acta Materialia, 52 (2004) 5397-5404.
[78] J. Musil, F. Kunc, H. Zeman, H. Polakova, Relationships between hardness, Young's modulus and elastic recovery in hard nanocomposite coatings, Surface and Coatings Technology, 154 (2002) 304-313.
[79] A. Leyland, A. Matthews, On the significance of the H/E ratio in wear control: a nanocomposite coating approach to optimised tribological behaviour, Wear, 246 (2000) 1-11.
[80] J. Malzbender, R. Steinbrech, Determination of the stress-dependent stiffness of plasma-sprayed thermal barrier coatings using depth-sensitive indentation, Journal of materials research, 18 (2003) 1975-1984.
[81] J. Woirgard, J. Dargenton, C. Tromas, V. Audurier, A new technology for nanohardness measurements: principle and applications, Surface and Coatings Technology, 100 (1998) 103-109.
[82] J. Roa, E. Jimenez-Pique, C. Verge, J. Tarragó, A. Mateo, J. Fair, L. Llanes, Intrinsic hardness of constitutive phases in WC–Co composites: Nanoindentation testing, statistical analysis, WC crystal orientation effects and flow stress for the constrained metallic binder, Journal of the european ceramic society, 35 (2015) 3419-3425.
[83] F. Deuerler, O. Lemmer, M. Frank, M. Pohl, C. Heßing, Diamond films for wear protection of hardmetal tools, International Journal of Refractory Metals and Hard Materials, 20 (2002) 115-120.
[84] F. Qin, Y. Chou, D. Nolen, R. Thompson, Coating thickness effects on diamond coated cutting tools, Surface and Coatings Technology, 204 (2009) 1056-1060.
[85] K. Kanda, S. Takehana, S. Yoshida, R. Watanabe, S. Takano, H. Ando, F. Shimakura, Application of diamond-coated cutting tools, Surface and Coatings Technology, 73 (1995) 115-120.
[86] M. Kang, G. Park, J.-G. Jung, B.-H. Kim, Y.-K. Lee, The effects of annealing temperature and cooling rate on carbide precipitation behavior in H13 hot-work tool steel, Journal of alloys and compounds, 627 (2015) 359-366.
[87] D.-s. Ma, J. Zhou, Z.-z. Chen, Z.-k. Zhang, Q.-a. Chen, D.-h. Li, Influence of thermal homogenization treatment on structure and impact toughness of H13 ESR steel, Journal of Iron and Steel Research International, 16 (2009) 56-60.
[88] J.-Y. Li, Y.-L. Chen, J.-H. Huo, Mechanism of improvement on strength and toughness of H13 die steel by nitrogen, Materials Science and Engineering: A, 640 (2015) 16-23.
[89] I. Souki, D. Delagnes, P. Lours, Influence of heat treatment on the fracture toughness and

crack propagation in 5% Cr martensitic steel, Procedia Engineering, 10 (2011) 631-637.
[90] D. Delagnes, P. Lamesle, M. Mathon, N. Mebarki, C. Levaillant, Influence of silicon content on the precipitation of secondary carbides and fatigue properties of a 5% Cr tempered martensitic steel, Materials Science and Engineering: A, 394 (2005) 435-444.
[91] P. Michaud, D. Delagnes, P. Lamesle, M. Mathon, C. Levaillant, The effect of the addition of alloying elements on carbide precipitation and mechanical properties in 5% chromium martensitic steels, ACTA materialia, 55 (2007) 4877-4889.
[92] M. Rahman, W. Seah, T. Teo, The machinability of Inconel 718, Journal of materials processing technology, 63 (1997) 199-204.
[93] E. Hosseini, V. Popovich, A review of mechanical properties of additively manufactured Inconel 718, Additive Manufacturing, 30 (2019) 100877.
[94] H. Qi, M. Azer, A. Ritter, Studies of standard heat treatment effects on microstructure and mechanical properties of laser net shape manufactured Inconel 718, Metallurgical and Materials Transactions A, 40 (2009) 2410-2422.
[95] A. Strondl, R. Fischer, G. Frommeyer, A. Schneider, Investigations of MX and γ′/γ ″precipitates in the nickel-based superalloy 718 produced by electron beam melting, Materials Science and Engineering: A, 480 (2008) 138-147.
[96] L.L. Parimi, G. Ravi, D. Clark, M.M. Attallah, Microstructural and texture development in direct laser fabricated IN718, Materials Characterization, 89 (2014) 102-111.
[97] X. Zhao, J. Chen, X. Lin, W. Huang, Study on microstructure and mechanical properties of laser rapid forming Inconel 718, Materials Science and Engineering: A, 478 (2008) 119-124.
[98] S. Mann, G.A. Ozin, Synthesis of inorganic materials with complex form, Nature, 382 (1996) 313-318.
[99] G.S. Upadhyaya, Cemented tungsten carbides: production, properties and testing, William Andrew1998.
[100] P. Angelo, R. Subramanian, B. Ravisankar, Powder metallurgy: science, technology and applications, PHI Learning Pvt. Ltd.2022.
[101] E. Jiménez-Piqué, M. Turon-Vinas, H. Chen, T. Trifonov, J. Fair, E. Tarrés, L. Llanes, Focused ion beam tomography of WC-Co cemented carbides, International Journal of Refractory Metals and Hard Materials, 67 (2017) 9-17.
[102] H.M. Ortner, P. Ettmayer, H. Kolaska, I. Smid, The history of the technological progress of hardmetals, International Journal of Refractory Metals and Hard Materials, 49 (2015) 3-8.
[103] P. Ettmayer, H. Kolaska, H.M. Ortner, History of Hardmetals, Comprehensive Hard Materials, 1 (2014) 3-27.
[104] M. Zhang, X. Wang, F. Jiao, Y. Niu, S. Chen, Residual stresses in ultrasonic vibration assistance turning cemented carbide, The International Journal of Advanced Manufacturing Technology, (2023) 1-11.
[105] P.K. Katiyar, P.K. Singh, R. Singh, A. Lava Kumar, Modes of failure of cemented tungsten carbide tool bits (WC/Co): A study of wear parts, International Journal of Refractory Metals and Hard Materials, 54 (2016) 27-38.
[106] A. Lisovsky, N. Tkachenko, V. Kebko, Structure of a binding phase in re-alloyed WC Co cemented carbides, International Journal of Refractory Metals and Hard Materials, 10 (1991) 33-36.
[107] J. Tarragó, C. Ferrari, B. Reig, D. Coureaux, L. Schneider, L. Llanes, Mechanics and mechanisms

of fatigue in a WC–Ni hardmetal and a comparative study with respect to WC–Co hardmetals, International Journal of Fatigue, 70 (2015) 252-257.
[108] X. Han, N. Lin, X. Zhang, W. Zhang, Z. Wang, C. Ma, Design and fabrication of bimetallic Co-Ni phosphides on WC-Co-Ni cemented carbide substrate for electrochemical hydrogen evolution reaction, Journal of Alloys and Compounds, (2023) 169603.
[109] G. Gille, J. Bredthauer, B. Gries, B. Mende, W. Heinrich, Advanced and new grades of WC and binder powder–their properties and application, International Journal of Refractory Metals and Hard Materials, 18 (2000) 87-102.
[110] C.J.H. Wort, Applications for superhard and ultra-hard materials, Microstructure-Property Correlations for Hard, Superhard, and Ultrahard Materials, (2016) 25-74.
[111] V. Kanyanta, Microstructure-property correlations for hard, superhard, and ultrahard materials, Springer2016.
[112] A. Eko, O. Fukunaga, N. Ohtake, The microstructure of cBN-metal composites synthesized from hBN with metallic solvents, International Journal of Refractory Metals and Hard Materials, 41 (2013) 73-77.
[113] M. Akaishi, T. Satoh, M. Ishii, T. Taniguchi, S. Yamaoka, Synthesis of translucent sintered cubic boron nitride, Journal of materials science letters, 12 (1993) 1883-1885.
[114] A.J. Perry, Y.P. Sharkeev, D.E. Geist, S.V. Fortuna, Dislocation network developed in titanium nitride by ion implantation, Journal of Vacuum Science & Technology A: Vacuum, Surfaces, and Films, 17 (1999) 1848-1853.
[115] Y.P. Sharkeev, A. Didenko, E. Kozlov, High dislocation density structures and hardening produced by high fluency pulsed-ion-beam implantation, Surface and Coatings Technology, 65 (1994) 112-120.
[116] K. Purushotham, L. Ward, N. Brack, P.J. Pigram, P. Evans, H. Noorman, R.R. Manory, The effect of MEVVA ion implantation of Zr on the corrosion behaviour of PVD TiN coatings, Corrosion Science, 50 (2008) 8-14.
[117] P. Shum, K. Li, Y. Shen, Improvement of high-speed turning performance of Ti–Al–N coatings by using a pretreatment of high-energy ion implantation, Surface and Coatings Technology, 198 (2005) 414-419.
[118] Y.-Y. Chang, H.-M. Lai, H.-Y. Kao, High temperature wettability of ion implanted multicomponent CrAlSiN films by molten glass, Surface and Coatings Technology, 237 (2013) 164-169.
[119] K. Bobzin, High-performance coatings for cutting tools, CIRP Journal of Manufacturing Science and Technology, 18 (2017) 1-9.
[120] K.M. Nasir, N.H.R. Sulong, M.R. Johan, A.M. Afifi, Synergistic effect of industrial-and bio-fillers waterborne intumescent hybrid coatings on flame retardancy, physical and mechanical properties, Progress in Organic Coatings, 149 (2020) 105905.
[121] I. Kartsonakis, E. Koumoulos, A. Balaskas, G. Pappas, C. Charitidis, G. Kordas, Hybrid organic–inorganic multilayer coatings including nanocontainers for corrosion protection of metal alloys, Corrosion Science, 57 (2012) 56-66.
[122] M. Barletta, A. Gisario, M. Puopolo, S. Vesco, Scratch, wear and corrosion resistant organic inorganic hybrid materials for metals protection and barrier, Materials & Design, 69 (2015) 130-140.
[123] F. Mei, Z. Zhijian, Y. Yang, L. Xiaoliang, G. Jiangxiong, Y. Tiechui, L. Jianguo, Microstructure,

mechanical, tribological, and oxidizing properties of AlCrSiN/AlCrVN/AlCrNbN multilayer coatings with different modulated thicknesses, Ceramics International, 48 (2022) 32973-32985.
[124] Y. Chen, H. Du, M. Chen, J. Yang, J. Xiong, H. Zhao, Structure and wear behavior of AlCrSiN-based coatings, Applied surface science, 370 (2016) 176-183.
[125] F. Ahmad, L. Zhang, J. Zheng, I. Sidra, S. Zhang, Characterization of AlCrN and AlCrON coatings deposited on plasma nitrided AISI H13 steels using ion-source-enhanced arc ion plating, Coatings, 10 (2020) 306.
[126] M. Bouroushian, T. Kosanovic, Characterization of thin films by low incidence X-ray diffraction, Cryst. Struct. Theory Appl, 1 (2012) 35-39.
[127] B.v. Brussel, J.T.M.D. Hosson, Glancing angle x-ray diffraction: A different approach, Applied physics letters, 64 (1994) 1585-1587.
[128] J. Chastain, R.C. King Jr, Handbook of X-ray photoelectron spectroscopy, Perkin-Elmer Corporation, 40 (1992) 221.
[129] W. Wu, W. Chen, S. Yang, Y. Lin, S. Zhang, T.-Y. Cho, G. Lee, S.-C. Kwon, Design of AlCrSiN multilayers and nanocomposite coating for HSS cutting tools, Applied Surface Science, 351 (2015) 803-810.
[130] Y. Yang, H. Shang, T. Shao, Influence of nitrogen implantation on adhesion strength of TiAlN film on γ-TiAl alloy, Applied Surface Science, 508 (2020) 145141.
[131] S. Hainsworth, W. Soh, The effect of the substrate on the mechanical properties of TiN coatings, Surface and Coatings Technology, 163 (2003) 515-520.
[132] S. Bull, Nanoindentation of coatings, Journal of Physics D: Applied Physics, 38 (2005) R393.
[133] L. Wang, Y. Wang, X. Sun, Z. Pan, J. He, C. Li, Influence of pores on the surface microcompression mechanical response of thermal barrier coatings fabricated by atmospheric plasma spray—Finite element simulation, Applied Surface Science, 257 (2011) 2238-2249.
[134] A. Pajares, L. Wei, B.R. Lawn, N.P. Padture, C.C. Berndt, Mechanical characterization of plasma sprayed ceramic coatings on metal substrates by contact testing, Materials Science and Engineering: A, 208 (1996) 158-165.
[135] E. Harry, M. Ignat, Y. Pauleau, A. Rouzaud, P. Juliet, Mechanical behaviour of hard PVD multilayered coatings, Surface and Coatings Technology, 125 (2000) 185-189.
[136] P. Fischer, R.M. Schwarz, M. Marinaro, M. Wachtler, L. Jörissen, Investigation of the Electrochemical Oxygen Reduction Reaction in Non-Aqueous, Magnesium-Ion-Containing Electrolytes for Magnesium Air Batteries, ECS Transactions, 75 (2017) 3.
[137] M. Swain, Mechanical property characterisation of small volumes of brittle materials with spherical tipped indenters, Materials Science and Engineering: A, 253 (1998) 160-166.
[138] E. Jiménez-Piqué, Indentation of Ceramics, (2021).
[139] W.C. Oliver, G.M. Pharr, An improved technique for determining hardness and elastic modulus using load and displacement sensing indentation experiments, Journal of materials research, 7 (1992) 1564-1583.
[140] W.C. Oliver, G.M. Pharr, Measurement of hardness and elastic modulus by instrumented indentation: Advances in understanding and refinements to methodology, Journal of materials research, 19 (2004) 3-20.
[141] A. International, ASTM E384-99-Standard Test Method for microindentation hardness of materials, ASTM International West Conshohocken, 1999.
[142] D. Shetty, I. Wright, P. Mincer, A. Clauer, Indentation fracture of WC-Co cermets, Journal of

materials science, 20 (1985) 1873-1882.
[143] H. Li, R. Bradt, The effect of indentation-induced cracking on the apparent microhardness, Journal of materials science, 31 (1996) 1065-1070.
[144] J. Wade, S. Ghosh, P. Claydon, H. Wu, Contact damage of silicon carbide ceramics with different grain structures measured by Hertzian and Vickers indentation, Journal of the European Ceramic Society, 35 (2015) 1725-1736.
[145] K. Fan, J.Y. Pastor, J. Ruiz-Hervias, J. Gurauskis, C. Baudin, Determination of mechanical properties of Al2O3/Y-TZP ceramic composites: Influence of testing method and residual stresses, Ceramics International, 42 (2016) 18700-18710.
[146] B.R. Lawn, Indentation of ceramics with spheres: a century after Hertz, Journal of the American Ceramic Society, 81 (1998) 1977-1994.
[147] R.B. Collier, K.P. Plucknett, Spherical indentation damage in TiC–Ni3Al composites, International Journal of Refractory Metals and Hard Materials, 30 (2012) 188-195.
[148] J. Yang, F.G. Marro, T. Trifonov, M. Odén, M. Johansson-Jõesaar, L. Llanes, Contact damage resistance of TiN-coated hardmetals: Beneficial effects associated with substrate grinding, Surface and Coatings Technology, 275 (2015) 133-141.
[149] C. Jin, K. Plucknett, Hertzian indentation response of TiC-316L stainless steel cermets, International Journal of Refractory Metals and Hard Materials, 72 (2018) 172-182.
[150] I. El Azhari, J. García, F. Soldera, S. Suárez, E. Jiménez-Piqué, F. Mücklich, L. Llanes, Contact damage investigation of CVD carbonitride hard coatings deposited on cemented carbides, International Journal of Refractory Metals and Hard Materials, 86 (2020) 105050.
[151] B.R. Lawn, A.G. Evans, D. Marshall, Elastic/plastic indentation damage in ceramics: the median/radial crack system, Journal of the American Ceramic Society, 63 (1980) 574-581.
[152] J. Roa, E. Jiménez-Piqué, R. Martínez, G. Ramírez, J.M. Tarragó, R. Rodríguez, L. Llanes, Contact damage and fracture micromechanisms of multilayered TiN/CrN coatings at micro-and nano-length scales, Thin Solid Films, 571 (2014) 308-315.
[153] D. Diao, K. Kato, K. Hokkirigawa, Fracture mechanisms of ceramic coatings in indentation, (1994).
[154] J. Von Stebut, R. Rezakhanlou, K. Anoun, H. Michel, M. Gantois, Major damage mechanisms during scratch and wear testing of hard coatings on hard substrates, Thin Solid Films, 181 (1989) 555-564.
[155] P. Steinmann, H. Hintermann, Adhesion of TiC and Ti (C, N) coatings on steel, Journal of Vacuum Science & Technology A: Vacuum, Surfaces, and Films, 3 (1985) 2394-2400.
[156] P. Mehrotra, D. Quinto, Techniques for evaluating mechanical properties of hard coatings, Journal of Vacuum Science & Technology A: Vacuum, Surfaces, and Films, 3 (1985) 2401-2405.
[157] L. Llanes, E. Tarrés, G. Ramírez, C. Botero, E. Jiménez-Piqué, Fatigue susceptibility under contact loading of hardmetals coated with ceramic films, Procedia Engineering, 2 (2010) 299-308.
[158] O. Knotek, B. Bosserhoff, A. Schrey, T. Leyendecker, O. Lemmer, S. Esser, A new technique for testing the impact load of thin films: the coating impact test, Surface and Coatings Technology, 54 (1992) 102-107.
[159] C. Mendibide, P. Steyer, J. Fontaine, P. Goudeau, Improvement of the tribological behaviour of PVD nanostratified TiN/CrN coatings—An explanation, Surface and Coatings Technology, 201 (2006) 4119-4124.
[160] M. Stoiber, M. Panzenböck, C. Mitterer, C. Lugmair, Fatigue properties of Ti-based hard

coatings deposited onto tool steels, Surface and Coatings Technology, 142 (2001) 117-124.
[161] E. Tarrés, G. Ramírez, Y. Gaillard, E. Jiménez-Piqué, L. Llanes, Contact fatigue behavior of PVD-coated hardmetals, International Journal of Refractory Metals and Hard Materials, 27 (2009) 323-331.
[162] B.R. Lawn, Y. Deng, P. Miranda, A. Pajares, H. Chai, D.K. Kim, Overview: damage in brittle layer structures from concentrated loads, Journal of Materials Research, 17 (2002) 3019-3036.
[163] Y. Kayali, S. Taktak, Characterization and Rockwell-C adhesion properties of chromium-based borided steels, Journal of Adhesion Science and Technology, 29 (2015) 2065-2075.
[164] D.B.A. Test, Richtlinien. No. 3198, Verein Deutscher Ingenieure (VDI), VDI-Verlag, Dusseldorf, 1992.
[165] N. Vidakis, A. Antoniadis, N. Bilalis, The VDI 3198 indentation test evaluation of a reliable qualitative control for layered compounds, Journal of materials processing technology, 143 (2003) 481-485.
[166] N. Vidakis, Determination of the fatigue strength of thin hard coatings for the prediction of their life time on hybrid bearings steel races, used in high speed spindles of machine tools, Greece: Aristoteles University of Thessaloniki, (1997).
[167] A. C-05, Standard test method for adhesion strength and mechanical failure modes of ceramic coatings by quantitative single point scratch testing, (2005).
[168] B. Eigenmann, B. Scholtes, E. Macherauch, X-ray residual stress determination in thin chromium coatings on steel, Surface Engineering, 7 (1991) 221-224.
[169] J. Rech, M. Djouadi, J. Picot, Wear resistance of coatings in high speed gear hobbing, Wear, 250 (2001) 45-53.
[170] S. Ma, D. Ma, Y. Guo, B. Xu, G. Wu, K. Xu, P.K. Chu, Synthesis and characterization of super hard, self-lubricating Ti–Si–C–N nanocomposite coatings, Acta Materialia, 55 (2007) 6350-6355.
[171] K. Bobzin, N. Bagcivan, P. Immich, S. Bolz, R. Cremer, T. Leyendecker, Mechanical properties and oxidation behaviour of (Al, Cr) N and (Al, Cr, Si) N coatings for cutting tools deposited by HPPMS, Thin Solid Films, 517 (2008) 1251-1256.
[172] I.-W. Park, D.S. Kang, J.J. Moore, S.C. Kwon, J.J. Rha, K.H. Kim, Microstructures, mechanical properties, and tribological behaviors of Cr–Al–N, Cr–Si–N, and Cr–Al–Si–N coatings by a hybrid coating system, Surface and Coatings Technology, 201 (2007) 5223-5227.
[173] S. Vepřek, S. Reiprich, L. Shizhi, Superhard nanocrystalline composite materials: The TiN/Si3N4 system, Applied physics letters, 66 (1995) 2640-2642.
[174] S. Veprek, M.G. Veprek-Heijman, P. Karvankova, J. Prochazka, Different approaches to superhard coatings and nanocomposites, Thin solid films, 476 (2005) 1-29.
[175] S. Veprek, H.-D. Männling, M. Jilek, P. Holubar, Avoiding the high-temperature decomposition and softening of (Al1− xTix) N coatings by the formation of stable superhard nc-(Al1− xTix) N/a-Si3N4 nanocomposite, Materials Science and Engineering: A, 366 (2004) 202-205.
[176] A.Y. Adesina, Z.M. Gasem, F.A. Al-Badour, Characterization and evaluation of AlCrN coated FSW tool: A preliminary study, Journal of Manufacturing Processes, 25 (2017) 432-442.
[177] T. Leyendecker, O. Lemmer, S. Esser, J. Ebberink, The development of the PVD coating TiAlN as a commercial coating for cutting tools, Surface and Coatings Technology, 48 (1991) 175-178.
[178] M. Van Stappen, L. Stals, M. Kerkhofs, C. Quaeyhaegens, State of the art for the industrial use of ceramic PVD coatings, Surface and Coatings Technology, 74 (1995) 629-633.
[179] G.G. Fuentes, E. Almandoz, R. Pierrugues, R. Martínez, R.J. Rodríguez, J. Caro, M. Vilaseca,

High temperature tribological characterisation of TiAlSiN coatings produced by cathodic arc evaporation, Surface and Coatings Technology, 205 (2010) 1368-1373.
[180] G.G. Fuentes, E. Almandoz, R.J. Rodríguez, H. Dong, Y. Qin, S. Mato, F.J. Pérez-Trujillo, Vapour deposition technologies for the fabrication of hot-forming tools: a review, Manufacturing Rev., 1 (2014) 1-17.
[181] J. Galeja, K. Lukaszkowicz, Comparison of the Structure of AlCrSiN Coating Produced by Planar and Rotating Arc Technology, Solid State Phenomena, Trans Tech Publ, 2019, pp. 141-153.
[182] E. Almandoz Sánchez, Desarrollo de recubrimientos PVD cuaternarios de tipo nitruro, óxido y oxinitruro para aplicaciones de trabajo en caliente, (2017).
[183] L. Aissani, C. Nouveau, M.J. Walock, H. Djebaili, A. Djelloul, Influence of vanadium on structure, mechanical and tribological properties of CrN coatings, Surface Engineering, 31 (2015) 779-788.
[184] M. Vardelle, A. Vardelle, P. Fauchais, Spray parameters and particle behavior relationships during plasma spraying, Journal of Thermal Spray Technology, 2 (1993) 79-91.
[185] R. Wang, H.Q. Li, R.S. Li, H.J. Mei, C.W. Zou, T.F. Zhang, Q.M. Wang, K.H. Kim, Thermostability, oxidation, and high-temperature tribological properties of nano-multilayered AlCrSiN/VN coatings, Ceramics International, 48 (2022) 11915-11923.
[186] Y.-Y. Chang, M.-C. Cai, Mechanical property and tribological performance of AlTiSiN and AlTiBN hard coatings using ternary alloy targets, Surface and Coatings Technology, 374 (2019) 1120-1127.
[187] B. Xiao, T.F. Zhang, Z. Guo, Z. Li, B. Fan, G. Chen, Z. Xiong, Q. Wang, Mechanical, oxidation, and cutting properties of AlCrN/AlTiSiN nano-multilayer coatings, Surface and Coatings Technology, 433 (2022) 128094.
[188] Q. Zhang, Y. Xu, T. Zhang, Z. Wu, Q. Wang, Tribological properties, oxidation resistance and turning performance of AlTiN/AlCrSiN multilayer coatings by arc ion plating, Surface and coatings technology, 356 (2018) 1-10.
[189] Z. Wu, P. Tang, Y. Wu, Q. Wang, Z. Qi, Wear behavior of AlCrSiVN coatings at elevated temperature up to 700° C, Vacuum, 169 (2019) 108876.
[190] J.C. Colombo-Pulgarín, A.J. Sánchez Egea, D.J. Celentano, D.M. Krahmer, V. Martynenko, N. López de Lacalle, Mechanical and chemical characterisation of TiN and AlTiSiN coatings on a LPBF processed IN718 substrate, Materials, 14 (2021) 4626.
[191] Y. Guanghua, H. Xinmin, W. Yanqing, Q. Xingguo, Y. Ming, C. Zuoming, J. Kang, Effects of heat treatment on mechanical properties of H13 steel, Metal Science and Heat Treatment, 52 (2010) 393-395.
[192] J. Calvo, M. Penalva, J.M. Cabrera, Characterization of strain-induced precipitation in Inconel 718 superalloy, Journal of Materials Engineering and Performance, 25 (2016) 3409-3417.
[193] D. Tovar-Vargas, E. Roitero, M. Anglada, E. Jiménez-Piqué, H. Reveron, Mechanical properties of ceria-calcia stabilized zirconia ceramics with alumina additions, Journal of the European Ceramic Society, 41 (2021) 5602-5612.
[194] Y. Deng, L. Tang, G. Zeng, H. Dong, M. Yan, J. Wang, W. Hu, J. Wang, Y. Zhou, J. Tang, Enhanced visible light photocatalytic performance of polyaniline modified mesoporous single crystal TiO2 microsphere, Applied Surface Science, 387 (2016) 882-893.
[195] A. Fernández-Abia, J. Barreiro, J. Fernández-Larrinoa, L.L. de Lacalle, A. Fernández-

Valdivielso, O. Pereira, Behaviour of PVD coatings in the turning of austenitic stainless steels, Procedia Engineering, 63 (2013) 133-141.
[196] R. Boxman, S. Goldsmith, Macroparticle contamination in cathodic arc coatings: generation, transport and control, Surface and Coatings Technology, 52 (1992) 39-50.
[197] S. Zhang, L. Wang, Q. Wang, M. Li, A superhard CrAlSiN superlattice coating deposited by a multi-arc ion plating: II. Thermal stability and oxidation resistance, Surface and Coatings Technology, 214 (2013) 153-159.
[198] J. Musil, M. Jirout, Toughness of hard nanostructured ceramic thin films, Surface and Coatings Technology, 201 (2007) 5148-5152.
[199] M. Chen, F. Cai, W. Chen, Q. Wang, S. Zhang, Influence of vacuum annealing on structures and properties of AlTiSiN coatings with corrosion resistance, Surface and Coatings Technology, 312 (2017) 25-31.
[200] S. Zhang, D. Sun, Y. Fu, H. Du, Effect of sputtering target power on microstructure and mechanical properties of nanocomposite nc-TiN/a-SiNx thin films, Thin solid films, 447 (2004) 462-467.
[201] Y.-C. Huang, S.-Y. Chang, C.-H. Chang, Effect of residual stresses on mechanical properties and interface adhesion strength of SiN thin films, Thin Solid Films, 517 (2009) 4857-4861.
[202] S.-Y. Chang, Y.-S. Lee, C.-L. Lu, Effect of plasma treatments on the interface chemistry and adhesion strength between Cu metallization and SiCN etch stop layer, Journal of The Electrochemical Society, 154 (2007) D241.
[203] S. Bull, D. Rickerby, New developments in the modelling of the hardness and scratch adhesion of thin films, Surface and Coatings Technology, 42 (1990) 149-164.
[204] L. Patnaik, S. Maity, S. Kumar, Evaluation of crack resistance and adhesive energy of AlCrN and Ag doped aC films deposited on chrome nitrided 316 LVM stainless steel, Advances in Materials and Processing Technologies, (2021) 1-22.
[205] H. Ju, L. Yu, D. Yu, I. Asempah, J. Xu, Microstructure, mechanical and tribological properties of TiN-Ag films deposited by reactive magnetron sputtering, Vacuum, 141 (2017) 82-88.
[206] Q. Wang, F. Zhou, J. Yan, Evaluating mechanical properties and crack resistance of CrN, CrTiN, CrAlN and CrTiAlN coatings by nanoindentation and scratch tests, Surface and Coatings Technology, 285 (2016) 203-213.
[207] Y. Chen, Z. Zhang, T. Yuan, F. Mei, X. Lin, J. Gao, W. Chen, Y. Xu, The synergy of V and Si on the microstructure, tribological and oxidation properties of AlCrN based coatings, Surface and Coatings Technology, 412 (2021) 127082.
[208] L.-M. Berger, Application of hardmetals as thermal spray coatings, International Journal of Refractory Metals and Hard Materials, 49 (2015) 350-364.
[209] A. Gant, R. Morrell, A. Wronski, H. Jones, Edge toughness of tungsten carbide based hardmetals, International Journal of Refractory Metals and Hard Materials, 75 (2018) 262-278.
[210] Y. Huang, Y.K. Chou, S.Y. Liang, CBN tool wear in hard turning: a survey on research progresses, The International Journal of Advanced Manufacturing Technology, 35 (2007) 443-453.
[211] M. Cook, P. Bossom, Trends and recent developments in the material manufacture and cutting tool application of polycrystalline diamond and polycrystalline cubic boron nitride, International Journal of Refractory Metals and Hard Materials, 18 (2000) 147-152.
[212] V. Bushlya, F. Lenrick, A. Bjerke, H. Aboulfadl, M. Thuvander, J.-E. Ståhl, R. M'Saoubi, Tool wear mechanisms of PcBN in machining Inconel 718: analysis across multiple length scale, CIRP

annals, 70 (2021) 73-78.
[213] S. Gordon, J. Roa, T. Rodriguez-Suarez, R. M'Saoubi, E. Jiménez-Piqué, L.F. Franca, L. Llanes, Influence of microstructural assemblage of the substrate on the adhesion strength of coated PcBN grades, Ceramics International, 48 (2022) 22354-22363.
[214] S. Gordon Pozuelo, Microstructural and mechanical properties correlation at the micro-and nanometric length scale of different cBN grade, (2018).
[215] S. Sveen, J. Andersson, R. M' saoubi, M. Olsson, Scratch adhesion characteristics of PVD TiAlN deposited on high speed steel, cemented carbide and PCBN substrates, Wear, 308 (2013) 133-141.
[216] A. Mosquera, L. Mera, G. Fox-Rabinovich, R. Martínez, I. Azkona, J. Endrino, Advantages of nanoimpact fracture testing in studying the mechanical behavior of CrAl (Si) N coatings, Nanoscience and Nanotechnology Letters, 2 (2010) 352-356.
[217] L.-h. Zhu, S. Cheng, W.-y. Ni, Y.-x. Liu, Effect of 10% Si addition on cathodic arc evaporated TiAlSiN coatings, Transactions of Nonferrous Metals society of china, 26 (2016) 1638-1646.
[218] W.-Y. Ho, C.-H. Hsu, C.-W. Chen, D.-Y. Wang, Characteristics of PVD-CrAlSiN films after post-coat heat treatments in nitrogen atmosphere, Applied Surface Science, 257 (2011) 3770-3775.
[219] Y. Gui, J. Zhao, J. Chen, Y. Jiang, Preparation and characterization of Ni spines grown on the surface of cubic boron nitride grains by electroplating method, Materials, 9 (2016) 153.
[220] J. Liang, E. Almandoz, L. Ortiz-Membrado, R. Rodríguez, J.F. de Ara, G.G. Fuentes, L. Llanes, E. Jiménez-Piqué, Mechanical Performance of AlCrSiN and AlTiSiN Coatings on Inconel and Steel Substrates after Thermal Treatments, Materials, 15 (2022) 8605.
[221] X. Zhang, X.-B. Tian, Z.-W. Zhao, J.-B. Gao, Y.-W. Zhou, P. Gao, Y.-Y. Guo, Z. Lv, Evaluation of the adhesion and failure mechanism of the hard CrN coatings on different substrates, Surface and Coatings Technology, 364 (2019) 135-143.
[222] Q. Wang, F. Zhou, Z. Zhou, L.K.-Y. Li, J. Yan, An investigation on the crack resistance of CrN, CrBN and CrTiBN coatings via nanoindentation, Vacuum, 145 (2017) 186-193.
[223] S.-Y. Chang, H.-C. Tsai, J.-Y. Chang, S.-J. Lin, Y.-S. Chang, Analyses of interface adhesion between porous SiOCH low-k film and SiCN layers by nanoindentation and nanoscratch tests, Thin Solid Films, 516 (2008) 5334-5338.
[224] L. Patnaik, S.R. Maity, S. Kumar, Evaluation of crack resistance and adhesive energy of AlCrN and Ag doped aC films deposited on chrome nitrided 316 LVM stainless steel, Advances in Materials and Processing Technologies, 8 (2022) 1048-1069.
[225] B. Casas, M. Anglada, V. Sarin, L. Llanes, TiN coating on an electrical discharge machined WC-Co hardmetal: surface integrity effects on indentation adhesion response, Journal of materials science, 41 (2006) 5213-5219.
[226] Y. Zheng, G. Fargas, O. Lavigne, M. Serra, D. Coureaux, P. Zhang, Z. Yao, Q. Zhang, J. Yao, L. Llanes, Contact fatigue of WC-6% wtCo cemented carbides: Influence of corrosion-induced changes on emergence and evolution of damage, Ceramics International, 48 (2022) 5766-5774.
[227] Y. Kong, X. Tian, C. Gong, P.K. Chu, Enhancement of toughness and wear resistance by CrN/CrCN multilayered coatings for wood processing, Surface and Coatings Technology, 344 (2018) 204-213.
[228] L. Ortiz-Membrado, N. Cuadrado, D. Casellas, J. Roa, L. Llanes, E. Jiménez-Piqué, Measuring the fracture toughness of single WC grains of cemented carbides by means of microcantilever

bending and micropillar splitting, International Journal of Refractory Metals and Hard Materials, 98 (2021) 105529.
[229] Y. Torres, R. Bermejo, F. Gotor, E. Chicardi, L. Llanes, Analysis on the mechanical strength of WC-Co cemented carbides under uniaxial and biaxial bending, Materials & Design, 55 (2014) 851-856.
[230] J.M. Tarragó, D. Coureaux, Y. Torres, E. Jiménez-Piqué, L. Schneider, J. Fair, L. Llanes, Strength and reliability of WC-Co cemented carbides: Understanding microstructural effects on the basis of R-curve behavior and fractography, International Journal of Refractory Metals and Hard Materials, 71 (2018) 221-226.
[231] J.M. Tarragó, E. Jiménez-Piqué, L. Schneider, D. Casellas, Y. Torres, L. Llanes, FIB/FESEM experimental and analytical assessment of R-curve behavior of WC–Co cemented carbides, Materials Science and Engineering: A, 645 (2015) 142-149.
[232] R. Polini, M. Barletta, On the use of CrN/Cr and CrN interlayers in hot filament chemical vapour deposition (HF-CVD) of diamond films onto WC-Co substrates, Diamond and Related Materials, 17 (2008) 325-335.
[233] Y.-Y. Chang, C.-H. Chung, Z.-H. Tsai, J.-M. Tsai, Tribological and mechanical properties of AlCrBN hard coating deposited using cathodic arc evaporation, Surface and Coatings Technology, 432 (2022) 128097.
[234] Y. Liu, T.-G. Wang, W. Lin, Q. Zhu, B. Yan, X. Hou, Microstructure and properties of the AlCrSi (O) N tool coatings by arc ion plating, Coatings, 10 (2020) 841.
[235] K. Bobzin, T. Brögelmann, N. Kruppe, M. Carlet, Nanocomposite (Ti, Al, Cr, Si) N HPPMS coatings for high performance cutting tools, Surface and Coatings Technology, 378 (2019) 124857.
[236] K. Bobzin, T. Brögelmann, N. Kruppe, M. Carlet, Wear behavior and thermal stability of HPPMS (al, ti, cr, si) ON,(Al, ti, cr, si) n and (ti, al, cr, si) n coatings for cutting tools, Surface and Coatings Technology, 385 (2020) 125370.
[237] R. Fu, S. Kwok, P. Chen, P. Yang, R. Ngai, X. Tian, P.K. Chu, Surface modification of cemented carbide using plasma nitriding and metal ion implantation, Surface and Coatings Technology, 196 (2005) 150-154.
[238] L. Ortiz-Membrado, S. García-González, J. Orrit-Prat, R. Bonet, J. Caro, J. Fernández de Ara, E. Almandoz, L. Llanes, E. Jimenez-Pique, Improved Adhesion of Cathodic Arc Pvd Alcrsin Coating on Ion-Implanted Wc-Co Substrates, Available at SSRN 4244016.
[239] A. Mitsuo, S. Uchida, N. Nihira, M. Iwaki, Improvement of high-temperature oxidation resistance of titanium nitride and titanium carbide films by aluminum ion implantation, Surface and Coatings technology, 103 (1998) 98-103.
[240] D.-Y. Wang, M.-C. Chiu, Characterization of TiN coatings post-treated by metal-plasma ion implantation process, Surface and Coatings Technology, 156 (2002) 201-207.
[241] R.R. Manory, S. Mollica, L. Ward, K.P. Purushotham, P. Evans, J. Noorman, A.J. Perry, The effects of MEVVA ion implantation on the tribological properties of PVD-TiN films deposited on steel substrates, Surface and Coatings Technology, 155 (2002) 136-140.
[242] B. Deng, Y. Tao, Z. Hu, The microstructure, mechanical and tribological properties of TiN coatings after Nb and C ion implantation, Applied surface science, 284 (2013) 405-411.
[243] B. Deng, Y. Tao, D. Guo, Effects of vanadium ion implantation on microstructure, mechanical and tribological properties of TiN coatings, Applied Surface Science, 258 (2012) 9080-9086.
[244] B. Tian, W. Yue, Z. Fu, Y. Gu, C. Wang, J. Liu, Microstructure and tribological properties of W-

implanted PVD TiN coatings on 316L stainless steel, Vacuum, 99 (2014) 68-75.
[245] K.-W. Weng, Y.-C. Chen, S. Han, C.-S. Hsu, Y.-L. Chen, D.-Y. Wang, Effects of ion implantation on the microstructure and residual stress of filter arc CrN films, Thin solid films, 516 (2008) 5330-5333.
[246] K.-W. Weng, T.-N. Lin, D.-Y. Wang, Tribological property enhancement of CrN films by metal vapor vacuum arc implantation of vanadium and carbon ions, Thin solid films, 516 (2008) 1012-1019.
[247] K. Chang, S. Han, J. Lin, J. Hus, H. Shih, The effect of MEVVA implanted Cr on the corrosion resistance of CrN coated low alloy steel by cathodic arc plasma deposition, Surface and Coatings Technology, 172 (2003) 72-78.
[248] Y.-Y. Chang, D.-Y. Wang, Corrosion behavior of CrN coatings enhanced by niobium ion implantation, Surface and Coatings Technology, 188 (2004) 478-483.
[249] K. Purushotham, L. Ward, N. Brack, P.J. Pigram, P. Evans, H. Noorman, R. Manory, Corrosion behavior of Zr modified CrN coatings using metal vapor vacuum arc ion implantation, Journal of Vacuum Science & Technology A: Vacuum, Surfaces, and Films, 25 (2007) 110-116.
[250] Y.-C. Zhu, K. Fujita, N. Iwamoto, H. Nagasaka, T. Kataoka, Influence of boron ion implantation on the wear resistance of TiAlN coatings, Surface and Coatings Technology, 158 (2002) 664-668.
[251] B. Deng, Y. Tao, H. Liu, P. Liu, Influence of niobium ion implantation on the microstructure and tribological properties of TiAlN coatings, Surface and Coatings Technology, 228 (2013) S554-S557.
[252] B. Liu, B. Deng, Y. Tao, Influence of niobium ion implantation on the microstructure, mechanical and tribological properties of TiAlN/CrN nano-multilayer coatings, Surface and Coatings Technology, 240 (2014) 405-412.
[253] G. Peggs, I. Leigh, Recommended procedure for micro-indentation Vickers hardness test, (1983).
[254] J. Chen, S. Bull, On the factors affecting the critical indenter penetration for measurement of coating hardness, Vacuum, 83 (2009) 911-920.
[255] X. Cai, H. Bangert, Hardness measurements of thin films-determining the critical ratio of depth to thickness using FEM, Thin Solid Films, 264 (1995) 59-71.
[256] K. Purushotham, L.P. Ward, N. Brack, P.J. Pigram, P. Evans, H. Noorman, R.R. Manory, Wear behaviour of CrN coatings MEVVA ion implanted with Zr, Wear, 257 (2004) 901-908.
[257] Y. Zeng, Y. Zhen, J. Bian, J. Zhang, J. Pi, G. He, A. Xu, X. Zhang, J. Jiang, Cubic AlN with high thermal stabilities in TiN/AlN multilayers, Surface and Coatings Technology, 364 (2019) 317-322.
[258] M. Gondal, T. Fasasi, U. Baig, A. Mekki, Effects of oxidizing media on the composition, morphology and optical properties of colloidal zirconium oxide nanoparticles synthesized via pulsed laser ablation in liquid technique, Journal of Nanoscience and Nanotechnology, 18 (2018) 4030-4039.
[259] A. Zaman, E.I. Meletis, Microstructure and mechanical properties of TaN thin films prepared by reactive magnetron sputtering, Coatings, 7 (2017) 209.
[260] M. Bartosik, R. Daniel, Z. Zhang, M. Deluca, W. Ecker, M. Stefenelli, M. Klaus, C. Genzel, C. Mitterer, J. Keckes, Lateral gradients of phases, residual stress and hardness in a laser heated Ti0. 52Al0. 48N coating on hard metal, Surface and Coatings Technology, 206 (2012) 4502-4510.